NTNU

Norwegian University of
Science and Technology

Temperature coefficients in compensated silicon materials for solar cells

Åsmund Skomedal

Master of Science in Physics and Mathematics
Submission date: December 2017
Supervisor: Ursula Gibson, IFY
Co-supervisor: Erik S Marstein, IFE

Norwegian University of Science and Technology
Department of Physics

Summary

The pricing of solar modules is closely connected to the rating at standard testing conditions (STC). Lately more emphasis has been put on the relationship between field performance of PV-modules and the temperature sensitivity of cells. As it turns out, a benefit in the performance of cells made of Elkem Solar Silicon®(ESS) in high temperature, high irradiance areas relative to polysilicon cells has been showed. This benefit has been ascribed better temperature coefficients (TCs) in the cell parameters. In this thesis the physical phenomena behind the TCs are investigated. Through temperature and injection dependent lifetime spectroscopy (TIDLS) measurements of wafers, and temperature dependent IV-measurements of Passivated Emitter and Rear Contact (PERC-) cells, made of both ESS and polysilicon, an experimental foundation for the understanding these phenomena is built.

More importantly, the experimental results are used in the development of an advanced cell-model in an updated version of the device modeling software PC1Dmod 6.2. The model is verified by comparison to the measurements. Further, the independent and joint effect of varying the material parameters (such as compensation level, effective doping level and bulk lifetime) on the performance and temperature sensitivity of solar cells of different quality is investigated. In the end, a comprehensive understanding of the phenomena involved is reached, and novel knowledge relevant for compensation engineering is acquired.

The conclusion is that the most decisive material parameters for the temperature sensitivity of the measured PERC-cells is the the bulk lifetime and its temperature coefficient, and that any benefit in the TCs of ESS-cells relative to similarly rated polysilicon-cells probably stems from higher bulk lifetimes. However, this should not lead to the conclusion that ESS-cells in general have higher lifetimes; instead this comes down to the fact that if an ESS-cell and a polysilicon-cell are to have similar efficiencies, the ESS-cell necessarily needs to have higher lifetimes, and thus it will have better TCs too. Still, this should be considered in the pricing of the cells, since it might lead to relatively high performance ratios in ESS-cells, compared to polysilicon cells, especially in hot locations with high levels of irradiation.

Preface

This work is a part of the PRINCESS-project, which is within the EnergiX program of the Norwegian Research Council. This is a commercial collaboration project between Elkem Solar and Institute of Energy Technology (IFE) with the aim of investigating and understanding the phenomena deciding the temperature sensitivity of cells made of Elkem Solar Silicon®. Several papers has been published within this project already, i.e. (Berthod et al., 2015, 2016). As such, the work presented in this thesis builds on the work of others, both published and unpublished.

Therefore I want to express my gratitude to all the guys at IFE who have been helping me the last few months. It has been fun. Thanks guys. I am looking forward to continue to work with you, somehow or other.

Erik, I always enjoy our discussions while they last, even though I rarely contribute, and even though I don't always comprehend it once I leave your office. You make me optimistic about the future of our planet, and you inspire me to continue working with solar energy as long as I'm able. I am very happy for your ability to gather threads and make the object at hand seem well within reach. Especially after having been at Halvards office.

Halvard, I have enjoyed your supervision the last few months. I am inspired by your light-hearted approach to serious problems, and encouraged by your ever bright mood. Thanks for being patient with the persistence in my questions, whether they are about my failure to understand physics, or my failure to understand how your pieces of code work (if they do).

Marie and Rune, thanks for helping out whenever I have questions. Both of you contributed much to my thesis, for instance by doing measurements previous to my coming, sharing Matlab-scripts and helping me to understand stuff.

And thanks to all you other guys at IFE; you make it worthwhile to travel for hours on hours every week to get to and from Kjeller.

Oh, and thanks to Linda who has made an unexpected thrill of the last few weeks of my non-thesis life, taking the coloring of potentially grey days to the limits of RGB and beyond.

Åsmund Skomedal, December 15, 2017, Kjeller

Table of Contents

List of Tables

List of Figures

Abbreviations

$A_{n/p}$	=	Auger recombination coefficient for electrons/holes
ARC	=	Anti-Reflection Coating
B	=	Boron
B_{rad}	=	Radiative recombination coefficient
BGN	=	Band Gap Narrowing
BSF	=	Back Surface Field
B_{rad}	=	Radiative recombination coefficient
$B_{n/p}$	=	SRH coefficient for electrons/holes
C_l	=	Compensation level
CB	=	Conduction Band
CP5	=	A 2:10:5 HF:HNO_3:CH_3COOH solution
D	=	Diffusion coefficient
E	=	Electric field
ERE	=	External Radiative Efficiency
E_g	=	Energy band gap
E_i	=	Intrinsic fermi level
E_t	=	Trap state energy level
ESS	=	Elkem Solar Silicon®
ESS 0.5	=	ESS material with a target resistivity $\rho = 0.5\,\Omega\mathrm{cm}$
EG-Si	=	Electronic Grade Silicon (9N-11N)
f_c	=	Collection fraction
FF	=	Fill Factor
G	=	Generation rate
GB	=	Grain Boundary
h	=	$6.626 \times 10^{-34}\,\mathrm{J\,s}$ = Planck's constant
I_{sc}	=	Short circuit current
I_{PL}	=	PL intensity
$i.i$	=	Incomplete Ionization
J	=	Current density
J_0	=	Reverse saturation current
J_s	=	Current density of surface recombination
J_{sc}	=	Short circuit current density
J_{Lg}	=	Ideal current
k_B	=	Boltzmann's constant
$L_{n/p}$	=	Diffusion length for electrons/holes
MG-Si	=	Metallurgical Grade Silicon
MPP	=	Maximum Power Point
m^*	=	Effective mass

Δn	=	Excess carrier density
n	=	Density of electrons
n	=	Ideality factor
$\hat{n}$	=	Density of trap state electrons
n_0	=	Density of electrons at equilibrium (zero injection)
n_i	=	Intrinsic carrier concentration
n_{maj}	=	Density of majority carriers at equilibrium
n_s	=	Density of surface electrons
n_1	=	Occupation density of surface trap states
N_A	=	Density of acceptor atoms
N_A^-	=	Density of ionized acceptor atoms
N_D	=	Density of donor atoms
N_D^+	=	Density of ionized donor atoms
N_t	=	Density of trap states
$N_{s,t}$	=	Density of surface trap states
P	=	Phosphorous
p	=	Density of holes
PERC	=	Passivated Emitter Rear Contact
PL	=	Photoluminescence
Δp	=	Excess carrier density
$\hat{p}$	=	Density of trap state holes
p_0	=	$N_A - N_D$ = Effective doping level
$p_{0,i.i}$	=	$N_A^- - N_D^+$ = Density of holes at equilibrium ($i.i$ taken into account)
p_1	=	Occupation density of surface trap states
p_s	=	Density of surface holes
P_{MPP}	=	Output power at MPP
q	=	Elementary charge
QssPC	=	Quasi-steady state Photoconductance
R_s	=	Series resistance
R_{sh}	=	Shunt resistance
REF 1.3	=	Polysilicon reference, with a target resistivity $\rho = 1.3\,\Omega\mathrm{cm}$
SG-Si	=	Solar Grade Silicon (6N)
SRH	=	Shockley Read Hall
S	=	Surface recombination velocity
SRV	=	Surface Recombination Velocity
STC	=	Standard Testing Conditions ($1000\,\mathrm{W/m^2}$ at $25\,^\circ\mathrm{C}$)
$S_{n0/p0}$	=	Surface recombination parameters of electrons/holes
T	=	Temperature
TC	=	Temperature coefficient (average)
TC_{FF}	=	Temperature coefficient of fill factor
$TC_{J_{sc}}$	=	Temperature coefficient of short circuit current
$TC_{V_{oc}}$	=	Temperature coefficient of open circuit voltage
TC_η	=	Temperature coefficient of efficiency
TC_τ	=	Temperature coefficient of lifetime

U	=	Recombination rate
U_{SRH}	=	SRH recombination rate
U_{rad}	=	Radiative recombination rate
U_{Aug}	=	Auger recombination rate
VB	=	Valence Band
v_d	=	Drift velocity
V_{oc}	=	Open circuit voltage
v_{th}	=	Thermal velocity
W	=	Wafer thickness
β	=	Temperature coefficient (derivative)
η	=	Efficiency
ε_s	=	Dielectric permittivity of semiconductor
μ	=	Carrier mobility
ν	=	Frequency
Φ_{PL}	=	PL emission rate
ϕ	=	Electrostatic potential
ρ	=	Resistivity [$\Omega\mathrm{cm}$]
ρ_{fixed}	=	Local density of fixed charge
σ	=	Conductivity
$\sigma_{n/p}$	=	Capture cross section of electrons/holes
τ	=	Charge carrier lifetime
$\tau_{Aug,n/p}$	=	Auger recombination lifetime of carrier electrons/holes
τ_{bulk}	=	Bulk minority carrier lifetime
τ_c	=	Scattering time
τ_{eff}	=	Effective minority carrier lifetime
$\tau_{n/p}$	=	Electron/hole carrier lifetime
$\tau_{n0/p0}$	=	Capture time constant of carrier electrons/holes
τ_{rad}	=	Radiative recombination lifetime
τ_{SRH}	=	SRH recombination lifetime
τ_{surf}	=	Surface recombination lifetime

Chapter 1

Introduction

As the annual global installed capacity of solar power continues to soar at around 30% of the global capacity (Solar Power Europe, 2016), the demand for competitive solar cell technologies is as high as ever. Although a lot has already been gained as to cost reduction in the production of solar cells, the material itself still constitutes a substantial part of the budget for a module manufacturer. Any reduction in the material cost is therefore welcomed by the industry.

One option for reducing the material cost is by replacing the energy demanding Siemens process, which is commonly used for producing polysilicon. Some parts of the solar industry have developed alternative, less energy demanding processes for making solar grade (SG) Silicon. A whole branch of alternatives, all imprecisely grouped under the term upgraded metallurgical grade Silicon (UMG-Si), involves direct purification of metallurgical grade Silicon. Some of the impurities left in the material when using these methods effectively works as dopants, and they have to be compensated by the addition of the opposite dopant until the desired effective doping level is reached. Thus these materials are often referred to as *compensated* Silicon.

Although compensated Silicon is commonly considered an inherently lower quality material, recent studies have shown that the actual field performance of modules of compensated Silicon coming from the Norwegian company Elkem Solar beats that of similarly rated modules of polysilicon in high irradiation areas (Tayyib et al., 2013, 2014a). This indicates favorable temperature coefficients (TCs), which has been confirmed by several studies on Elkem Solar Silicon®(ESS) (Tayyib et al., 2014b,c; Søndenå et al., 2015; Berthod et al., 2015). Although some of the specific traits of these TCs have been pointed out, the physical reason why ESS is behaving as it is is still in the blue.

In this thesis a comprehensive approach will be used in order to investigate ESS and its behavior as a response to temperature. Firstly, temperature dependent charge carrier lifetime measurements on wafers made from three different Silicon materials, of which two are ESS and one is polysilicon, will be presented. The lifetime is decisive for the diffusion length of the carriers, and therefore decisive for the current as well as the voltage of the device. Secondly, temperature dependent IV-measurements on cells made of the same

materials will be presented. Thus it will be possible to correlate the lifetime measurements to the cell parameters and their temperature sensitivity, Thirdly, the lifetime measurements will be used as input to advanced device modeling of solar cells in the modeling software PC1Dmod 6.2, so as to possibly recreate the temperature behavior of the measured cells. The comparison between model and measurement results will give an increased understanding of what impacts the temperature sensitivity of the cells, as well as serving to validate the model. Lastly, the same modeling software will be used to do a sensitivity analysis of the different material parameters on the IV-parameters and their temperature coefficients.

The goals of this thesis are:

1. to measure the minority carrier lifetime in wafers made of ESS and polysilicon,
2. to measure the IV-parameters and temperature coefficients (TCs) of cells made of ESS and polysilicon,
3. to assess the impact of lifetime and doping levels on the IV-parameters and their TCs of solar cells made from ESS and polysilicon, and
4. ultimately to explain the reason for the previously measured advantages in the TCs of ESS-cells.

The structure of the thesis is as follows. First, a foundation for understanding the phenomena involved has to be laid. Thus, the thesis starts with a revision of the relevant theoretical considerations. First going through Silicon production technologies, it quickly moves on to theory on material parameters like doping, mobility, lifetime and carrier transport. After this, the topics lean more towards the experimental, going from the measurement of lifetimes on to the effect of lifetime on solar cell performance, and in the end to the core concern of the thesis: temperature sensitivity.

The next part of the thesis is a short introduction to the practicalities entailed in the thesis work. This involves a description of the samples, a short walk-through of the measurement techniques, and an introduction to the modeling framework.

The Results and Discussion part is divided into four. In the first three parts, lifetime measurement results, IV-measurement results and modeling results are presented and discussed. At the end of each of these parts, the main results and their implications will be summarized. This all culminates in the general discussion, where, drawing upon all the partial conclusions that have been made previously, a comprehensive understanding of how, how much, and why compensation and lifetime affects the IV-parameters and their TCs, and what this means for our understanding of compensation, will be laid down.

Although there already exists analytical and experimental investigations on the TCs of solar cells made of compensated Silicon in general (Xiao et al., 2014), and ESS in specific (Tayyib et al., 2014b,c; Søndenå et al., 2015; Berthod et al., 2015), the scientific community have yet to apply extensive device simulation in order to investigate the independent and combined impact of compensation and lifetime. Thus the results of this thesis will contribute with novel knowledge in the field, deepening our understanding of the temperature sensitivity of solar cells, as well as improving the foundation for doing compensation engineering. Possibly this may increase the incentive for using compensated Silicon for solar cells, ultimately contributing to the continued lowering of the price of solar energy.

As is mentioned in the Preface, this thesis is a part of the PRINCESS project, within the EnergiX program of the Norwegian Research Council. This means that not all the measurements used in this thesis have been performed, and not all the Matlab-code that has been run has been written, by its author. However, wherever work done by others has been used, this is stated in the Experiments and Modeling part. The rest has been performed by me.

Chapter 2

Theory and Literature Review

In this chapter the foundation for understanding the remainder of the thesis will be laid.

When it comes to making a functioning solar cell, several demands on the material has to be fulfilled. First of all a sufficiently pure material has to be achieved. This will be covered in section 2.1. Secondly, in order to attain the required electrical properties, the material has to be doped, which will be covered in section 2.2. Of the electrical properties, the ones most relevant for this thesis are mobility μ and minority carrier lifetime τ, which will be covered in the two subsequent sections. In order to estimate τ, some basic transport equations have to be applied, which will be derived in section 2.5. In the next section the theory behind the measuring of τ will be further developed, before the effect of τ on the performance of the solar cell will be discussed in section 2.7. The last section of this chapter will deal with the way material properties, as well as the performance of a PV module, responds to changing temperatures.

2.1 Silicon Production Technology

This section is a rough introduction to the most used Silicon production technologies that exists and that are relevant to this thesis. It is based on (Pizzini, 2012), and interested readers are encouraged to seek more information there, or in the many references therein.

Although Silicon is not the only material used for photovoltaic (PV) applications, it currently holds about 95% of the market share (ISE, 2017), and it is the only material which is considered in this thesis.

Almost all Silicon production routes used in PV applications today starts with the initial step of a carbothermic reduction of quartz (SiO_2) to make metallurgical grade Silicon (MG-Si). This is a crude form of Silicon, and due to its low purity (generally between 96% and 99%) it cannot be used in PV applications without further refining. In short, the carbothermic reduction of quartz is a process in which quartz and coal is mixed together in an electric arc furnace, as shown in **Figure 2.1**. Generally, energy is added through three carbon electrodes submerged in the mix, resulting in MG-Si being formed and collected at the bottom of the furnace, which may then be tapped.

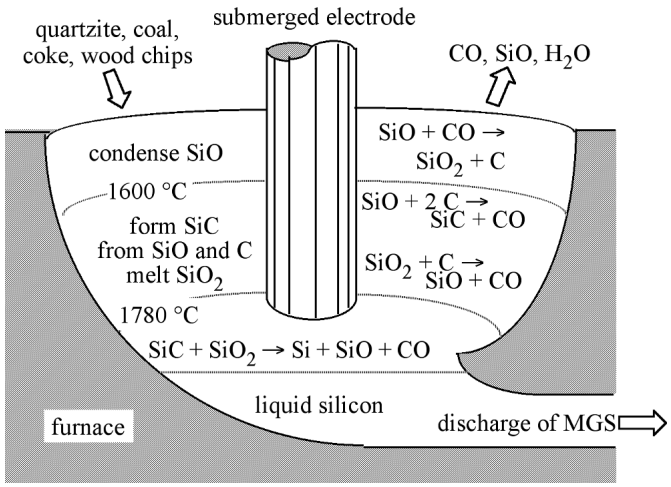

Figure 2.1: A submerged electric arc furnace for the carbothermic reduction of quartz to make metallurgical grade Silicon. Taken from `http://cnx.org/contents/bGvrPT9L@3/Semiconductor-Grade-Silicon`

2.1.1 The Siemens Process

When it comes to Silicon for PV applications, by far the most common way of refining pure Silicon from MG-Si is called the *Siemens process.* In short, this process involves fractional evaporation or condensation of a volatile Silicon compound, like trichlorosilane ($SiHCl_3$), through rectification or distillation to achieve ultra high purity. Then the volatile compound is decomposed into elemental Silicon by blowing it onto heated Silicon seed rods ($\sim 1150\,^{\circ}\mathrm{C}$), onto which the trichlorosilane decomposes and Silicon crystallites forms. The conventional version of this process leads to electronic grade polycrystalline Silicon (EG-Si) which is more than 9N, or $99.999\,999\,9\,\%$ clean, commonly referred to as *polysilicon*. There exists, however, a modified Siemens process that is dedicated to making solar grade polysilicon (SG-Si). This process uses a fluidized bed reactor, and is less energy demanding, but not as clean (6N) as EG-Si.

2.1.2 Upgraded Metallurgical Route

An alternative to the Siemens process is the upgraded metallurgical route, which is really a range of alternative routes in which MG-Si is further refined in order to make upgraded metallurgical grade Silicon (UMG-Si). The application of hydro- and pyrometallurgical processes might be the most common route, although other alternatives exists, like fluoride, plasmochemical and electrochemical processes, or simply producing high-grade MG-Si directly by using high-purity raw materials. This wide range of physical processes lead to an equally wide range of Silicon products, differing in impurity contents and making any attempt to give a common term to these materials ambiguous, to say the least. What they all bear in common, however, is the need for compensation. Since, in any of

the upgraded metallurgical routes, it has proven hard to remove enough impurities to reach the same degree of purity as polysilicon, some impurities remain (for instance boron) that effectively act as dopants. To compensate for this effect, other dopants (for instance phosphorous) have to be added in order to reach the desired effective doping level. Thus one may dub these materials *compensated Silicon*.

Even though the mobility is expected to be lower in compensated Silicon than in polysilicon, it has been shown that the lifetime may be significantly higher (Dubois et al., 2008; Pizzini, 2012; Xiao et al., 2012a), which may make up for the low mobility. This will be discussed further in section 2.7.

Some of the compensated materials have proven to be clean enough to deserve the term SG-Si. One of these is called the Elkem Solar Silicon®(ESS).

2.1.3 Elkem Solar Silicon®

ESS, which is refined through the hydro- and pyrometallurgical process, was developed on the industrial level by Elkem. It is a five step process, involving the creation of MG-Si, slag treatment, leaching, (directional) solidification and post treatment (see **Figure 2.2**).

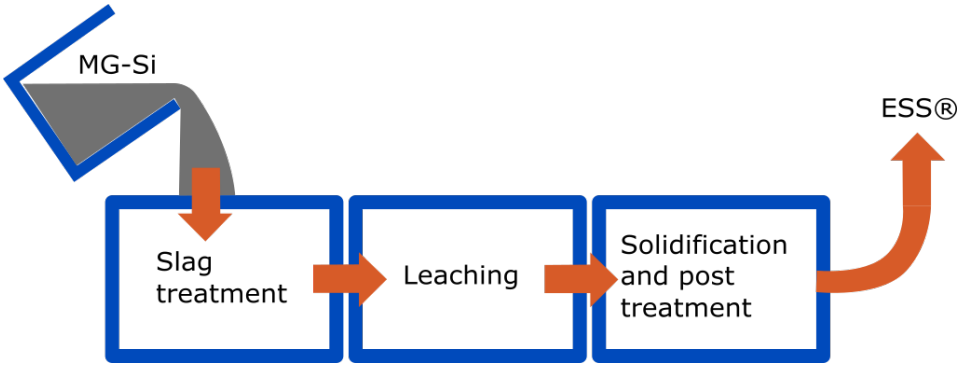

Figure 2.2: The ESS process.

The slag treatment is a pyrometallurgical process in which molten MG-Si is mixed with slag, taking advantage of different solubility of impurities in the Silicon and in the slag, or the existence of components in the slag that may form stable compounds with some of the impurities. Thus it is possible to reduce the content of Boron (B) and Phosphorous (P) to below $5\,\mathrm{ppmw}$ and $1\,\mathrm{ppmw}$ respectively.

In the leaching step, the fact that easily oxidizable impurities tend to diffuse towards grain boundaries is taken advantage of. The Silicon is ground to a powder, presumably divided at the grain boundaries, so that when acids (e.g. HCl, HF and HNO_3) are applied to this powder the impurities are etched off.

Directional solidification is a method that takes advantage of the fact that some of the impurities have higher solubility in liquid than in solid Silicon. Thus, during the solidification the impurities will tend to stay in the liquid, a process known as segregation. If the solidification process is controlled to happen from one end of the ingot to the other (it is directional), the concentration of impurities will increase in the liquid side, until the

whole ingot is solid. In the end, most of the impurities will be concentrated in the part of the ingot that solidified last, which may be cut off. In an ideal situation (i.e. 0 diffusion in the solid, infinitely fast diffusion in the liquid and equilibrium at the presumably straight solid-liquid interface) this is described by Scheil's equation;

$$C_s(x) = k_{eff} C_0 (1-x)^{k_{eff}-1}. \tag{2.1}$$

Here $C_s(x)$ is the concentration of the given element in the solid at relative height x, C_0 is the starting concentration in the molten Silicon, $k_{eff} = \xi_{(s)}/\xi_{(l)}$ is the effective segregation coefficient, and $\xi_{(s/l)}$ is the atomic fraction of the impurity in solid/liquid Silicon.

The post processing step is mostly concerned with making the ingots suitable for sale and transport. This involves making the top and bottom cut, as well as cutting the ingot into suitably sized blocks.

In the end a very high purity material is obtained, which has proven to perform excellently, yielding efficiencies above 20% at STC when the passivated emitter and rear cell (PERC) architecture is applied (REC, 2016). Further, advantageous temperature coefficients make cells made of ESS especially potent in high irradiation areas (Tayyib et al., 2013, 2014a), which will be discussed further in section 2.8.

2.2 Doping and Ionization

Intrinsic Silicon is in itself a bad conductor. For this reason, and in order to make a pn-junction, it is necessary to dope it. Usually the whole Silicon wafer is background doped with electron acceptors (e.g. B) to become p-type, and then an electron donor (e.g. P) is diffused in at the emitter side to make an n-type region (Reinders et al., 2017). The concentration of acceptor atoms is denoted N_A, while the concentration of donor atoms is denoted N_D.

As already mentioned, in compensated Silicon the content of acceptors may be too high from the onset. In order to reach the desired doping level it is therefore necessary to dope the whole wafer with additional donors, earning it the name of compensated Silicon. The compensation level C_l is defined as

$$C_l = \frac{N_A + N_D}{n_{maj}}, \tag{2.2}$$

where n_{maj} is the equilibrium majority carrier concentration. The donor atoms contribute with carriers as long as they are ionized. The concentration of ionized acceptors and donors are denoted N_A^- and N_D^+ respectively, so that the majority carrier concentration at equilibrium is $n_{maj} = n_i + |N_A^- - N_D^+|$. For simplicity, it is often assumed that all donors and acceptors are ionized, an assumption dubbed *complete ionization*. This means that $N_A^- = N_A$ and $N_D^+ = N_D$. If in addition $|N_A - N_D| \gg n_i$, which is almost always the case, we may say that the concentration of majority carriers equals the net doping concentration. In a p-region that would be $p_0 = N_A - N_D$, and in an n-region $n_0 = N_D - N_A$, where p_0 and n_0 is the equilibrium concentration of holes and electrons respectively. p_0 (and n_0) are also called the *effective doping level*.

The assumption of complete ionization may be a good approximation for non-compensated Silicon with doping concentrations of less than $1 \times 10^{17}\,\mathrm{cm}^{-3}$, but recent studies have shown that the assumption doesn't hold for compensated Silicon with more than $5 \times 10^{16}\,\mathrm{cm}^{-3}$ of B or $2 \times 10^{16}\,\mathrm{cm}^{-3}$ of Ga (Forster et al., 2013a,b). Incomplete ionization ($i.i$) is insignificant for acceptor dopants at these doping levels in Silicon (Cuevas et al., 2012) because the degeneracy factor is twice that of donors (see Neamen, 1997, pp. 110). This holds for both compensated and non-compensated Silicon. The density of holes at equilibrium if $i.i$ is taken into account is $p_{0,i.i} = N_A^- - N_D^+$ in a p-type material. $i.i$ may have considerable effects on the electrical properties of the material, and may prove to be essential to understand the behavior of compensated Silicon with changing temperatures.

2.3 Mobility

Following the formalism of (Reinders et al., 2017), the basic theory of the carrier mobility μ will now be introduced. As the name implies, μ characterizes how quickly a charge carrier moves through a metal or a semiconductor. It is defined as the proportionality factor relating the drift velocity v_d and the electric field E:

$$v_d = \frac{q\tau_c}{m^*} E \equiv \mu E, \tag{2.3}$$

where τ_c is the scattering time and m^* is the effective mass of the carrier. In other words, μ is proportional to τ_c, which is the average time a carrier is accelerated in an electric field until it scatters. Thus it is the different scattering mechanisms in the material that determines μ. According to Matthiessen's rule the effect of the different scattering mechanisms may be added up according to

$$\frac{1}{\mu} = \sum_{i=1}^{N} \frac{1}{\mu_i}, \tag{2.4}$$

where μ_i is the mobility due to scattering mechanism i.

The relationship between mobility and conductivity σ becomes apparent when looking at the drift current, which is $J_{n,drift} = nq \cdot v_d$ for electrons and $J_{p,drift} = pq \cdot v_d$ for holes. The drift current is generally the sum of the contribution from electrons and holes, so that

$$J_{drift} = J_{n,drift} + J_{p,drift} = q(n\mu_n + p\mu_p)E, \tag{2.5}$$

where

$$q(n\mu_n + p\mu_p) \equiv \sigma = \frac{1}{\rho}, \tag{2.6}$$

is the conductivity and ρ is the resistivity. This is an alternative formulation of Ohm's law.

A mobility model was developed by Klaassen that successfully predicts the mobility for non-compensated Silicon (Klaassen, 1992b,a). However, the model has been shown not to hold for compensated Silicon (Forster et al., 2013a,b; Cuevas et al., 2012), especially not the minority carrier mobility (Rougieux et al., 2010). Compensation serves to reduce

μ. This has been attributed to increased impurity scattering, due to reduced screening as well as incomplete ionization. In 2013 a new empirical model was proposed where the mobility's dependency on C_l was included (Schindler et al., 2014). This model has been implemented in update 6.1 and 6.2 of PC1D (Haug et al., 2015), the latter being the version which has been used in the modeling of solar cells in this thesis.

2.4 Minority Carrier Lifetime

The following sections, up to section 2.7, are based on (Haug, 2014), (Nelson, 2003) and (Rein, 2005) unless otherwise stated.

A material property decisive for the performance of a solar cell is the lifetime of the minority carriers, denoted $\tau_{n/p}$ in p/n-type material. In essence the lifetime is the average time an excited carrier will stay in the conduction band before relaxing, or recombining, back to the valence band. As will be discussed later, the lifetime determines the diffusion length L, which again determines the likelihood of the carrier to be collected by a contact, and thus the performance of the solar cell.

However, τ is not constant; it depends on other cell parameters, especially temperature T and injection level Δn. As will be seen in chapter 3, it may well vary by a factor of more than 10 within the range of normal operating temperatures and injection levels. Thus, in order to make an accurate cell model realistically describing operation in the field it is vital to incorporate $\tau = \tau(T, \Delta n)$.

As already mentioned, what limits the lifetime are the recombination mechanisms, including the intrinsic recombination mechanisms, Shockley Read Hall recombination and surface recombination, which are the topics of the following sections.

2.4.1 Intrinsic Recombination Mechanisms

The reason why radiative recombination and Auger recombination are called intrinsic recombination mechanisms is because they are inevitable mechanisms that exist due to the physical properties of the semiconductor, and not due to any defects.

Radiative recombination is the mechanism in which an electron in the conduction band (CB) releases energy in the form of a photon and falls down from the CB to recombine with a hole in the valence band (VB) (see **Figure 2.3**). The frequency of the emitted light corresponds to the change in energy, in other words; $h\nu = \Delta E$, where h is Planck's constant, ν is its frequency and ΔE is the change in energy. It can be shown that the radiative recombination rate U_{rad} is proportional to $(np - n_i^2)$:

$$U_{rad} = B_{rad}(np - n_i^2), \tag{2.7}$$

where B_{rad} is the radiative recombination coefficient which is carrier density independent and a property of the material.

Neglecting carrier trapping, so that $\Delta n = \Delta p$, we may write $(np - n_i^2) = (n_0 + \Delta n)(p_0 + \Delta n) - n_0 p_0 = (p_0 + n_0 + \Delta n)\Delta n$. Then U_{rad} may be expressed by the the excess minority carrier density $\Delta n = n - n_0$;

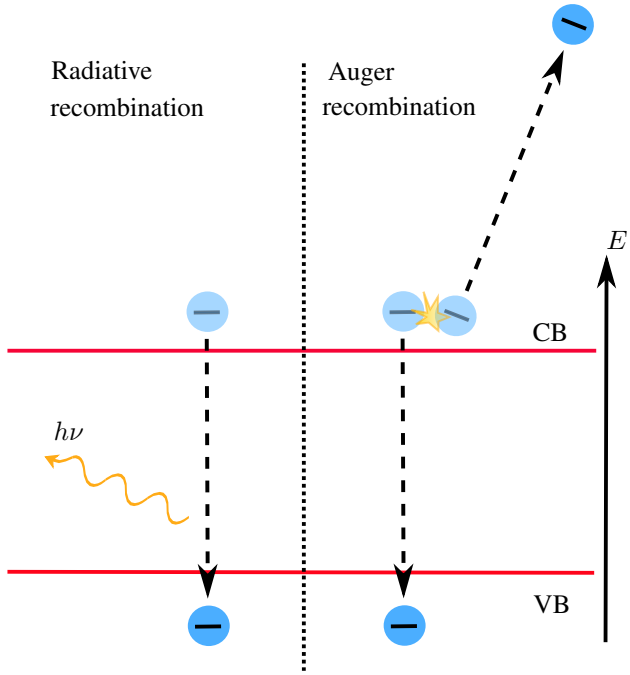

Figure 2.3: To the left: Radiative recombination, in which an electron in the conduction band (CB) relaxes down to the valence band (VB), recombining with a hole, and in the process releases a photon with energy $h\nu = \Delta E$, where h is Planck's constant, ν is its frequency and ΔE is the change in energy. To the right: Auger recombination, in which two electrons in the CB collide and one electron gives off its energy to the other, causing the first electron to relax and recombine with a hole in the VB, and the other electron to rise to a higher energy level in the CB. The energy axis is for electrons; for holes it is reversed.

$$U_{rad} = \frac{\Delta n}{\tau_{rad}}, \tag{2.8}$$

where

$$\tau_{rad} = \frac{1}{B_{rad}(p_0 + n_0 + \Delta n)}, \tag{2.9}$$

is the minority carrier radiative lifetime. In a compensated p-type material, where $p_0 \gg n_0$, this may be reduced to

$$\tau_{n,rad} = \frac{1}{B_{rad}p}, \tag{2.10}$$

where $p = p_0 + \Delta n$. The radiative recombination of holes in n-type material is completely analogous.

In Silicon, which is an indirect bandgap material, the probability of radiative recombination is low, and recombination is dominated by the other recombination mechanisms.

Auger recombination is the mechanism in which two electrons (or holes) in the CB (VB) collide and one give off some of its energy to the other, causing the first to relax and recombine in the VB (CB), and the other to rise to a higher (kinetic) energy level in the CB (VB). The extra energy of the second electron (hole) will then quickly be dissipated via thermalization, or in other words be given off to the material as heat as the charge carriers transfer their energy to atomic vibrations in the material, thus relaxing back to the band edge. Thus this energy is lost. Similarly to radiative recombination, the minority carrier Auger lifetime in p-type material at low injection may be expressed as

$$\tau_{n,Aug} = \frac{1}{A_n p^2}, \tag{2.11}$$

and as

$$\tau_{p,Aug} = \frac{1}{A_p n^2}, \tag{2.12}$$

in n-type material, where $A_{n/p}$ is the Auger recombination coefficient for electrons/holes.

Since the momentum of the involved electrons may change in Auger recombination, i.e. they may move in k-space (though the total k must be conserved), the fact that a bandgap is indirect does not limit the rate of recombination. Thus, in indirect bandgap materials, like Silicon, Auger recombination is the dominant intrinsic recombination mechanism.

Also, as can be seen from equation (2.11) and (2.12), the Auger lifetime decreases with increasing doping levels. Also, the Auger lifetime decreases with injection level, which can be seen in **Figure 2.5**.

2.4.2 Shockley Read Hall Recombination

The well known picture of available energy states in a semiconductor being exclusively below the VB edge or above the CB edge is, of course, a simplification. In reality there are available energy states between the band edges due to impurities, defects and dislocations in the material. These energy states are called *defect states*, and depending on the distance from the band edges they may exhibit different properties. If a defect state is located close to the CB edge, the probability of an electron to occupy this state and for it to jump up to the CB again is high, but the probability of the electron to fall down from the defect state to the VB and recombine is low. Thus it effectively traps the electron, earning it the name *trap state*. A trap state close to the VB edge does the same for a hole. In general, trap states that are close to the bandgap edges will enhance either τ_p or τ_n.

If, on the other hand, the defect state is located around the middle of the bandgap (i.e. *deep* in the bandgap), and an electron occupies it, chances are a hole will be excited to recombine with the electron before the electron is excited back up to CB. Thus this will increase the recombination rate of the material, earning it the name of a *recombination centre*. The process, which is referred to as Shockley Read Hall (SRH) recombination, is usually non-radiative, emitting a phonon instead of a photon, which serves to heat up

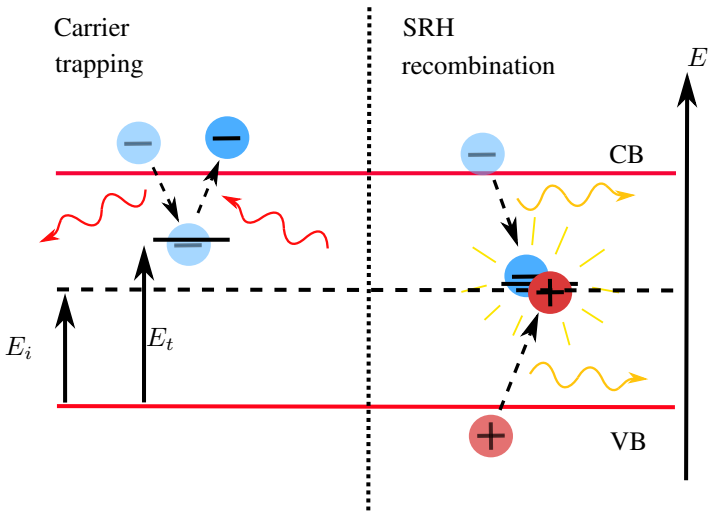

Figure 2.4: To the left: Carrier trapping, in which an electron in the conduction band (CB) relaxes down to a trap state at E_t, releasing a phonon, and after a while is re-excited back to CB. To the right: SRH recombination, in which an electron in CB relaxes down to a trap state, there to recombine with a hole from VB. The energy axis is for electrons; for holes it is reversed.

the material. This loss mechanism is the practical limiting mechanism of most solar cells (Reinders et al., 2017).

The SRH recombination rate may be derived, and yields

$$U_{SRH} = \frac{np - n_i^2}{\tau_{p0}(n + \hat{n}) + \tau_{n0}(p + \hat{p})}, \tag{2.13}$$

where

$$\tau_{p0/n0} = \frac{1}{v_{th}\sigma_{p/n}N_t}, \tag{2.14}$$

is the capture time constant of holes/electrons, and

$$\hat{p} = n_i e^{(E_i - E_t)/k_B T}, \tag{2.15}$$

$$\hat{n} = n_i e^{(E_t - E_i)/k_B T}. \tag{2.16}$$

Here $v_{th} \sim 10^7\,\mathrm{cm/s}$ (at 300 K) is the thermal velocity, $\sigma_{p/n}$ is the capture cross section of holes/electrons, N_t is the trap density and $(E_t - E_i)$ is the distance between the trap state energy E_t and the middle of the bandgap.

By assuming $\Delta n = \Delta p$, and remembering that $np - n_i^2 = (p_0 + n_0 + \Delta n)\Delta n$, we see that we may rewrite equation (2.13) to

$$U_{SRH} \approx \frac{\Delta n}{\tau_{SRH}}, \tag{2.17}$$

where

$$\tau_{SRH} = \frac{\tau_{p0}(n_0 + \Delta n + \hat{n}) + \tau_{n0}(p_0 + \Delta n + \hat{p})}{p_0 + n_0 + \Delta n}. \tag{2.18}$$

From this we can see that at low injection in a p-type material ($p_0 \gg \Delta n$ and $p_0 \gg n_0$), the majority carriers will dominate, so that $\tau_{SRH} \approx \tau_{n0}$. At high injection ($\Delta n \gg p_0$ and $\Delta n \gg n_0$) you get $\tau_{SRH} \approx \tau_{n0} + \tau_{p0}$.

A comprehensive method for doing temperature- and injection-dependent lifetime spectroscopy (TIDLS) has been developed by (Rein, 2005), and further refined by, among others, (Murphy et al., 2012). From equation (2.18), assuming p-type Silicon so that n_0 may be neglected, we derive

$$\frac{\tau_{SRH}}{\tau_{n0}} \approx 1 + \frac{\hat{p}}{p_0} + k\frac{\hat{n}}{p_0} + \left(k - \frac{\hat{p}}{p_0} - k\frac{\hat{n}}{p_0}\right) Y \tag{2.19}$$

$$= A(k, E_t) + B(k, E_t) \cdot Y, \tag{2.20}$$

where $k = \tau_{p0}/\tau_{n0}$ and $Y = \frac{n}{p} \approx \frac{\Delta n}{p}$. Using this equation, a linear regression may be applied to find A and B for a single defect. If there are more defects in the material, their contributions to τ_{SRH} may be added up inversely. Each value of A and B may be represented by a range of combinations of k and E_t. When doing TIDLS, these combinations are mapped for each temperature, and a minimum error fit is found. Thus it is possible to find k and E_t of one or more defects in a material.

2.4.3 Surface Recombination

The trap density is often much higher at the surfaces due to dangling unpassivated bonds and absorbed impurity molecules (Reinders et al., 2017). These defect states may form an almost continuous distribution of states in the bandgap which effectively works as an infinite sink for recombination. This is obviously detrimental for the performance of a solar cell. To deal with this you have to passivate the recombination centres. In solar cells with high quality bulk material, surface recombination is a limit to the performance of the solar cells, and the development of better (and cheaper) methods of surface passivation is of major concern to the solar industry. One way of achieving surface passivation is the introduction of electric fields. Since any recombination event necessarily involves both an electron and a hole, it is possible to limit the surface recombination by reducing the density of just one of the carrier types. Since the carriers are charged, the introduction of an electric field will repel one of the carrier types. Surface passivation by electric field may be implemented with a doping profile, or by depositing stable electrostatic charges in an overlying insulator. These methods are called field-effect passivation, and the former is what is used in a Aluminum-back surface field (Al-BSF). Often both means of passivation are implemented simultaneously.

Mathematically the recombination rate by surface trap states U_{surf} may be treated similarly to SRH recombination, and may be expressed as

$$U_{surf} = \frac{N_{s,t} v_{th} (n_s p_s - n_i^2)}{\frac{n_s + n_1}{\sigma_p} + \frac{p_s + p_1}{\sigma_n}} \equiv S \Delta n_s, \tag{2.21}$$

where $\sigma_{n/p}$ is the capture cross section of electrons/holes of the surface states, $\Delta n_s = n_s - n_0$ and $\Delta p_s = p_s - p_0$ are the excess surface electron and hole density, n_1 and p_1 are the occupation densities of the surface trap states, and S is the surface recombination velocity (SRV) (Aberle, 1999). In the case of a single defect state, and flatband conditions, i.e. no electric fields at the given surface, we have $\Delta n_s = \Delta p_s$, and

$$S(\Delta n_s) = \frac{n_0 + p_0 + \Delta n_s}{\frac{n_0 + n_1 + \Delta n_s}{S_{p0}} + \frac{p_0 + p_1 + \Delta n_s}{S_{n0}}} \tag{2.22}$$

where $S_{n0/p0} = N_{t,s} \sigma_{n/p} v_{th}$ are the surface recombination parameters for electrons/holes.

If, however, there is band bending at the surface, which is the case when a passivating electric field has been introduced, the assumption that $\Delta n_s = \Delta p_s$ does not hold. Consequently equation (2.22) cannot be used, and an analytical expression of the SRV does not exist. Instead an extended SRH formalism (B M Girisch et al., 1988) has to be applied, n_s and p_s have to be estimated numerically, leading to U_{surf} through equation (2.21). From these equations it can be shown that the SRVs depend on the effective doping level p_0 (or n_0 if n-type); the higher p_0, the higher the SRVs are (Aberle, 1999). For low doping levels ($p_0 < 5 \times 10^{15}\,\mathrm{cm}^{-3}$) this has shown to have a linear dependency on p_0 (Brody and Rohatgi, 2001).

A current density of surface recombination may be defined as

$$J_s \equiv qS(\Delta n_s). \tag{2.23}$$

In general the front SRV, S_f, is different from the rear SRV, S_r, and the total contribution of surface recombination to the effective minority carrier lifetime of a cell, τ_{eff}, is given by

$$\frac{1}{\tau_{eff}} = \frac{1}{\tau_{bulk}} + \alpha_0^2 D, \tag{2.24}$$

where D is the diffusion coefficient and α_0 is the smallest eigenvalue solution of the equation

$$\tan(\alpha_0 W) = \frac{S_f + S_r}{\alpha_0 W + \frac{S_f S_r}{\alpha_0 W}}, \tag{2.25}$$

and W is the cell thickness (Haug, 2014). However, it can be shown that if $S_f = S_r = S$, τ_{eff} may be approximated to

$$\frac{1}{\tau_{eff}} \approx \frac{1}{\tau_{bulk}} + \frac{2S}{W} + D \left(\frac{\pi}{W} \right)^2, \tag{2.26}$$

which will be within 5% of the actual value of τ_{eff} for all S (Sproul, 1994).

The recombination rates due to the different mechanisms may be summed up to give a total recombination rate

$$U_{eff} = U_{rad} + U_{Aug} + U_{SRH} + U_{surf}. \tag{2.27}$$

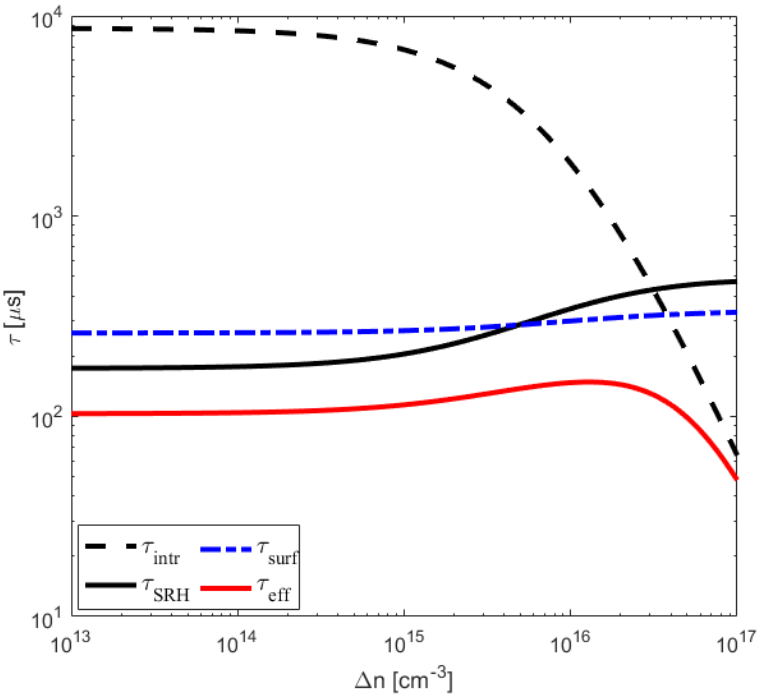

Figure 2.5: Example of the effective minority carrier lifetime τ_{eff}, which equals the inverse sum of all its components, and is thus limited by its smallest component.

Since all the different recombination rates can be expressed as

$$U = \frac{\Delta n}{\tau}, \tag{2.28}$$

it is possible to sum up the inverse of the lifetimes to yield the effective lifetime;

$$\frac{1}{\tau_{eff}} = \frac{1}{\tau_{int}} + \frac{1}{\tau_{SRH}} + \frac{1}{\tau_{surf}}, \tag{2.29}$$

where

$$\frac{1}{\tau_{int}} = \frac{1}{\tau_{rad}} + \frac{1}{\tau_{Aug}}. \tag{2.30}$$

Since τ_{eff} equals to the inverse sum of its components, it will always be limited by its smallest component. This can be seen in the example of **Figure 2.5**.

2.5 Carrier Transport

Charge carriers in a semiconductor may be generated, recombined or transported. Generation is the process in which an electron is excited from the VB to the CB, or the hole from the CB to the VB, thus *generating* a carrier. Due to charge conservation, the change in number of electrons (or holes) within a section of the semiconductor must equal the generation minus the recombination, plus the change due to transport of carriers in and out of the section, as depicted in **Figure 2.6**. This may be stated mathematically in one dimension as

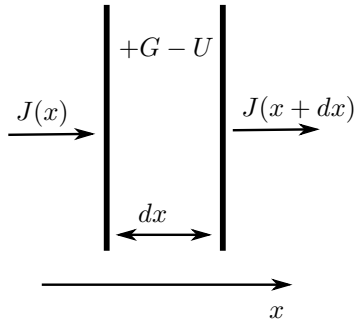

Figure 2.6: The change in charge carriers within a section of a semiconductor equals the change in carriers caused by the sum of current into the section, current out of the section, generation and recombination. Also, $\frac{J(x+dx)-J(x)}{dx} = \frac{\partial J}{\partial x}$.

$$\frac{\partial n}{\partial t} = \frac{1}{q}\frac{\partial J_n}{\partial x} + G_n - U_n \tag{2.31a}$$

$$\frac{\partial p}{\partial t} = -\frac{1}{q}\frac{\partial J_p}{\partial x} + G_p - U_p, \tag{2.31b}$$

for electrons and holes respectively. Here J is the current density, G is the generation rate and U is the recombination rate.

There are two mechanisms that drive current in a semiconductor: drift due to an electric field, and diffusion due to gradients in the charge carrier density. The contributions from each may be summed up to yield the total current due to electrons and holes respectively;

$$J_n = J_{n,drift} + J_{n,diff} = q\mu_n nE + qD_n\frac{\partial n}{\partial x}, \tag{2.32a}$$

$$J_p = J_{p,drift} + J_{p,diff} = -q\mu_p pE - qD_p\frac{\partial p}{\partial x}, \tag{2.32b}$$

where E is the local electric field. D_n and D_p are the diffusion coefficients for electrons and holes. Inserting (2.32) into (2.31) yields

$$\frac{\partial n}{\partial t} = \mu_n \left(n\frac{\partial E}{\partial x} + E\frac{\partial n}{\partial x} \right) + D_n \frac{\partial^2 n}{\partial x^2} + G_n - U_n \tag{2.33a}$$

$$\frac{\partial p}{\partial t} = \mu_p \left(p\frac{\partial E}{\partial x} + E\frac{\partial p}{\partial x} \right) + D_p \frac{\partial^2 p}{\partial x^2} + G_p - U_p. \tag{2.33b}$$

2.6 Measuring the Lifetime

When measuring τ_{eff} you take advantage of the carrier transport equations. By illuminating a wafer homogeneously there will be no gradients in E or n, so that equation (2.33a) and (2.33b) reduces to

$$\frac{\partial \Delta n}{\partial t} = G_n - U_n, \tag{2.34a}$$

$$\frac{\partial \Delta n}{\partial t} = G_p - U_p, \tag{2.34b}$$

respectively. Here we have assumed high injection, so that $\Delta n = n - n_0 \approx n$ and $\Delta n = \Delta p$. Then, since the recombination rate may be expressed as $U = \Delta n/\tau_{eff}$, we arrive at an equation expressing τ_{eff} solely by G and Δn;

$$\tau_{eff} = \frac{\Delta n}{G - \frac{\partial \Delta n}{\partial t}}. \tag{2.35}$$

2.6.1 Quasi-steady state Photoconductance (QssPC)

Now, going back to the illuminated wafer; if the light source is kept at a constant intensity we are operating in steady state, i.e. $\frac{\partial \Delta n}{\partial t} = 0$, so that equation (2.35) becomes

$$\tau_{eff} = \frac{\Delta n}{G}. \tag{2.36}$$

If you slowly vary G, and measure Δn at each G, you can estimate τ_{eff} at each Δn. This is the *quasi-steady state* case.

Conversely, if the light is turned off, you will have $G = 0$ while the carriers recombine, and equation (2.35) becomes

$$\tau_{eff} = -\frac{\Delta n}{\frac{\partial \Delta n}{\partial t}}, \tag{2.37}$$

meaning the lifetime can be found from the decay rate of excess carriers. This is the *quasi-transient* case. The problem with this method is that the decay rate may change with Δn.

In general, however, it is possible to estimate both G and $\frac{\partial \Delta n}{\partial t}$ at the same time. You then make use of the whole of equation (2.35). This is the *general* case. With the use of a coil a current is induced in the sample, making it possible to deduce its conductivity σ. From this the excess carrier density Δn may be determined via the equation

$$\Delta n(t) = \frac{\Delta \sigma(t)}{q(\mu_n + \mu_p)W}, \tag{2.38}$$

where W is the wafer thickness. Further, there is a calibrated reference cell next to the sample measuring the light intensity I. Then G may be determined from the equation

$$G(t) = OC \cdot \frac{I(t)}{qW}, \tag{2.39}$$

where the optical constant OC is an empirically determined factor quantifying the fraction of photons that are absorbed in the sample times the charge per unit light intensity.

In general, in quasi-steady state photoconductance (QssPC) measurements all three methods are used. It is also possible to adjust the duration of the flash, and by doing so changing the relative size of the terms in the denominator of equation (2.35).

2.6.2 Photoluminescence Imaging

Photoluminescence imaging (PL-I), as the name alludes to, is a technique in which optical generation of carriers is used to acquire 2D maps of the effective lifetime over a wafer. Usually a short wavelength (relative to the band gap) laser is used to excite the carriers. The PL emission rate Φ_{PL} is equal to the rate of radiative recombination U_{rad};

$$\Phi_{PL} = B_{rad}(np - n_i^2), \tag{2.40}$$

from equation (2.7). In a moderately doped p-type material, where $p = N_A^- - N_D^+ + \Delta n$, $n = \Delta n$ and n_i may be neglected, this becomes

$$I_{PL} = C_{cal} B_{rad}(N_A^- - N_D^+ + \Delta n)\Delta n, \tag{2.41}$$

where I_{PL} is the measured intensity and C_{cal} is a sample- and instrument specific calibration constant. Equation (2.41) may be solved as a second degree polynomial of Δn. In a non-compensated p-type material in low injection you may simplify further and set $p = N_A$. Then you may write

$$\Delta n(x, y) = \left(\frac{1}{C_{cal} B_{rad} N_A} \right) \cdot I_{PL}(x, y). \tag{2.42}$$

Either way it is possible to apply equation (2.36) to get the lifetime of the sample. Notice that a dependency on (x, y) has been introduced in equation (2.42) to emphasize the fact that PL-I gives you an image of the variation of the effective lifetime over the area of a wafer. There is nothing in the way of introducing a dependency on (x, y) into equation (2.41) and (2.36) as well.

2.7 Lifetime and Solar Cell Performance

The effect of the minority carrier lifetime τ on the performance of the solar cell has already been alluded to. As was mentioned, τ affects the performance through the *diffusion length* L. This is the distance a carrier will diffuse on average before recombination, and is given by $L = \sqrt{\tau D}$, where $D = \mu k_B T/q$ is the diffusion coefficient, $k_B = 1.381 \times 10^{-23}\,\mathrm{J\,K^{-1}}$ is Boltzmann's constant, T is the temperature and $q = 1.602 \times 10^{-19}\,\mathrm{C}$ is the elementary charge. The number of minority carriers that are extracted from the cell, and thus the size of the output current J, is dependent upon the number of minority carriers that are generated within L of a contact. This means that the larger τ, the larger L and J, and thus the larger output power P_{out} and efficiency η.

(Nelson, 2003) derives the analytic solution to the transport problem (equation (2.31)), showing the exact relationship between the photocurrent J and the effective lifetime. The analytical relationship is complicated, and here it is enough to state that the effect of decreasing the lifetime is detrimental to the performance of the solar cell, and vice versa. In fact, as a study of the influence of different material- and process-based parameters on the variance of η in Passivated Emitter and Rear Contact (PERC) cells showed, the bulk minority carrier lifetime τ_{bulk} accounted for half the variance that could be found (Wasmer et al., 2017). This clearly points out the importance of τ_{bulk} for the performance of PERC solar cells. It is worth to note that this influence is expected to be smaller in lower quality cells, like the industry standard Al-BSF cell, that has poor surface passivation, and thus higher surface recombination currents. This gives low surface recombination lifetimes which will limit τ_{eff} in spite of high τ_{bulk}, thus limiting the performance.

However, τ_{eff} does not only affect the current of the solar cell, but also its voltage and fill factor FF. This can be seen in the common equation for the open circuit voltage V_{oc} derived from the one diode model of the solar cell:

$$V_{oc} = \frac{kT}{q} \ln\left(\frac{J_{sc}}{J_0}\right), \tag{2.43}$$

where

$$J_0 = \frac{qD}{Ln_{maj}} \cdot n_i^2, \tag{2.44}$$

is the the reverse saturation current, n_{maj} is the majority carrier density and n_i is the intrinsic carrier density. As is seen, $J_0 \propto \frac{1}{L} \propto \frac{1}{\sqrt{\tau_{eff}}}$. This means that when τ_{eff} increases, J_0 decreases while J_{sc} increases, both leading to an increase in V_{oc}.

The FF may be approximated by the *ideal fill factor* FF_0, which is given by

$$FF_0 = \frac{v_{oc} - \ln(v_{oc} - 0.72)}{v_{oc} + 1}. \tag{2.45}$$

This is the value of FF if the shunt and series resistance effects are removed (Green, 2003). Here, $v_{oc} = \frac{q}{nk_BT} V_{oc}$ and n is the ideality factor. So even though FF is not directly dependent on τ_{eff}, its dependency on V_{oc} gives it a positive correlation with τ_{eff} too.

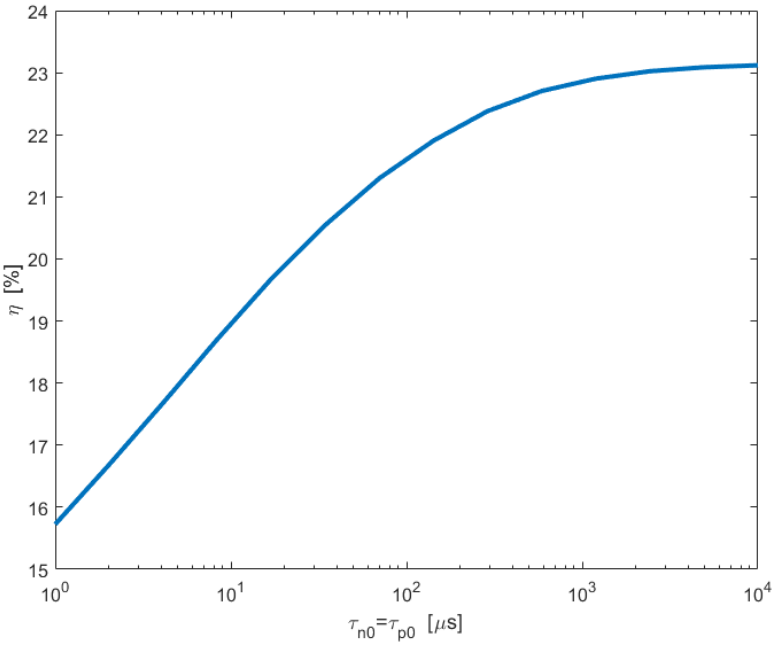

Figure 2.7: Efficiency of a solar cell as it changes with SRH recombination lifetime, based on a PC1D simulation. The cell model is an ideal cell, i.e. there is no surface recombination.

To illustrate the net effect of changing lifetime, a simulation has been made in PC1D in which the SRH lifetime is varied over 5 orders of magnitude, shown in **Figure 2.7**. The simulation was run with an ideal cell model, meaning the surface recombination was turned off.

As already mentioned, τ may increase with the compensation level of a material. This is mainly due to the change in bulk and surface SRH lifetimes. Let us consider a p-type material. The compensation level C_l may be changed by increasing N_d, and thus decreasing p_0. Considering equation (2.18) at a high injection level, so that we can neglect n_0, $\hat{p}$ and $\hat{n}$, we get

$$\tau_{SRH} \approx \frac{\tau_{p0}\Delta n + \tau_{n0}(p_0 + \Delta n)}{p_0 + \Delta n} \tag{2.46}$$

$$= \frac{\Delta n}{p_0 + \Delta n}\tau_{p0} + \tau_{n0}. \tag{2.47}$$

It is clear from inspection that τ_{SRH} decreases with p_0 in this case.

Looking at a low injection level, equation (2.18) becomes

$$\tau_{SRH} \approx \frac{\tau_{p0}(n_0 + \hat{n}) + \tau_{n0}(p_0 + \hat{p})}{p_0 + n_0} \tag{2.48}$$

$$\approx \tau_{p0}\frac{(n_0 + \hat{n})}{p_0} + \tau_{n0}(1 + \hat{p}/p_0), \tag{2.49}$$

where we have assumed $p_0 \gg n_0$ in the second line, implying a p-type material. Also in this case it is clear that τ_{SRH} decreases with p_0.

This means that τ_{SRH} decreases with the effective doping level $p_0 \approx N_A - N_D$ in a p-type material. Thus, if you increase the compensation level while keeping N_A constant, p_0 is reduced, and τ_{eff} is increased at injection levels where τ_{SRH} is a limiting lifetime component. This has been pointed out by others before (Dubois et al., 2008; MacDonald and Cuevas, 2011; Xiao et al., 2012a). However, if you want to make a compensated material with similar resistivity to an non-compensated one, the compensated material has to be doped more heavily (due to reduced mobility) (Berthod et al., 2016). This means that p_0 is usually larger in a compensated than a non-compensated material of similar resistivity, and the benefit of better τ_{SRH} is lost. Any benefit in the lifetime of a compensated material, with similar resistivity to an non-compensated material, thus has to be explained by another mechanism. Of course, you could argue that the main importance when comparing compensated and non-compensated Silicon is not their resistivity. For instance, it might be more fruitful to find the optimal resistivity of each material, and compare cells made of those. However, in the lack of a known optimal doping level, materials of similar resistivity has been chosen for comparison in this thesis.

Further, a beneficial impact of compensation on lifetime may be balanced out by a detrimental effect on mobility, as mentioned in section 2.3. Mobility is related to the diffusion coefficient D through the equation $D = \mu k_B T/q$. Thus, $L \propto \sqrt{\tau\mu}$, and there is a trade-off between increased lifetime and decreased mobility that has to be taken into account when doing compensation engineering (MacDonald and Cuevas, 2011). However, it has been noted that the mobility changes much less with compensation level than lifetime, and the net effect of compensation on L may well be positive (Xiao et al., 2012a, 2014).

2.8 Temperature Sensitivity

Solar modules are rated under standard testing conditions (STC), which is an incoming irradiance of $1000\,\mathrm{W\,m^{-2}}$ at $25\,^{\circ}\mathrm{C}$. However, it is well known that the module temperature under normal operating conditions are very often substantially higher than this, and often above $50\,^{\circ}\mathrm{C}$ (Rand et al., 2007). This means that the temperature sensitivity of the solar cells, measured by its temperature coefficients (TCs), is of major concern when trying to predict the field performance of modules.

The TC of parameter X at temperature T is defined as

$$TC_X(T) \equiv \frac{X(T) - X(25\,^{\circ}\mathrm{C})}{T - 25\,^{\circ}\mathrm{C}} \cdot \frac{100\%}{X(25^{\circ}\mathrm{C})}. \tag{2.50}$$

In the literature it is common to operate with a different definition, where the derivative $\frac{dX}{dT}$ is used instead of the relative difference $\frac{X(T)-X(25\,^{\circ}\mathrm{C})}{T-25\,^{\circ}\mathrm{C}}$, yielding

$$\beta_X(T) \equiv \frac{dX(T)}{dT} \cdot \frac{100\%}{X(25°\mathrm{C})}. \tag{2.51}$$

Because of noise, a β_X based on measurements often fluctuates a lot with T, and an average value over a range of temperatures has to be taken to get a useful value. If, however, the average of β_X over the temperatures between $25\,°\mathrm{C}$ and T is taken, you get TC_X. Also, when doing simulations, speed is of a major concern. If you use TC_X, in principle you only need to simulate two temperatures, because the values of X between $25\,°\mathrm{C}$ and T are not interesting. In the modeling part of this thesis, however, a small number of temperatures have been simulated, so as to assess the accuracy of the assumption of linearity. Therefore the definition expressed in equation (2.50) is deemed to be most suitable, and will be used in the remainder of this thesis.

2.8.1 Temperature Coefficient of the Minority Carrier Lifetime

The effective minority carrier lifetime τ_{eff} depends on temperature. The main cause of this temperature dependence is surface and bulk SRH recombination. The temperature dependence of $\tau_{SRH}(T)$ comes down to the temperature dependence of the capture time constants $\tau_{n0/p0}$ of electrons/holes, and the densities of defect state holes $\hat{p}(T)$ and electrons $\hat{n}(T)$. The defect state densities scale as $T^{3/2} \cdot e^{\frac{|E_t - E_i| - E_g}{k_B T}}$, where E_g is the band gap energy, E_i is the middle of the band gap, and E_t is the trap state energy level. This always scales positively with T. However, if $\hat{p}(T)$ is at least an order of magnitude smaller than the majority carrier concentration, it is the temperature dependence of $\tau_{n0/p0}(T)$ that dominates the expression for $\tau_{SRH}(T)$. Thus, which parameter dominates in the expression for $\tau_{SRH}(T)$ depends on the size of $\hat{p}$ (or $\hat{n}$), which depends on the energy level E_t of the defect trap state. Long story short, if it is a deep trap state, i.e. $|E_t - E_i|$ is small, $\hat{p}$ (or $\hat{n}$) is small, and it is the temperature dependence of $\tau_{n0/p0}(T)$ that dominates. $\tau_{n0/p0}(T) \propto T^{-0.5}$, giving it a negative T-dependency. If it is a shallow trap state, i.e. $|E_t - E_i|$ is big, it is the exponential term of the defect density that dominates, giving $\tau_{SRH}(T)$ a positive T-dependency.

If there are several defects, the total SRH lifetime is the inverse sum of the contributions from each defect. This means that a defect with small capture time constants may be more decisive to the total τ_{SRH} than one with large capture time constants. Thus the sign of the temperature dependency of the SRH lifetime depends on E_t, as well as τ_{n0} and τ_{p0}, of each defect.

As is clear, the temperature dependence of $\tau_{eff}(T)$ is not straightforward to derive. In the lifetime measurements presented in this thesis, however, the temperature dependence of $\tau_{SRH}(T)$ is positive, as will be seen in section 4.1.

2.8.2 Temperature Coefficient of the IV-Parameters

The IV-parameters open-circuit voltage V_{oc}, short-circuit current J_{sc} and fill factor FF all depend on temperature. While V_{oc} and FF decreases with T, J_{sc} actually increases with T. There are two important physical phenomena determining the temperature sensitivity

of solar cells: band gap narrowing (BGN) and thermal generation, the latter being the phenomenon that n_i increases with T. These phenomena affects the different IV-parameters in different ways, both due to optical and electrical effects, the extent to which will become clear in the following discussion.

Starting with the effect of BGN on J_{sc}; when the band gap is smaller, photons with lower energy than before may be absorbed. This causes a net increase in photo-generation, which directly leads to an increase in J_{sc}. Given that J_{sc} can be expressed as $J_{sc} = J_{Lg}G$, where the ideal current $J_{Lg} = qG$ is the total generated current (if all photons with $E > E_g$ contribute with one electron), and f_c is the collection fraction, the temperature dependence of J_{sc} may be expressed by

$$\frac{1}{J_{sc}}\frac{dJ_{sc}}{dT} = \frac{1}{J_{Lg}}\frac{dJ_{Lg}}{dE_g}\frac{dE_g}{dT} + \frac{1}{f_c}\frac{df_c}{dT}. \tag{2.52}$$

From this equation it is easy to see that BGN is important for determining $TC_{J_{sc}}$.

The temperature dependence of V_{oc} accounts for around 80% to 90% of the temperature dependence of η (Green, 2003). V_{oc} first of all depends on $n_i(T)$, and $n_i(T)$ depends on both T and BGN. Mathematically this may be described by considering the temperature dependence of the reverse saturation current J_0. According to equation (2.43);

$$V_{oc} = \frac{kT}{q}\ln\left(\frac{J_{sc}}{J_0}\right),$$

where we see that V_{oc} also depends on J_{sc}, which is weakly dependent on BGN. Further,

$$J_0 = \frac{qD}{Ln_{maj}} \cdot n_i^2,$$

where

$$n_i^2 = 4\left(\frac{2\pi k_B T}{h^2}\right)^3 (m_e^* m_h^*)^{3/2} e^{\frac{-E_g}{k_B T}} \tag{2.53}$$

$$\approx BT^3 e^{-E_{g0}/k_B T}, \tag{2.54}$$

is the intrinsic carrier density. Here $B = 4\left(\frac{2\pi k_B}{h^2}\right)^3 (m_e^* m_h^*)^{3/2}$ is independent of T, m_e^* and m_h^* are the effective masses of electrons and holes respectively, and E_{g0} is the linear extrapolation of the band gap at $T = 0\,\mathrm{K}$. This gives

$$J_0 = \frac{qD}{Ln_{maj}} BT^3 e^{-E_{g0}/k_B T} = B'T^3 e^{-E_{g0}/k_B T}. \tag{2.55}$$

Inserting this into (2.43) and molding a bit yields

$$V_{oc} = \frac{k_B T}{q}\left(\ln(J_{sc}) - \ln(B') - 3\ln(T) + \frac{E_{g0}}{k_B T}\right). \tag{2.56}$$

Taking the derivative with regards to T, and neglecting the temperature dependency of J_{sc}, we arrive at

$$\frac{1}{V_{oc}}\frac{dV_{oc}}{dT} = -\frac{1}{V_{oc}}\left[\frac{V_{g0}-V_{oc}}{T} + \gamma\frac{k_B}{q}\right], \tag{2.57}$$

where $V_{g0} = E_{g0}/q$, and the 3 in the second term of equation (2.56) has been replaced by γ. Dupré et al. showed that by introducing

$$\gamma = 1 - \frac{d\ln ERE_{oc}}{d\ln T} + \left(2\frac{d\ln E_g}{d\ln T} - \frac{d\ln J_{Lg}}{d\ln T}\right),$$

where ERE is the external radiative efficiency, you can account for the temperature sensitivity of the other mechanisms that determines V_{oc} (Dupré et al., 2015).

From equation (2.57) it is easy to see that the higher V_{oc} is, the smaller $\frac{dV_{oc}}{dT}$ is. This, and the fact that V_{oc} increases with τ_{eff}, means that the temperature sensitivity of V_{oc} decreases with τ_{eff}.

The fill factor FF is determined to a large degree by shunt resistance R_{sh} and series resistance R_s in the cell, as well as the ideality factor. The ideality factor is determined by the recombination lifetime in the emitter region, which is much lower than in the bulk of the cell. However, as was discussed in section 2.7, for most solar cells the most decisive value for FF is the V_{oc} (see equation (2.45)). It can be shown that

$$\frac{1}{FF}\frac{dFF}{dT} \approx (1-1.02FF_0)\left[\frac{1}{V_{oc}}\frac{dV_{oc}}{dT} - \frac{1}{T}\right] - \frac{R_s}{V_{oc}/J_{sc}-R_s}\left(\frac{1}{R_s}\frac{dR_s}{dT}\right), \tag{2.58}$$

if the shunt resistance, as well as the ideality factor of the cell, varies little with temperature (Dupré et al., 2015). From equation (2.58) it is easy to see that a decisive factor for the temperature dependence of the fill factor is the temperature dependence of V_{oc}.

2.8.3 Temperature Coefficients in Compensated Silicon

Recent studies have shown that the compensated Elkem Solar Silicon®(ESS) have beneficial traits compared to polysilicon in high temperature and high incoming irradiation (Tayyib et al., 2014a,b,c, 2013; Berthod et al., 2015; Søndenå et al., 2015). A difference in power yield between similarly rated modules with cells made of ESS and polysilicon of between 1% and 2% over a year has been shown (Tayyib et al., 2013, 2014a). This has been explained by a less negative TC_η in ESS-cells compared to that of polysilicon-cells. In other words, the effect of increasing the operating temperature is not as detrimental to ESS-cells as to standard polysilicon-cells.

One effect that could explain this is a higher density of BO-complexes in the B-rich compensated Silicon (F. Tanay, S. Dubois and Veirman, 2011). These defects act as recombination centers, effectively reducing the recombination lifetime. The hole capture cross-section of the BO-complexes has been shown to decrease with temperature. This means that an important limiting factor to the hole lifetime in ESS decreases with temperature. This is not the case in polysilicon, thus providing a possible explanation for the beneficial TCs of ESS. However, it has been argued that the oxygen content of ESS is not any higher than in typical polysilicon, in which case this explanation doesn't hold (Søndenå et al., 2015).

However, it has been shown that the benefit in TCs mostly happens in the wavelength region $800\,\mathrm{nm}$ - $1100\,\mathrm{nm}$ (Tayyib et al., 2014b; Søndenå et al., 2015). Since the absorption coefficients at these wavelengths are lower in Silicon (Green, 2008), it suggests that this is due to bulk effects, likely connected to recombination lifetime τ and mobility μ. The temperature sensitivity of the lifetime does not necessarily vary with compensation level. However, the high density of dopants in ESS means that at $25\,^{\circ}\mathrm{C}$, it has a lower μ than in polysilicon due to scattering by ionized impurities. But as the temperature increases the average thermal velocity of the charge carriers goes up, in effect making the scattering probability at the ionized impurities smaller, rendering this effect less important (Modanese et al., 2012). This results in a relative increase in μ of ESS compared to that of polysilicon as the temperature increases. This could serve to partly explain the improved temperature sensitivity of ESS.

On the other hand, V_{oc} has been shown to increase with p_0 (MacDonald and Cuevas, 2011). As was discussed in the previous section, the TCs of the IV-parameters are to a large degree linked with the magnitude of V_{oc}. Thus, if p_0 is raised, V_{oc} is raised, which results in smaller $TC_{V_{oc}}$ and TC_{FF}. Raising the compensation level is often done by increasing [P] in the feedstock, which serves to lower p_0. However, when doing compensation engineering it might be beneficial to increase both [B] and [P] in order to raise p_0. This has positive effects on V_{oc}, which results in smaller $TC_{V_{oc}}$ and TC_{FF}.

Another effect that might give a less negative $TC_{V_{oc}}$ and TC_{FF} in a compensated material is the effect of the lifetime itself. Since τ_{bulk} accounts for more than half the variance of the material parameters to the performance of a cell (Wasmer et al., 2017), the explanation may be that the magnitude of τ_{bulk} or TC_{τ} is what makes the big difference. As was discussed in section 2.7, a reduction in p_0 may lead to an increase in the SRH recombination lifetimes, and thus an increase in τ_{bulk}. Increasing τ_{bulk} leads to an increase in both V_{oc} and J_{sc} (MacDonald and Cuevas, 2011), which again leads to improved TCs. Further, it is fairly obvious that an increase in TC_{τ} would lead to an increase in $TC_{V_{oc}}$ and in $TC_{J_{sc}}$.

Previously, there has not been any research linking temperature dependent lifetime measurements to temperature dependent IV-measurements in compensated Silicon, as far as the literature study of this thesis goes. Therefore a big part of this thesis will focus on exactly this, also applying the comprehensive device simulation machinery that has been developed for this purpose. This will hopefully show to give a deepened understanding of the processes involved, contributing with novel knowledge to the field.

2.8.4 Literature Values

To get an idea of typical magnitudes of the TCs of solar cells, a literature study has been done. In **Table 2.1, 2.2, 2.3** and **2.4** values obtained in this study are presented. The cells have been marked with what material they are of, and which cell architecture has been used, since this plays a large role in determining the TCs. The materials are either electronic grade Silicon (EG-Si), Elkem Solar Silicon®(ESS), or other upgraded metallurgical grade Silicon materials (UMG-Si). In the comment section it is noted whether the material is monocrystalline/Czochralski (Cz) or multicrystalline (multi), if this is not already implicitly stated. Also, the cell measured by (Berthod et al., 2016) are based on the same ingots as was used in this thesis, and to emphasize this they are written in bold type. The

values measured by (Zhao et al., 1994) are old and not in the range of the others. These should be taken lightly. If the material is multicrystalline EG-Si, which is the industry standard today, it has been marked with polysilicon. The polysilicon material of (Berthod et al., 2016) had a certain blend-in ratio of silicon produced with a fluidized bed reactor (FBR), and is marked with FBR

Table 2.1: Literature values of temperature coefficient of V_{oc} at 1 sun ($1000\,\mathrm{W/m^2}$).

Material	Cell arch.	Comment	$\beta_{V_{oc}}$ [%/K]	Reference
ESS	**PERC**	**multi**	$\mathbf{-0.31 \pm 0.01}$	**(Berthod et al., 2016)**
ESS	Al-BSF	multi	-0.329	(Tayyib et al., 2014a)
polysilicon	**PERC**	**FBR**	$\mathbf{-0.32 \pm 0.01}$	**(Berthod et al., 2016)**
polysilicon	Al-BSF		-0.334	(Tayyib et al., 2014a)
polysilicon	PERC		-0.268	(Zhao et al., 1994)
EG-Si	Al-BSF	Cz	-0.353 ± 0.003	(Ponce-Alcántara et al., 2014)
polysilicon	Al-BSF		-0.336 ± 0.005	(Ponce-Alcántara et al., 2014)
UMG-Si	Al-BSF	Cz	-0.359 ± 0.009	(Ponce-Alcántara et al., 2014)
UMG-Si	Al-BSF	multi	-0.348 ± 0.009	(Ponce-Alcántara et al., 2014)

Table 2.2: Literature values of temperature coefficient of J_{sc} at 1 sun ($1000\,\mathrm{W/m^2}$).

Material	Cell arch.	Comment	$\beta_{J_{sc}}$ [%/K]	Reference
ESS	**PERC**	**multi**	$\mathbf{0.06 \pm 0.02}$	**(Berthod et al., 2016)**
ESS	Al-BSF	multi	0.062	(Tayyib et al., 2014a)
polysilicon	**PERC**	**FBR**	$\mathbf{0.055 \pm 0.01}$	**(Berthod et al., 2016)**
polysilicon	Al-BSF		0.048	(Tayyib et al., 2014a)
polysilicon	PERC		0.071	(Zhao et al., 1994)
EG-Si	Al-BSF	Cz	0.028 ± 0.006	(Ponce-Alcántara et al., 2014)
polysilicon	Al-BSF		0.040 ± 0.008	(Ponce-Alcántara et al., 2014)
UMG-Si	Al-BSF	Cz	0.050 ± 0.014	(Ponce-Alcántara et al., 2014)
UMG-Si	Al-BSF	multi	0.070 ± 0.008	(Ponce-Alcántara et al., 2014)

Table 2.3: Literature values of temperature coefficient of FF at 1 sun ($1000\,\mathrm{W/m^2}$).

Material	Cell arch.	Comment	β_{FF} [%/K]	Reference
ESS	**PERC**	**multi**	$\mathbf{-0.13 \pm 0.01}$	**(Berthod et al., 2016)**
ESS	Al-BSF	multi	-0.124	(Tayyib et al., 2014a)
polysilicon	**PERC**	**FBR**	$\mathbf{-0.145 \pm 0.01}$	**(Berthod et al., 2016)**
polysilicon	Al-BSF		-0.140	(Tayyib et al., 2014a)
polysilicon	PERC		-0.123	(Zhao et al., 1994)
EG-Si	Al-BSF	Cz	-0.147 ± 0.006	(Ponce-Alcántara et al., 2014)
polysilicon	Al-BSF		-0.141 ± 0.015	(Ponce-Alcántara et al., 2014)
UMG-Si	Al-BSF	Cz	-0.139 ± 0.01	(Ponce-Alcántara et al., 2014)
UMG-Si	Al-BSF	multi	-0.134 ± 0.013	(Ponce-Alcántara et al., 2014)

Table 2.4: Literature values of temperature coefficient of η at 1 sun ($1000\,\mathrm{W/m^2}$).

Material	Cell arch.	Comment	β_{η} [%/K]	Reference
ESS	**PERC**	**multi**	$\mathbf{-0.38 \pm 0.04}$	**(Berthod et al., 2016)**
ESS	Al-BSF	multi	-0.384	(Tayyib et al., 2014a)
polysilicon	**PERC**	**FBR**	$\mathbf{-0.42 \pm 0.02}$	**(Berthod et al., 2016)**
polysilicon	Al-BSF		-0.413	(Tayyib et al., 2014a)
EG-Si	PERC	Cz	-0.319	(Zhao et al., 1994)
EG-Si	Al-BSF	Cz	-0.47 ± 0.02	(Ponce-Alcántara et al., 2014)
polysilicon	Al-BSF		-0.43 ± 0.03	(Ponce-Alcántara et al., 2014)
UMG-Si	Al-BSF	Cz	-0.43 ± 0.03	(Ponce-Alcántara et al., 2014)
UMG-Si	Al-BSF	multi	-0.42 ± 0.02	(Ponce-Alcántara et al., 2014)

Chapter 3

Experiments and Modeling

This chapter is divided into three parts. The first part is a description of the samples. Then comes a description of the measurements that were done on these samples, and lastly a description of the modeling that was performed and how the modeling results were compared to the measurement results.

3.1 Samples

Wafers and cells made from three different p-type Silicon ingots were used in this thesis. Two of the ingots were based on Elkem Solar Silicon®(ESS), while the third was based on polysilicon, the role of which was being a reference to compare the ESS samples with. However, a certain mix-in ratio of the polysilicon reference was made in a fluidized bed reactor, which is an alternative, cheaper method of producing polysilicon. Thus we are comparing ESS to another second rate Silicon material. The ingots were casted at REC, Singapore. Each ingot had a target resistivity, as listed in **Table 3.1**. The resistivity is determined by the effective doping level of the material, so the ESS ingot with a resistivity ρ at $0.5\,\Omega\mathrm{cm}$ is more heavily doped than those with $\rho \sim 1.3\,\Omega\mathrm{cm}$.

Table 3.1: Ingots used in this thesis.

Alias	Material type	Resistivity [$\Omega\,\mathrm{cm}$]	C_l	p_0 [$10^{16}\,\mathrm{cm}^{-3}$]
ESS 0.5	ESS	0.5	1.3-1.9	3.6-4.4
ESS 1.3	ESS	1.3	2.0-4.8	~ 1.3
REF 1.3	polysilicon	1.3	1.0	0.95-1.3

The doping levels as they vary with height in the ingots has been determined using Scheil's equation (2.1) with initial ingot doping levels from the manufacturer. A plot of the estimated doping levels is shown in **Figure 3.1**.

The ingots were processed as if they were going into solar cell production. After a top and a bottom cut, the ingots were cut into $\sim 190\,\mu\mathrm{m}$ thick wafers. Of these, a selection of

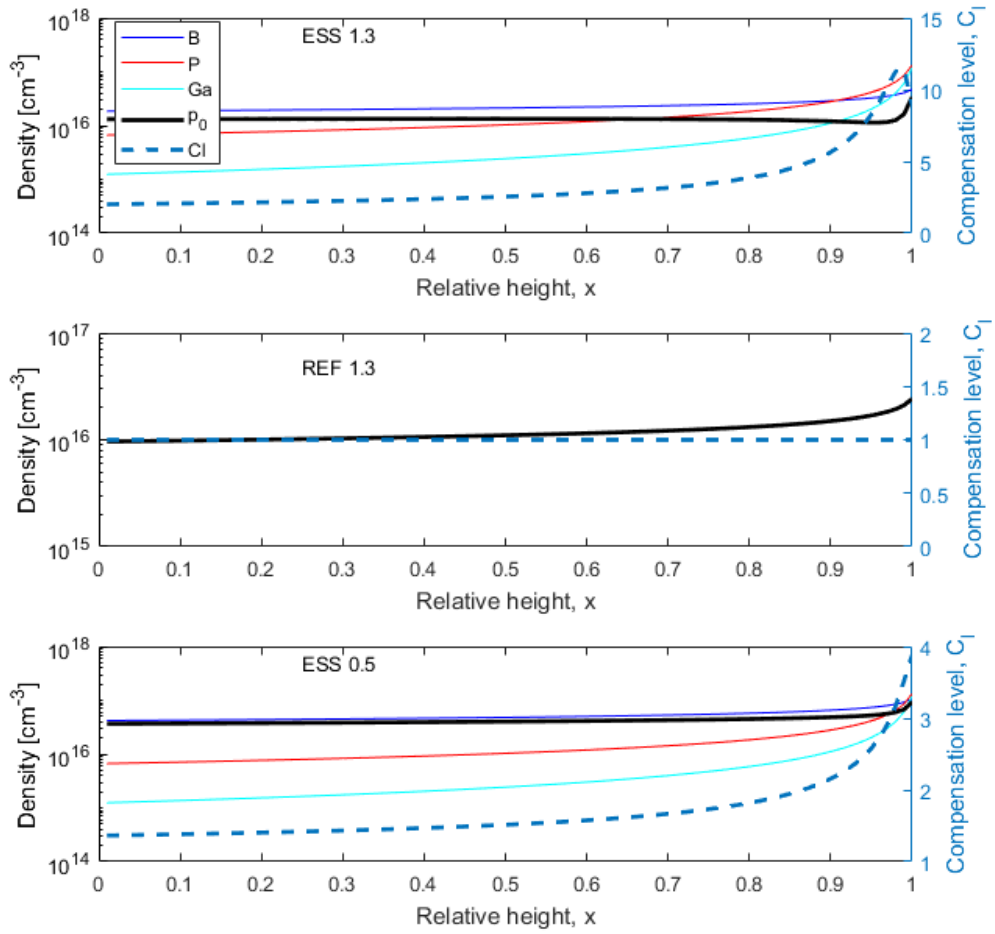

Figure 3.1: Doping levels of the ingots listed in **Table 3.1**, as estimated from Scheil's equation, (2.1). Incomplete inoization has been neglected in this plot. The top 5% and bottom $\sim 11\%$ of the ingots were removed before being cut into wafers.

wafers from different ingot positions were used for the measurements in this thesis. Some of them were taken to Institute of Energy Technology (IFE) in Kjeller to be prepared for lifetime measurements, and some were sent to ISC Konstanz to be made into cells.

The wafers that were prepared for lifetime measurements were, by employees at IFE, taken through the solar cell production processes necessary to make a solar cell, except contacting. Thus the wafers resembled the bulk of the corresponding cells as much as possible. Firstly the wafers were etched in a 2:10:5 HF:HNO_3:CH_3COOH solution (dubbed

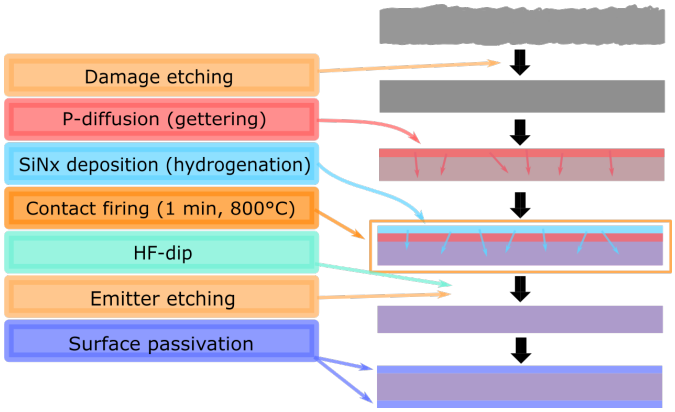

Figure 3.2: The sample preparation steps.

CP5), in order to clean the wafers and remove any damages on the surface. The wafers were then Phosphorous diffused, so as to create the emitter region. This also leads to gettering of impurities, so even though the emitter is etched away in the 6th step, this is an important step. Then an anti-reflection coating (ARC) of SiN_x was deposited on the wafers, and they were fired for 1 min in $800\,^{\circ}C$ (to simulate contact firing). This leads to hydrogenation. The ARC was then removed by dipping in a HF-solution. Lastly all wafers were emitter etched with CP5, and subsequently surface passivated with amorphous Silicon. Thus the samples were Phosphorous diffusion gettered and hydrogenated (PDG-H) wafers (Antonio Luque, 2011).

The wafers that were sent to ISC Konstanz, on the other hand, were made into Passivated Emitter Rear Contact (PERC) cells by employees there. PERC cells are expected to take over as the main industrial cell type in the near future, replacing the conventional Aluminum Back Surface Field (Al-BSF) cell (Min et al., 2017). Ideally, a monocrystalline PERC cell is expected to work with an efficiency of $\sim 19-21\%$, but this demands a finely tuned production process. The best PERC cells used for IV-measurements in this thesis performed at $\sim 18.2\,\%$ at standard testing conditions.

3.2 Measurements

3.2.1 PL-I Measurements

Prior to the QssPC measurements recorded in the next section, a BT Imaging LS-R1 Photoluminescence-imaging (PL-I) instrument was used by employees at IFE to take PL-images of the wafers. The images show the effective lifetime as it varies over the wafers. Thus the areas of the wafers containing high and low densities of defects are mapped. These images were in turn used to determine the optimal position to do QssPC measurements, as will be discussed in the next section. **Figure 3.3** shows the PL-images.

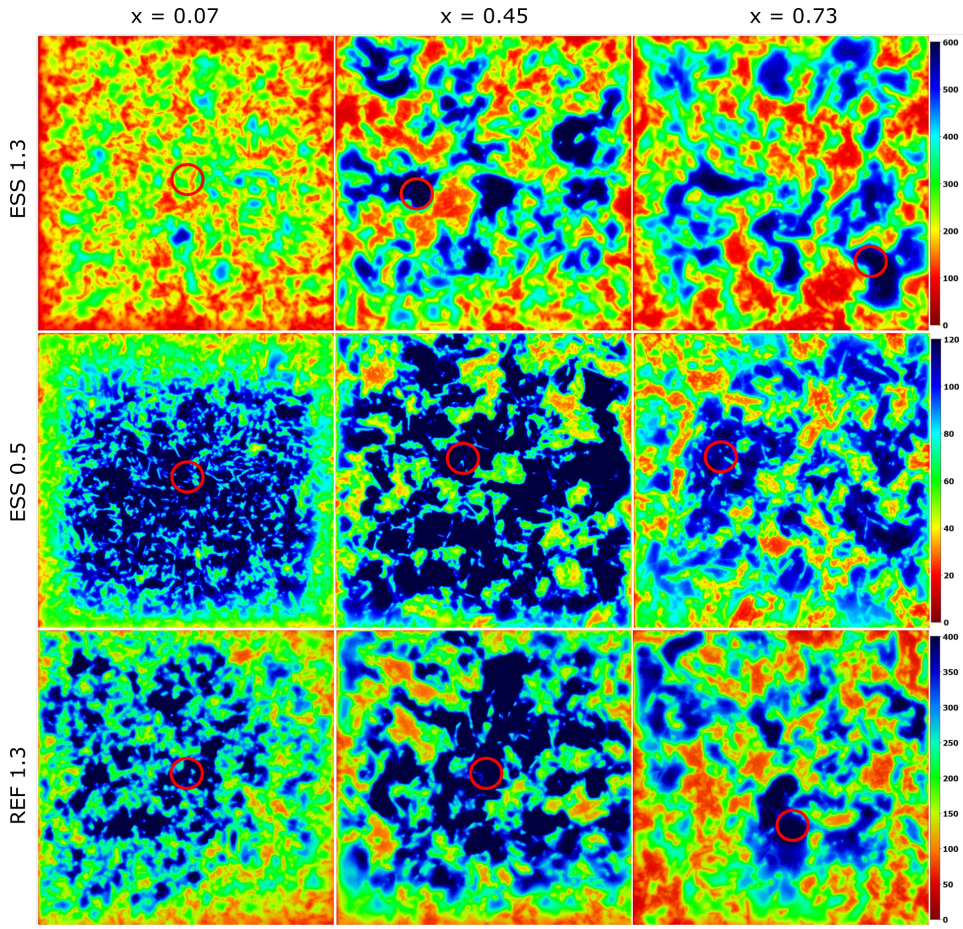

Figure 3.3: Photoluminescence-images of the wafers on which the quasi-steady state photoconductance (QssPC) measurements were done. The location of the inducing coil during the QssPC-measurements is marked with a red circle. Generally the QssPC instrument measures the lifetime in a donut-shaped region surrounding the coil. The color scale is the same for each row.

3.2.2 QssPC Measurements

Using a Sinton Instruments WCT-120TS quasi-steady state photoconductance-instrument (QssPC) with an integrated hotplate (see **Figure 3.5**), the bulk minority carrier lifetime τ_{bulk} as a function of injection level and temperature could be measured on the wafers. 9 wafers were picked out from three different positions (low, middle and high) in the three different ingots, corresponding to the ingot positions of the cells that was measured (as described in section 3.2.3). The temperature was varied between 25 °C and 130 °C and a measurement was taken at each 5 °C-step. An example of a single-temperature QssPC-measurement is shown in **Figure 3.4**.

As can be seen, the lifetime of this particular sample varies by a factor of more than

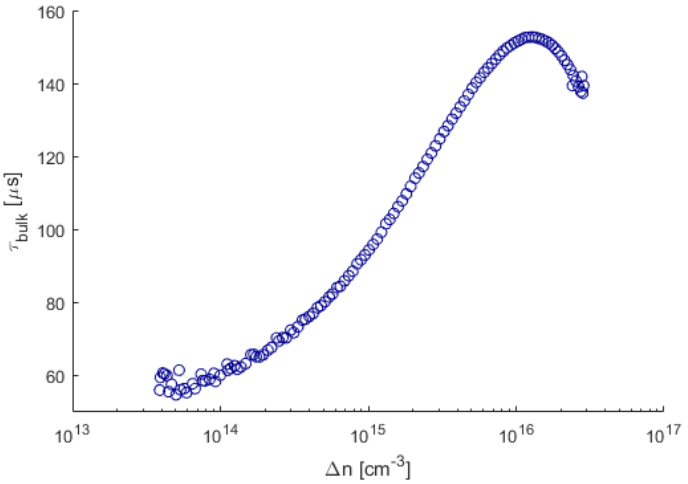

Figure 3.4: A QssPC-measurement of bulk lifetime τ_{bulk} as a function of injection level Δn.

2.5 within the range of injection levels, peaking at just above $\Delta n = 1 \times 10^{16}\,\mathrm{cm}^{-}3$. The noise in the data-points at low injection levels is a result of the low signal strength when the number of excess carriers is low. The amount of noise depends both on the material quality, and the mode of the QssPC measurement. After advice from Sinton Instruments, the measurements performed in this thesis were made with the general mode with a short flash when the lifetime was above $100\,\mu\mathrm{s}$, and a long flash when it was below. The results are presented in section 4.1.

Further, the QssPC tool can only measure a small section of a wafer at a time (the measuring coil has a diameter of $\sim 16.5\,\mathrm{mm}$), and a randomly placed measurement is not necessarily representative of the whole wafer. The defects are usually smaller and more dispersed in the lower part of an ingot, and become bigger and more localized as you go higher in the ingot (Sio et al., 2017). This can be seen in **Figure 3.3**. Although the areas with few defects might not be representative for the lifetime of the whole wafer, it was important to get QssPC measurements with as little noise as possible. Thus the measurements were done on large, high lifetime grains wherever possible. Still, as will be seen in section 4.1, there is generally a lot of noise in the lifetime measurements of this thesis.

3.2.3 IV-Measurements

A Wavelabs SINUS-220 LED solar simulator (shown in **Figure 3.5**) was used to do IV-measurements on 10 PERC cells made at ISC Konstanz. There was not enough time to measure a large amount of cells, so a choice as to which cells would be more relevant had to be made. In the end the decision was made to measure cells from four different positions in the ESS and the polysilicon reference ingot with a resistivity (ρ) of $1.3\,\Omega\mathrm{cm}$. These ingots are deemed to be comparable since they have an equal target resistivity. Also

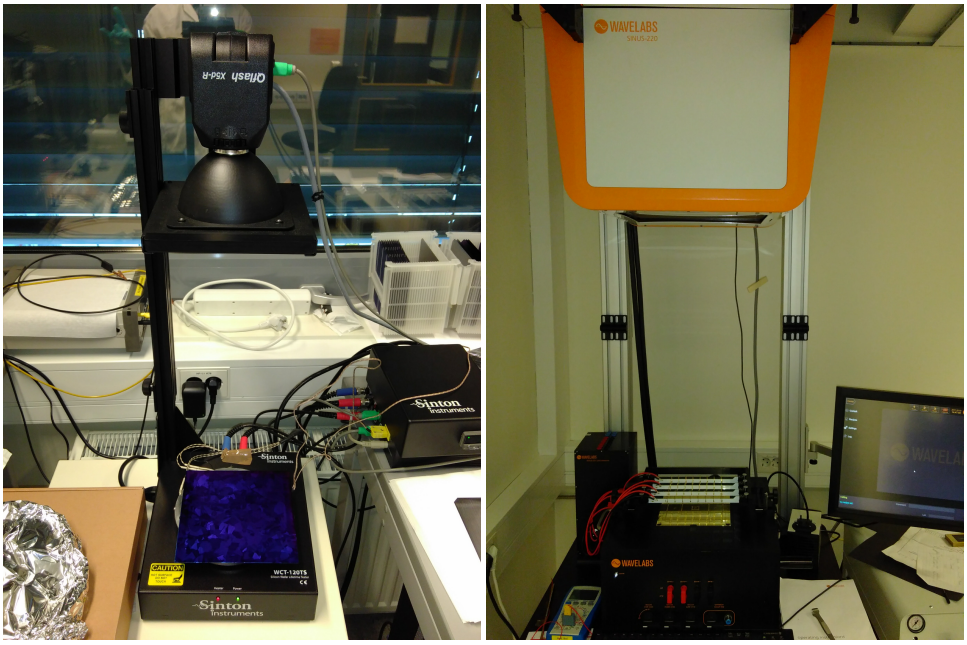

Figure 3.5: The left image shows the Sinton WCT-120TS QssPC instrument used to do minority carrier lifetime measurements, while the right image shows the Wavelabs SINUS-220 LED solar simulator used to do IV-measurements in this thesis. A sample wafer is placed on the QssPC instrument.

two cells from the ESS material with $\rho = 0.5\,\Omega\mathrm{cm}$ were chosen, so as to see the relative impact of high doping levels.

The solar simulator that was used has a hot-plate, making it possible to do measurements on cells of varying temperature. The temperature was raised from $25\,^{\circ}\mathrm{C}$ to $80\,^{\circ}\mathrm{C}$, and a measurement was done on every 5th degree. In this way the response in the cell-parameters to changing temperatures could be measured. The temperature was then lowered to $25\,^{\circ}\mathrm{C}$ again, and a measurement was done at $25\,^{\circ}\mathrm{C}$ to confirm that no change had happened either in the cell or in the solar simulator. The results, including temperature dependent IV-parameters (V_{oc}, J_{sc}, FF and η), and temperature coefficients (TCs) of these parameters, are presented in section 4.2.

3.3 Modeling

The goals of the modeling part in this thesis are:

1. to relate temperature dependent lifetime measurements to solar cell measurements,

2. to make a realistic model for the PERC cells that are measured,

3. to do a sensitivity analysis of the material parameters on the IV-parameters of a PERC cell

In order to achieve this, two PC1D-models have been developed. The first one is a PERC-model, in which the cell parameters have as much as possible been adapted to fit with the measurements of the PERC cells at hand. The second one is an ideal model, in which the series and shunt resistances have been turned off, there is no internal diode, and the front and back surface recombination has been turned off. The motivation of creating the ideal model is to reduce the loss mechanisms so as to magnify the effects of changing the material parameters. Thus the PERC-model will first be assessed by comparison to the measurements, possibly validating the accuracy of the model. If it turns out to be a good model, it can be used to analyze the response to changing material parameters in the measured PERC cells. The ideal model, on the other hand, can be used to analyze the 'ultimate' response to changes in the material parameters. If no significant response is observed in the ideal cell-model when changing one material parameter, you can usually expect an even smaller response in the PERC-model.

The models were developed in cooperation with IFE employees. The Matlab-code that was used to run the models and produce the results was built on scripts written by IFE employees, but the vast amount of coding was done by me.

A summary of the model parameters can be seen in **Table 3.2**.

Table 3.2: Cell parameters of the two cell-models used in this thesis. If there is a - sign, the parameter is not relevant.

Parameter [unit]	PERC	Ideal
Background doping type	p	p
Cell thickness [µm]	190	180
Device area [cm^2]	243.3	243.3
Front shading [%]	9.2	5
Front surface texture depth [µm]	3	3
Front surface charge [cm^{-2}]	$1 \cdot 10^{12}$	-
Front diffusion peak density [cm^{-3}]	$2 \cdot 10^{20}$ (ecv)	$1 \cdot 10^{20}$ (gaussian)
Front diffusion depth [µm]	0.45	0.4
Lifetime in depletion region [µs]	1	τ_{bulk}
Series resistance [Ω]	$2.1 \cdot 10^{-3}$	0
Shunt resistance [Ω]	9	-
Internal diode [A]	$1 \cdot 10^{-4}$	-
Front surface recomb., s_n [cm/s]	$1 \cdot 10^7$	0
Front surface recomb., s_p [cm/s]	$8 \cdot 10^5$	0
Back surface recomb., $s_n = s_p$ [cm/s]	$100 \cdot \frac{p_0}{1.32 \cdot 10^{16}}$	0

The PERC-model may be said to resemble industry standard cells, although the performance probably is in the low end of the scale. Thus the sensitivity to temperature found by the simulations of this model is assumed to represent the reality of similarly rated cells. The ideal cell-model, however, may be closer to laboratory record cells. Although 0 surface recombination will never be achieved, the ideal cell represents, as its name indicates,

the 'ideal' which the industry is working towards. Thus the knowledge acquired from the simulations of the ideal cell may be closer to the truth of future cells, whether they are PERC or of a completely different cell architecture.

In order to simulate solar cells with temperature and injection dependent lifetime values, as well as the accurate compensation levels, a modified version of cmd-PC1D 6.2 has been utilized (Haug and Greulich, 2016). In this version of PC1D it is possible to implement injection dependent SRH-lifetime data, as well as setting the bulk levels of Boron, Gallium and Phosphorous for each simulation. The program interpolates between the different lifetime-data points and use this, together with a calculation of the intrinsic lifetime values, as input to the bulk lifetime τ_{bulk}. Doing this for a set of temperatures it is possible to get temperature dependent simulations of solar cells with injection and temperature dependent SRH lifetimes.

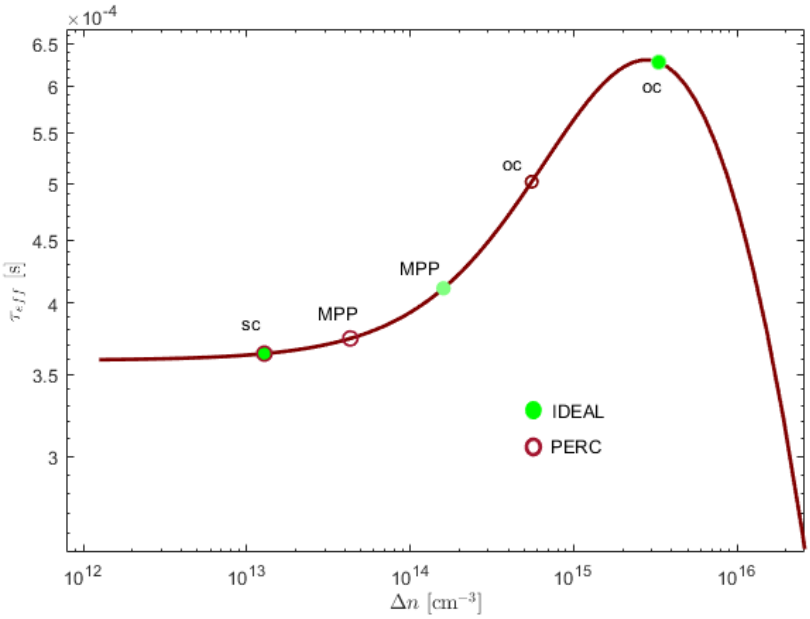

Figure 3.6: The short circuit (sc) point, maximum power point (MPP) and open circuit (oc) point on the $\tau_{eff}(\Delta n)$-curve in the ideal cell- and PERC-model. τ_{eff} is the effective lifetime and Δn is the injection level.

Due to the large amount of noise in the lifetime measurements it is not straightforward to implement the measured lifetimes in the software. Further, since short-circuit operation of a solar cell corresponds to low injection levels (often below $\Delta n \sim 1 \times 10^{13}\,\mathrm{cm}^{-3}$), in order to simulate the whole IV-curve you need lifetime values at injection levels below what could be measured. To solve these two problems a fitting algorithm was applied. This algorithm, developed by IFE employees, uses the τ_{bulk}-measurements of the QssPC tool and subtracts the intrinsic recombination lifetime (see section 2.4.1) to get τ_{SRH}. As was mentioned in section 2.4.2, temperature- and injection-dependent lifetime

spectroscopy (TIDLS) gives a framework for mapping the defects of a material by using lifetime measurements. In this thesis, however, we are not interested in k and E_t of each defect. Instead we are merely looking for a fit for the measured τ_{SRH}-curves by A and B in equation (2.20), so as to get analytical representations of the measured SRH recombination lifetimes. Thus, at each temperature, the measured τ_{SRH}-data are fitted to two defects to give analytical τ_{SRH}-curves. The new τ_{SRH}-curves, which are naturally smooth and cover all injection levels, are then used in the PC1D-simulations.

A plot of such an analytical lifetime-curve is shown in **Figure 3.6**. Also, the short circuit (sc) point, maximum power point (MPP) and open circuit (oc) point of the ideal cell- and PERC-model have been drawn in. This shows that the operating point is at higher injection levels in the ideal model, and that this affects the lifetime of the charge carriers.

The effect of p_0 on the surface recombination velocities (SRVs) has to be taken into account. This is discussed in section 2.4.3, where it is stated that the SRVs scale linearly with p_0 at low doping levels. Assuming this approximation to be good enough for high doping levels too, the back SRV was tuned linearly with p_0 in the PERC-model. The least doped and the most doped ESS-cells were used as reference points for this, and the SRVs of the other cells were scaled accordingly.

Another factor that had to be taken into account is the fact that the short circuit current J_{sc} of a solar cell increases with temperature. As mentioned in section 2.8.2, the increase in J_{sc} with T is due to the optical effect of band gap narrowing (BGN). This effect is not included in the original version of PC1D. Thus, in order for the PC1D-model to predict a correct behavior in J_{sc}, the optical effect of BGN had to be implemented. This is most easily done by introducing a temperature dependent absorption coefficient. Data from (Green, 2008; Nguyen et al., 2014) was used and implemented in all simulations.

Chapter 4

Results and Discussion

The order in which the results are presented is intended to be from the most fundamental to the most derived. Thus, the measurements of the bulk minority carrier lifetime τ_{bulk} is presented in section 4.1. The lifetimes of these wafers is an indicator of the material quality, and of the expected performance of cells based on this material. Therefore the next section deals with temperature dependent IV-measurements of the PERC cells made of neighbouring wafers of the lifetime-samples. In order to say anything about exactly what mechanisms have caused the differences in performance of the cells, a modeling framework has to be applied, in which the different material parameters may be changed independently, and their impact on the IV-parameters can be assessed. This framework was described in section 3.3, and is presented in section 4.3. In section 4.4 the results of the previous sections will be compared and discussed, in order to approach a holistic understanding of the phenomena deciding the TCs of solar cells.

4.1 Lifetime Measurement Results

Using the QssPC method, bulk minority carrier lifetimes τ_{bulk} of the wafers described in section 3.1 could be measured. The results are presented according to relative height x in the ingots, starting at $x = 0.07$ in **Figure 4.1**, $x = 0.45$ in **Figure 4.2** and $x = 0.73$ in **Figure 4.3**.

As can be seen, for all three heights τ_{bulk} is highest in ESS 1.3 (meaning the wafers made of ESS material with a target resistivity $\rho = 1.3\,\Omega\mathrm{cm}$), and lowest in ESS 0.5, although the lifetime of ESS 1.3 and REF 1.3 (the polysilicon reference) completely overlap at $x = 0.07$. Further, τ_{bulk} increases with x in all materials when going from $x = 0.07$ to $x = 0.45$, but only in ESS 1.3 (with any considerable magnitude) when going from $x = 0.45$ to $x = 0.73$.

The relative magnitude of τ_{bulk} in the different samples may be attributed partly to their doping levels. Since both the effective doping level $p_0 = N_A - N_D$ and compensation level $C_l = (N_A + N_D)/p_0$ changes from sample to sample, it is hard to isolate the effect of each parameter. It has been pointed out, however, that decreasing p_0 has a positive impact

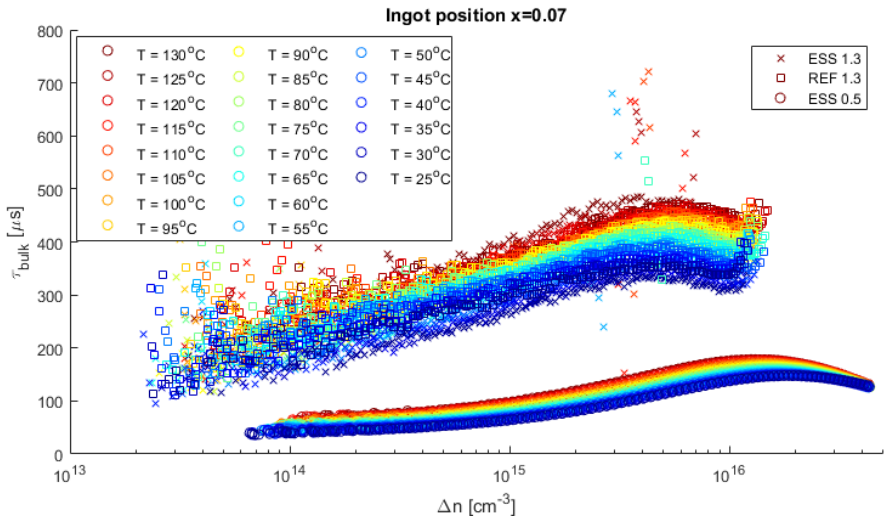

Figure 4.1: Bulk minority carrier lifetimes as a function of injection level Δn and temperature T at ingot position $x = 0.07$ in ESS 1.3 (crosses), REF 1.3 (squares) and ESS 0.5 (circles). The lifetime of ESS1.3 and REF 1.3 overlap.

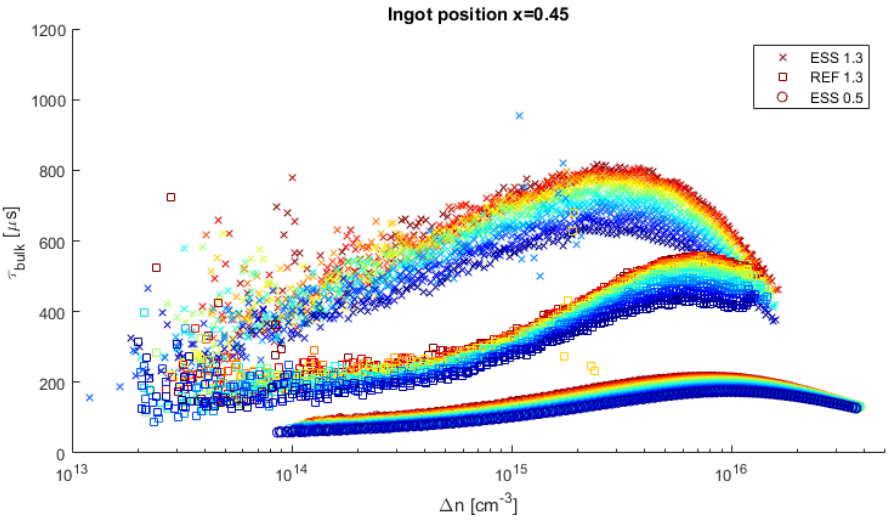

Figure 4.2: Bulk minority carrier lifetimes as a function of injection level Δn and temperature T at ingot position $x = 0.45$. The color legend is the same as in **Figure 4.1**.

on lifetime due to the reduced recombination strength of recombination centres when the density of carriers is low (Dubois et al., 2008). This holds if the acceptor density N_A is kept constant, and p_0 is decreased by increasing N_D. What happens if p_0 is decreased by increasing both N_A and N_D, but increasing the latter the most, is not as straightforward.

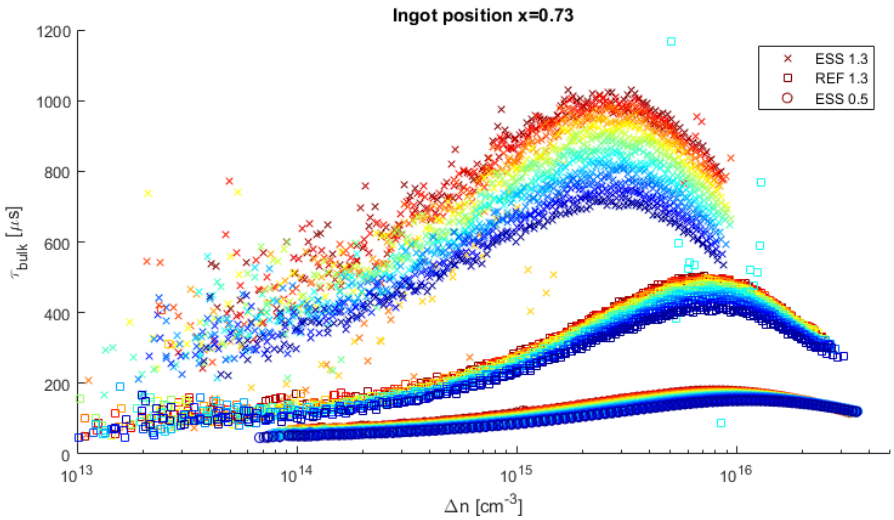

Figure 4.3: Bulk minority carrier lifetimes as a function of injection level Δn and temperature T at ingot position $x = 0.73$. The color legend is the same as in **Figure 4.1**.

These measurements show that τ_{bulk} may be higher in a material with a higher p_0 (as it is in ESS 1.3 relative to REF 1.3).

Of course, there may be several reasons why τ_{bulk} is higher in ESS 1.3 than in REF 1.3 other than a different p_0. After all, the difference in p_0 between these two materials is inconsiderable at low x. As we will come back to, the two ingots are (necessarily) of different feedstocks, and there may be impurities and defects present in the reference material that are not present in ESS which may explain the difference.

When comparing the lifetime of the differently doped ESS materials, however, ESS 0.5 is considerably lower than ESS 1.3. Since the two ESS-materials are expected to contain roughly the same impurities, the relatively low lifetime of ESS 0.5 is likely due to its high doping levels. In specific, ESS 0.5 has a higher p_0 than ESS 1.3 (which is what gives it the low resistivity). This fits well with the expected theoretical relationship between p_0 and τ.

Something else that comes into play is the fact that the wafers are not homogeneous. As is discussed in section 3.2.2, in order to get as little noise as possible, areas with low defect densities, and thus relatively high lifetimes, were picked out for the QssPC measurements. This means the measurement areas are not necessarily, or even necessarily not, representative of the whole wafers. As can be seen in the PL-images (**Figure 3.3**), the grain sizes, as well as the difference in lifetime between good and bad grains, increase with x. This means that at low x, the measurements have been performed over both good and bad areas, giving an average value which presumable represents the average over the whole wafer. At higher x, however, the measurements have been performed on large, high lifetime grains, and the measured lifetimes are higher than the average lifetimes of the wafers. This has to be accounted for when discussing the magnitude of the measured lifetimes in the remainder of the thesis.

It may be argued that doing the measurements on more representative areas of the

wafers, or scaling them by the harmonic average over the wafers, would be more interesting. This would permit a more consistent discussion when comparing to IV-measurements of corresponding cells. However, the maximum value of τ_{bulk} of a wafer is interesting in and of itself, since it tells you something about the quality of the feedstock in the absence grain boundaries. The effects of grain boundaries and dislocations are not trivial (and not one-dimensional), and difficult to account for. Thus, some information is lost either way, but as long as this disclaimer about the magnitude of τ_{bulk} is kept in mind, and the results are discussed in light of this, it is acceptable.

Note also that τ_{bulk} increases with temperature at all injection levels in all cases (except at high injection levels and high x in ESS 0.5), but it increases the most in ESS 1.3. This is not to say that the temperature coefficient of the bulk lifetime, $TC_{\tau_{bulk}}$, is much higher in ESS 1.3 than in the other blocks, since $TC_{\tau_{bulk}}$ is normalized by the absolute value of τ_{bulk} (see equation (2.50)).

In the remainder of the thesis, $TC_{\tau_{bulk}}$ will be written simply as TC_τ.

One point to note about these measurements is that it is implicitly assumed that surface recombination is negligible. This assumption may be defended by pointing to the excellent passivation properties of amorphous Silicon. The same passivation technique has been shown to permit effective lifetimes in the millisecond range in the same laboratory using the same process as in this work. This suggests the surface recombination velocities are below $5\,\mathrm{cm/s}$, in which case the choice of neglecting them is warranted.

4.1.1 Temperature Coefficient of the Lifetime

As is clear from **Figure 4.4**, $TC_\tau(75\,^\circ\mathrm{C})$ is almost independent of injection level Δn, except for in ESS 0.5, where it decreases with Δn from $\Delta n \sim 2 \times 10^{15}\,\mathrm{cm}^{-3}$. ESS 0.5 has the highest TC_τ at low and middle ingot positions. Also, TC_τ of REF 1.3 is on par with that of ESS 1.3 in the low and middle part of the ingot. Even though ESS 1.3 seems to be slightly higher at $x = 0.07$, and REF 1.3 seems to be slightly higher in $x = 0.45$, their values lie within the uncertainties of each other, and no statement can be made as to which one is higher at these positions. However, TC_τ of ESS 1.3 is considerably higher at $x = 0.73$. This goes for all injection levels.

As was discussed in section 2.8.1, the temperature dependence of the lifetime depends on the defect; it can be either negative or positive, depending on the position of the defect energy level relative to the band gap edges. Since ESS and the reference material are of different feedstock, they naturally contain different impurities. This explains the difference in TC_τ between ESS 1.3 and REF 1.3.

When it comes to ESS 0.5, its TC_τ is considerably higher than those of ESS 1.3 and REF 1.3 in the low and middle part of the ingot, and comparable to ESS 1.3 high in the ingot. The main difference between ESS 1.3 and ESS 0.5 is a larger effective doping level p_0 and a smaller compensation level C_l in the latter. This either suggests a beneficial effect of p_0 or a detrimental effect of C_l on TC_τ. The lifetime is negatively correlated with p_0. Thus it is natural to assume that TC_τ is positively correlated with p_0. However, since TC_τ is normalized by τ_{bulk} (see equation (2.50)), a lower TC may be explained by a higher lifetime. This means that the high TC_τ in ESS 0.5 may be due to its low τ_{bulk}. Thus a correlation between TC_τ and p_0 may be indirectly caused by the phenomenon that $\tau bulk$ decreases with p_0.

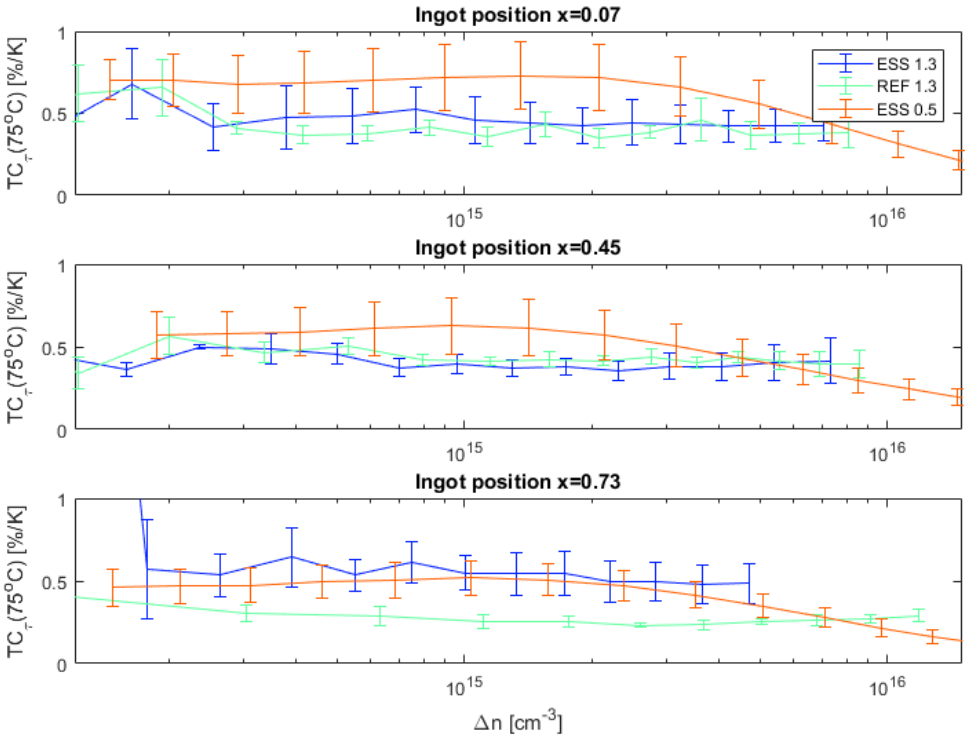

Figure 4.4: The temperature coefficients $TC_\tau(75\,^\circ\mathrm{C})$ of the lifetimes of ESS 1.3, REF 1.3 and ESS 0.5 at three different ingot positions, calculated from the QssPC-lifetime measurements. Each data point is an average over its surrounding Δn. Further, at each point, $TC_\tau(75\,^\circ\mathrm{C})$ has been estimated as the mean of $TC_\tau(T)$ when T goes from 70 °C to 80 °C, and the error bars correspond to the standard deviation of these.

The compensation level C_l is two to five times higher in ESS 1.3 than in the other materials (as can be seen in **Table 3.1**). The difference in C_l increases with x, which seems to correlate with a benefit in TC_τ. Thus there might be a positive correlation between TC_τ and C_l.

All in all, TC_τ might depend on both C_l and p_0, as well as feedstock quality. No definitive conclusion as to the correlation can be made at this point. In the remainder of the thesis, the effect of C_l and p_0 on τ and TC_τ will not be investigated further, but the independent impact of C_l, p_0, τ and TC_τ (the material parameters) on V_{oc} and J_{sc}, FF and η (the IV-parameters) and their TCs, in cells made of the same materials, will be investigated.

4.1.2 Section Summary

The lifetimes turn out to be highest in ESS 1.3, lowest in ESS 0.5, and REF 1.3 is somewhere in between. There is a large amount of scatter in the measurements, forcing us to make the measurements at large grains wherever possible. The grain size increases with x. This means that the lifetime measurements at high x are unrepresentatively large, compared to the average lifetime of the wafers. τ_{bulk} is negatively correlated with p_0, when comparing the ESS-wafers.

Further, the lifetime increases with temperature in all cases. TC_τ is highest in ESS 0.5 for all x. The high TC_τ of ESS 0.5 may be ascribed its low τ_{bulk}. ESS 1.3 and REF 1.3 have similar TC_τ at low and middle x, but ESS 1.3 is higher at high x. No conclusion as to a potential correlation between C_l or p_0 and TC_τ can be made.

4.2 IV-measurement Results

4.2.1 The IV-Parameters

The measured IV-parameters of the PERC cells are presented in **Figure 4.5**. As can be seen in **d)**, there is a spread of $\sim 2\%_{abs}$ in the efficiencies (η) of the different cells at $25\,^\circ\mathrm{C}$. Also, the absolute value of $\eta(25\,^\circ\mathrm{C})$ is between 16.3% and 18.2%, which is more in the range of industry standard Aluminum-Back Surface Field (Al-BSF) cells than PERC cells. The REF 1.3-cell at $x = 0.45$ was measured to $\eta(25\,^\circ\mathrm{C}) \approx 12.5\%$. This cell was deemed broken and taken out of the results. Even though the cells may not be representative for state of the art PERC cells, there is an internal consistency that makes it valuable to compare the cells within this study to each other.

However, an important point is the fact that the small amount of measured cells renders the statistical significance of these results very low. On this basis there can be made no generalization as to the performance of ESS-cells relative to polysilicon-cells. However, having this disclaimer in mind, arguments may still be made as to the correlation between the IV-parameters and their TCs, and the lifetime measurements and the doping levels. Also, large amounts of measurements comparing cells based on ESS to cells based on polysilicon have been made already (Berthod, 2016; Berthod et al., 2016), and the knowledge gained from adding on this is limited. Thus, the results will be discussed and compared in light of the lifetime measurements in the previous section, and in light of what we know about the doping levels of the materials.

For starters, it can be noted that η, V_{oc} and J_{sc} of the cells made of wafers from the relative ingot position $x \approx 0.08$ and $x \approx 0.17$ in ESS 1.3 and REF 1.3 are almost overlapping at all temperatures. This points to a consistency in the cell processing at ISC Konstanz, since they are the most similar cells in terms of effective doping level and lifetime. The ESS 1.3 cell from high in the ingot performs better than the REF 1.3 from high in the ingot. More spesifically, it has a higher V_{oc} and J_{sc}, and a lower FF. This correlates well with the measured lifetimes, since a benefit in the bulk lifetime was measured for ESS 1.3 at high x, but not at low x. However, bulk lifetime is positively correlated with all IV-parameters. The lower FF of ESS 1.3 thus has to be explained by something else.

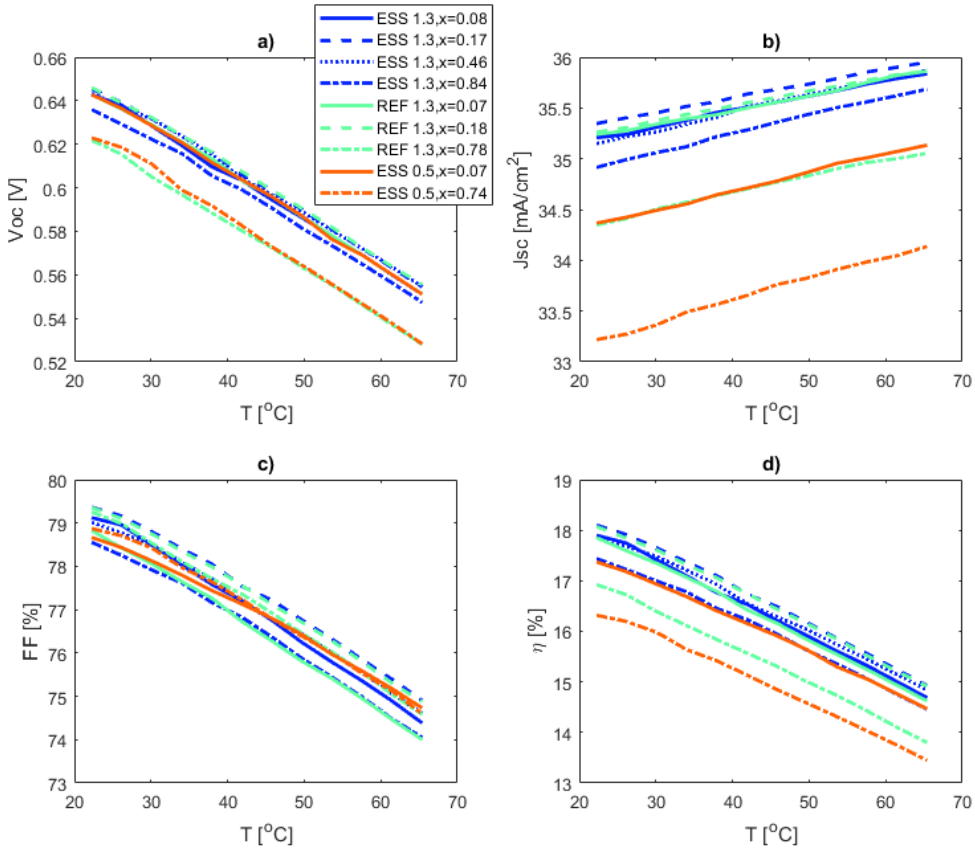

Figure 4.5: Results of IV-measurements performed on the PERC cells made at ISC Konstanz, including a) V_{oc}, b) J_{sc}, c) FF and d) η. The cells were measured at every fifth temperature between $23\,^{\circ}\mathrm{C}$ and $65.5\,^{\circ}\mathrm{C}$. The legend refers to what material type (ESS or the polysilicon reference (REF)), what ingot resistivity ($1.3\,\Omega\mathrm{cm}$ or $0.5\,\Omega\mathrm{cm}$) and what ingot position ($x \in (0, 1)$) the wafers that the cells are made of are from.

Note that the η of the cells made from a high ingot position in all three ingots is between 0.5% and 2% lower than the cells made from a low ingot position. This seems not to correlate with the measured lifetimes. It might be caused by a random error due to mistakes in the cell processing, or it might be due to a lower material quality that is not caught in the lifetime measurements. The low number of measured cells makes it hard to determine which explanation is true. However, as was discussed in section 4.1, the lifetime measurements were made on especially favorable areas of the wafers, meaning the absolute value of the lifetime measurements are not necessarily representative of the wafer as a whole. In fact, the lifetimes are probably overrated in the middle positions, and even more so high in the ingot. Thus the average lifetime may actually decrease

with ingot height, even though this is not seen in the lifetime measurements. Further, this explanation seems logical since it is known that the dislocation cluster density increases with x (Sio et al., 2017). Although the density of grain boundaries (GB) is higher at low ingot positions, these defects are passivated more effectively during the wafer preparation process of hydrogenation. Thus you expect to see a lower average lifetime higher in the ingot, reflected in a lower cell efficiency. Thus the lower performance of the cells at high x are probably due to lower material quality, or, in other words, lower bulk lifetimes.

Both the ESS 0.5 cells have lower η than most of the other cells. The ESS 0.5 material is highly doped (high p_0, which is what gives it the low resistivity), and a high p_0 is connected to low SRH lifetimes, and thus low effective lifetimes. This is confirmed by the lifetime measurements, where the ESS 0.5 wafers consequently have the lowest bulk lifetimes. Low effective lifetimes affects all the IV-parameters negatively. This is see in **Figure 4.5**, except maybe in V_{oc}. However, p_0 is positively correlated with V_{oc}, due to the splitting of the quasi-Fermi levels, which depends on the carrier densities in the base and the emitter (Xiao et al., 2012b). This serves to explain both the low η of the ESS 0.5-cells and the decent V_{oc} of the cell at $x = 0.07$.

To see the relative performance of the cells as it varies with temperature, a plot of normalized efficiencies is given in **Figure 6.1** in the Appendix.

4.2.2 Temperature Coefficients

The temperature coefficients (TCs), as defined by equation (2.50), of the IV-parameters of the measured PERC cells are presented in **Figure 4.7**. Three observations may be pointed out immediately:

(a) The TCs at $\sim 60\,^{\circ}\mathrm{C}$ are in the range of the literature values (see section 2.8.4),

(b) high in the ingot, TC_η of ESS 1.3 is smaller (less negative) than TC_η of REF 1.3,

(c) the absolute value of the TCs increases with T in all cases, and

(d) the TCs, except $TC_{V_{oc}}$, of the ESS 0.5-cells are relatively good.

(a) Initially this was not the case. The first estimation yielded TCs that were considerably smaller than the literature values. This indicated the presence of a possible systematic error. The obvious candidate for this systematic error was the temperature measurement of the cells. There is a built-in thermometer in the solar simulator that was used for this. To check this hypothesis, a thermocouple was used to measure the temperature of the hotplate. The thermocouple systematically showed lower temperatures than the solar simulator, strengthening the hypothesis. Of course, the thermocouple cannot be trusted completely either. However, by re-scaling the temperature given by the solar simulator according to the values acquired with the thermocouple, new values of the TCs were estimated. These new values, which are the ones that are presented here, showed to be in the value-range of the literature values. Still, these numbers have to be taken very lightly. This is reflected in a large uncertainty, which can be seen in **Figure 4.7**. This also means that the temperature measurements, which were intended to go between $25\,^{\circ}\mathrm{C}$ and $80\,^{\circ}\mathrm{C}$ only goes between $23\,^{\circ}\mathrm{C}$ and $65.5\,^{\circ}\mathrm{C}$.

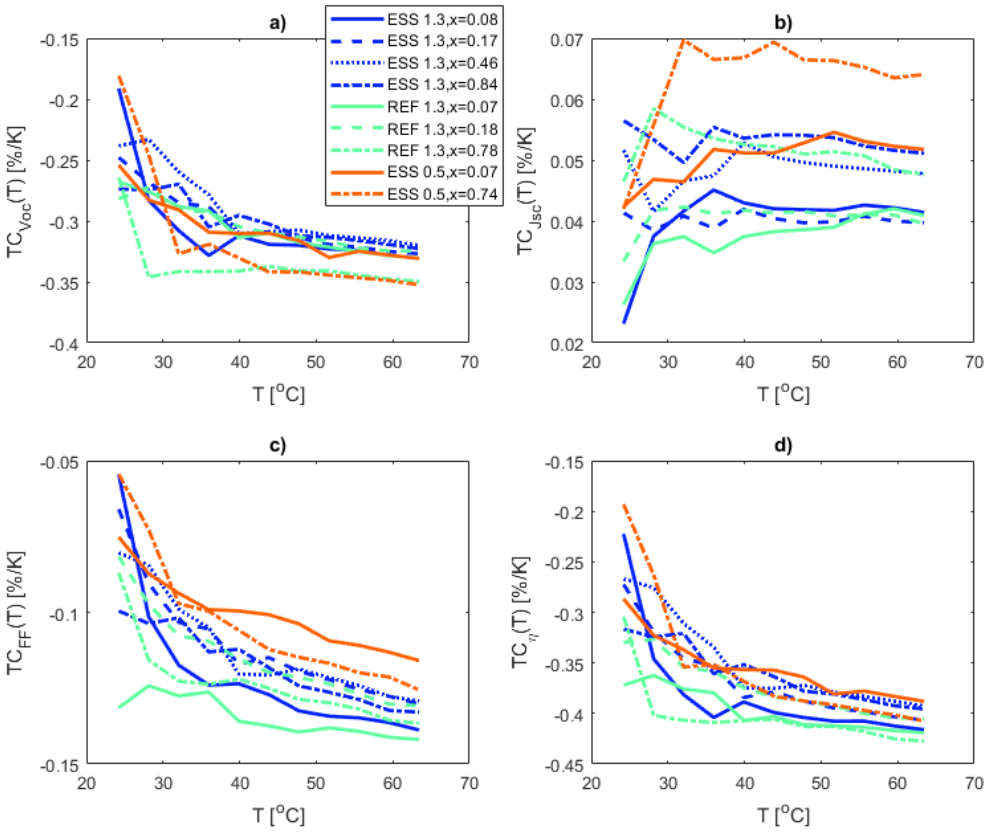

Figure 4.6: Temperature coefficients of a) V_{oc}, b) J_{sc}, c) FF and d) η as a function of T, derived from the IV-measurements of the PERC cells.

(b) This correlates well with the measured TC_τ, shown in **Figure 4.4** suggesting a correlation between TC_τ and TC_η, which is not surprising, given the correlation between τ and η. TC_τ of ESS 1.3 and REF 1.3 are similar in the low and middle part of the ingot, while that of ESS 1.3 is bigger high in the ingot. Further, V_{oc} of ESS 1.3 is higher at this ingot position, which is also correlated with less negative $TC_{V_{oc}}$ and TC_{FF}.

(c) The fact that the TCs are not constant with respect to T is not surprising. The physical effects of changing the temperature are not in general linear. However, the apparent linearity in the IV-parameters in figure **Figure 4.5** makes it tempting to assume that a linear dependency on T is a good approximation. In **Figure 4.6** we see that the TCs change with a factor of up to 2 when going from 23 °C to 60 °C. Thus the accuracy of a liner approximation of the temperature dependency of the IV-parameters has to be assessed. This is done in section 4.2.3.

(d) The fact that the TCs of ESS 0.5 are good is interesting. TC_τ is higher in ESS

0.5 than in the other materials at low and middle ingot positions (see **Figure 4.4**), but it is on par with ESS 1.3 high in the ingot. And indeed, it is the low ingot position that yields the best TC_η, while the high ingot position yields an averagely good TC_η. This further strengthens the hypothesis of a correlation between TC_τ and TC_η.

One factor that has to be taken into account when discussing these results is surface recombination. One may assume that surface recombination is relatively high in the PERC cells dealt with here, since their efficiencies at 25 °C are between 16.3% 18.2%. When surface recombination is high, the advantage of having a high bulk lifetime is lost, since it will be the surface recombination that limits the effective lifetime, and not the bulk recombination. Thus the effect of increased bulk lifetime due to increased temperature may be lost, or at least inhibited, in the samples with the highest bulk lifetimes, namely ESS 1.3.

Further, as discussed in section 2.4.3, surface recombination velocities (SRVs) are affected by p_0. As the effective doping level rises, the SRVs increases. Thus the SRVs are relatively high in ESS 0.5, and, even though τ_{bulk} is low, the effective lifetime may be limited by surface recombination in ESS 0.5 too. In fact this may be one of the reasons for the low performance of the ESS 0.5-cells. This will be investigated further in section 4.3.

In order to see the dependency of the TCs on x, as well as illustrating the large uncertainty in their magnitudes, the TCs at 60 °C is plotted against ingot position x in **Figure 4.7**. The value itself is taken as the mean of $TC(T)$ with $T = (53.5, 57.5, 61.5, 65.5)$°C, and the error-bar reflects the uncertainty of the acquired values. As can be seen, the uncertainty in the TCs is relatively large. This is mainly due to the large uncertainty in the temperature measurements. The choice of 60 °C may seem high, considering the normal operating temperatures of solar cells, even in hot environments (Rand et al., 2007). And admittedly, the temperature was chosen rather arbitrarily. Still, as will be clear in section 4.2.3, if the value of the TCs at 60 °C is used to estimate the IV-parameters as they vary with T, it does not give an error of more than 1.1% in any of the IV-parameters at any temperature, which seems to be acceptable.

It is immediately clear that the difference between ESS 1.3 and REF 1.3 is inconsiderable for all TCs at low ingot positions. At $x \approx 0.8$ the difference in TC_η is bigger. Although large parts of the uncertainty-bars overlap also here, one may state that TC_η of ESS 1.3 is almost certainly smaller, mostly due to $TC_{V_{oc}}$. This reflects exactly what was seen of TC_τ in section 4.1, suggesting a strong correlation between TC_τ and TC_η.

However, there is a slight problem with comparing TC_η of ESS 1.3 and REF 1.3 at high x, since the values of $\eta(25\,°\mathrm{C})$ are not equal. This comes into play in the definition of the TCs. Since the TCs are normalized by the value of the given IV-parameter at 25°C, the magnitude of $\eta(25\,°\mathrm{C})$ plays a big role in the magnitude of TC_η. If $\eta(25\,°\mathrm{C})$ is high, this causes the absolute value of TC_η to be low, and vice versa. Of course, this is taken into account when using the TCs, and it doesn't make the TCs of two cells with a different $\eta(25\,°\mathrm{C})$ incomparable. However, when it comes to comparing two different materials in terms of their TCs, it might be misleading to compare two cells with different values of $\eta(25\,°\mathrm{C})$. We see that all the TCs of ESS 1.3 and REF 1.3 are similar at low ingot positions, where their IV-parameters are also similar. To assess the impact of normalization, the un-normalized TCs were plotted (these can be found in **Figure 6.2** in the Appendix). In the un-normalized TCs there is still a benefit for ESS 1.3 at high x, although slightly smaller.

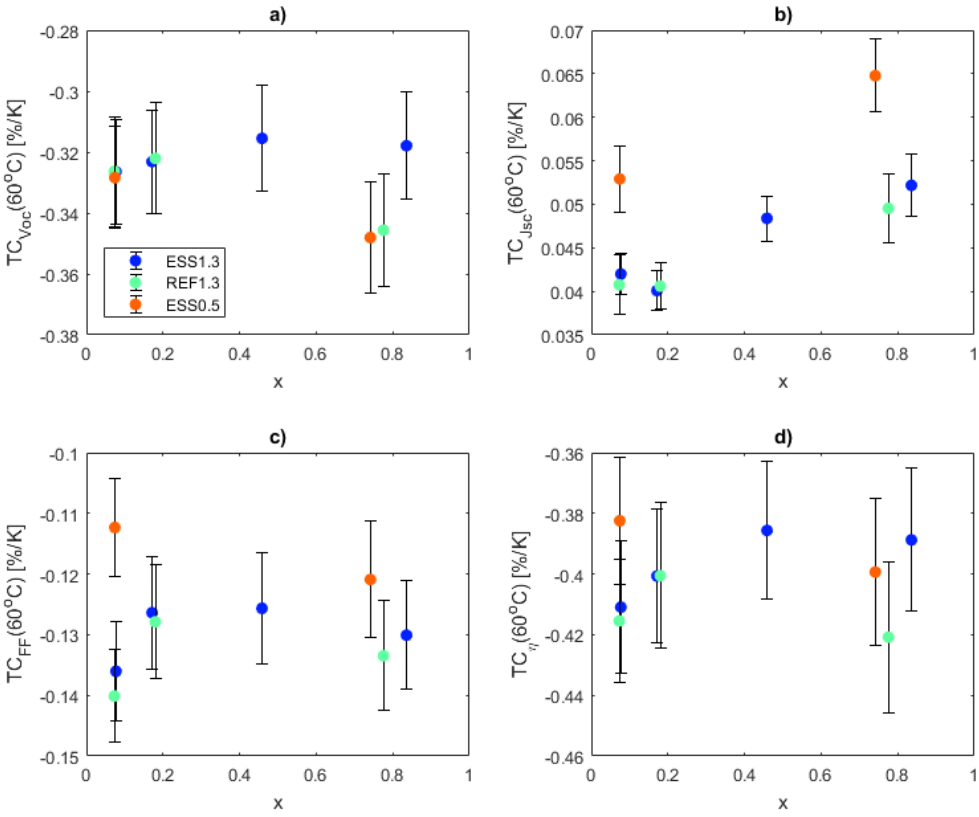

Figure 4.7: Temperature coefficients at 60 °C of a) V_{oc}, b) J_{sc}, c) FF and d) η derived from the IV-measurements of the PERC cells.

This means that the benefit in the normal TCs of ESS 1.3 at high x is not due to the difference in the magnitude of the IV-parameters. Of course, TC_τ was measured to be advantageous in ESS 1.3, which makes a good explanation for the difference. At any rate, as long as there is only one measurement showing a benefit in the TCs of ESS 1.3, we are far from a statistically significant conclusion.

ESS 0.5 generally has a small TC_η all along the ingot, but not a small $TC_{V_{oc}}$. The unnormalized TCs of ESS 0.5 are even better (relative to the other materials) than its normal TCs. This means that the relatively small TCs of ESS 0.5 are not due to low values of the IV-parameters, but rather due to a property of the material itself. The benefit in TC_η of ESS 0.5 comes from $TC_{J_{sc}}$ and TC_{FF}. The reason for this is not clear.

4.2.3 Assessment of the Assumption of Linearity

The temperature dependent curve of each IV-parameter may be approximated by two numbers: the value at $25\,^{\circ}\mathrm{C}$, and the temperature coefficient. This may be dubbed the *linearity approximation*. In order to assess the accuracy of the linearity approximation one may look at the relative error E_X of the approximation of IV-parameter X to the real value, defined as $E_X = \frac{X_a - X_r}{X_r}$, where X_a is the approximated value of the IV-parameter, and X_r is the real value. This was done, and the error is at most 1.1% in η, $\sim 0.8\%$ in V_{oc}, 0.4% in FF and only $\sim 0.1\%$ in J_{sc}.

A 1.1% error seems to be acceptable within the constraints of this thesis. It may be argued that a statistical significant amount of cells would yield a standard deviation larger than 1.1% in all the IV-parameters. And since the PERC-model presented in section 3.3 is fitted to the IV-parameters of the measured PERC-cells, we have to give the absolute values of the simulated IV-parameters an even greater uncertainty. Thus, in the rest of the thesis, unless the error of the linear approximation exceeds 2%, it will be only the value of the IV-parameters at $25\,^{\circ}\mathrm{C}$ that will be presented, along with the TCs.

4.2.4 Section Summary

The efficiency of all the measured PERC-cells are reduced by $2\%_{abs}$ when going from $25\,^{\circ}\mathrm{C}$ to $55\,^{\circ}\mathrm{C}$. The measured ESS 1.3- and the REF 1.3-cells perform equally well at low x, but ESS 1.3 is better at high x. The cells based on ESS 0.5 have lower efficiencies than the other cells. In spite of a certain amount of scatter in the data, this correlates well with the measured lifetimes. The apparent low performance, relative to the lifetimes, of the cells at high ingot positions may be explained by the overestimation of the lifetimes at these positions explained in section 4.1.

After an adjustment of the temperatures, a consistent set of TCs of the cells are found. The magnitudes of the TCs are in the range of earlier measured TCs of both ESS- and polysilicon-cells, although with large uncertainties. A benefit in the TCs of ESS 1.3 relative to the reference is only found at high ingot positions, which comes from a benefit in TC_τ and V_{oc}. A relative benefit in the TCs of ESS 0.5 also points to a correlation between TC_η and TC_τ.

4.3 Modeling Results

The order in which the modeling results are presented is intended to have a natural progression. The first simulation is an attempt to recreate the measurements. The discrepancy between this simulation and the measurements leads to questions about the relative impact of each material parameter. This calls for further investigations, which is a new set of simulations. Each subsequent simulation is designed to investigate the impact of a (set of) parameter(s). This order also happens to be the order in which the simulations were performed in reality.

In the discussion, the PC1D-models will sometimes be treated as a 'black boxes' of physics, of which the contents are unknown. This is not to say that the implemented physical models are unknown. (For a detailed summary of what physical models are entailed

in PC1Dmod 6.2, see (Haug and Greulich, 2016).) Even though it is possible to make qualitative statements as to the trends caused by the different phenomena by assessing the physical models themselves, the relative impact of each phenomenon can only be accurately evaluated through simulations. Still, it is not always straightforward to deduce which mechanism causes which behavior. Thus the simulation results will be discussed with the goal of mapping the importance of each mechanism in each case. It is important to keep in mind that some of the phenomena are coupled in reality (like the effect of p_0 on τ), but not in the model. In section 4.4, the effect of the different mechanisms and their relative importance will be summed up, and a comprehensive understanding about what mechanisms are important for the performance and temperature sensitivity of solar cells will be reached.

4.3.1 Modeling of PERC cells, all effects taken into account

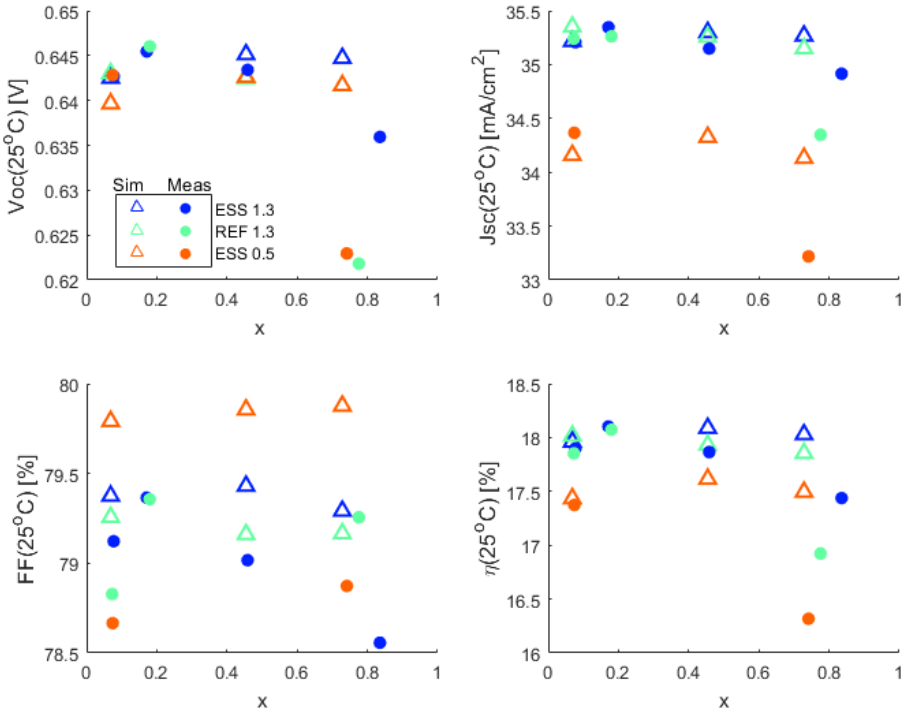

Figure 4.8: IV-parameters of the PERC-model (triangles), simulated with real lifetimes from the measurements in section 4.1 and real compensation and doping levels from Scheil's equation. The IV-parameters of the measured cells have also been included (dots).

IV-parameters. As is explained in section 3.3, the goal of the PERC-model is to recreate the results of the measurements as much as possible. Starting with the most realistic simulation possible within the framework described there, comparing the simulation to the measurements, it is easy to see where the model falls short. The full set of known material parameters of the measured PERC-cells has been applied in the PERC cell-model, including the doping levels determined by Scheil's equation and the measured lifetimes from section 4.1 .

As can be seen in **Figure 4.8**, the efficiency is predicted to be $\eta(25\,^{\circ}\mathrm{C}) \sim 18\%$ for cells based on ESS 1.3, slightly lower for REF 1.3, and $\eta(25\,^{\circ}\mathrm{C}) \sim 17.5\%$ for ESS 0.5. These efficiencies are all quite constant with x, although there is a slight increase when going from low to middle ingot positions, and a slight decrease when going from middle to high ingot positions, in all the materials. The biggest difference between ESS 1.3 and REF 1.3 is a benefit to ESS 1.3 in V_{oc}, while the biggest difference between ESS 1.3 and ESS 0.5 is a benefit to ESS 1.3 in J_{sc}.

The simulated IV-parameters align very well with the measurements at low x, at least in V_{oc}, J_{sc} and η. In the middle of the ingot the simulations seem to align well with the measurements of ESS 1.3, but there are no measurements of the other two materials in this position. High in the ingot, the simulations seem to overestimate the performance of the cells. It is not surprising that the simulation and measurement results align well at low x, since these are the measurements that the parameters of the PERC-model were adjusted to fit with. Apparently there is some mechanism affecting the performance as we go to higher x that is not caught in the model. An initial question is therefore what this mechanism is.

The most obvious cause of this is the overestimation of lifetimes at high x. As was discussed in section 4.1, the lifetimes were measured at large grains. Thus the lifetime input to the simulations is higher than the average lifetime over the wafers, which leads to overestimation of the performance of the cells. This overestimation only comes into play at higher x, since there are no large grains at low x (see **Figure 3.3**). Of course, the inhomogeneity of the wafers could have been accounted for either by using a 2D or 3D device model, or by scaling the lifetime curves to a harmonic mean over the surface of the wafers. It has been shown that the latter method may give a prediction within an error of 1% (Haug et al., 2016). However, to do this is a very time-consuming task far outside the scope of this thesis. At least the resulting overestimation in the prediction of the performance of the cells at high x can be accounted for.

According to the model, ESS 1.3 and REF 1.3 are almost equal in all parameters at all x. The η of ESS 1.3 is slightly higher at middle and high ingot positions, and the η of REF 1.3 is slightly higher at low ingots positions. Remember that the lifetime varies with x in all the materials, and is equal in ESS 1.3 and REF 1.3 at low x, and considerably higher at middle and high x. Thus the measured IV-parameters are more strongly correlated with the lifetime, qualitatively, than what the PERC-model predicts. This indicates that the effect of the lifetime is counterbalanced, or inhibited, by something in the model. A possible candidate for this is surface recombination. If the SRVs are high, τ_{surf} will be low, restricting τ_{eff} so that any change in τ_{bulk} only has a small effect. A quick calculation shows that a SRV given by $S_{0p} = S_{0n} = 100\,\mathrm{cm/s}$ (which is the case for ESS 1.3 at low x) gives a $\tau_{surf} < \tau_{bulk}$ for ESS 1.3 at $T = 298\,\mathrm{K}$. The same goes for ESS 0.5, with $S_{0p} = S_{0n} = 440\,\mathrm{cm/s}$. This means the surface recombination is limiting τ_{eff} more than

τ_{bulk} is, and the effect of the bulk lifetime is lost to a certain degree. This explains the small difference between ESS 1.3 and REF 1.3 at high x in spite of very different bulk lifetimes.

In general there is less variation with x in the simulation than in the measurements. This is likely not due to doping levels. For starters, p_0 does not change considerably with x in ESS. However, both N_A and N_D (and thus C_l) increases with x. This leads to a higher amount of ionized impurity scattering, thus reducing the mobility (Rougieux et al., 2010). However, the effect of compensation is included in the mobility model (Schindler et al., 2014), so this should not be a limitation in the model.

Something that is not included in the model is the effect of grain boundaries and dislocations. The density and geometry of these change with ingot position, as is easily seen in **Figure 3.3**. In addition to affecting the lifetime at each position of the cell, this leads to 2D/3D effects in the carrier logistics that can only be correctly emulated by a 2D/3D model. Since PC1D is a 1D modeling software, the lateral variation in the bulk cannot be emulated. This partly explains the smaller variation with x in the simulations than in the measurements.

Also, the collector architecture of the cells is not represented in the PC1D-models. While an Al-BSF cell has a uniform back surface, the PERC-cell has local back contacts. This means that the carriers have to move laterally to a certain degree in order to be collected, meaning the effect of lateral movement by the carriers is lost in the simulations. This may be partly accounted for by a correction factor, but the exact carrier logistics and its effects on the performance of the cell can only be correctly emulated by a 2D- or 3D-device simulator. Doing this falls outside the scope of this thesis, but the resulting uncertainty will be kept in mind in the remainder of the discussion.

Temperature Coefficients. The TCs predicted by the PERC-model can be seen in **Figure 4.9**, together with the measured TCs. The TCs previously measured by (Berthod et al., 2016) on PERC-cells based on the same ingots as the ones used in this thesis are shown as dashed lines. According to this simulation, it is the ESS 0.5-cells that have the least negative TC_η. This is mostly due to a benefit in TC_{FF}. The ESS 1.3- and REF 1.3-cells have almost equal TC_ηs, but ESS 1.3 is slightly less negative. The change with x is small.

The model recreates the magnitude of the measured TCs well. Also, both the simulated and the measured TCs are in the range of what was measured by (Berthod et al., 2016), although they measured slightly higher $TC_{V_{oc}}$ and $TC_{J_{sc}}$, and slightly lower TC_{FF}. As in the IV-parameters, the tendency is that there is less spread between the simulated values than the measured values, especially between ESS 1.3 and REF 1.3, and especially in $TC_{V_{oc}}$. For the IV-parameters, this was argued to be due to high values of SRV in the PERC-model, making τ_{surf} more important than τ_{bulk}, as well as random scatter caused by grain boundaries and dislocation clusters. If $\tau_{surf} < \tau_{bulk}$, it means that the temperature dependency of τ_{bulk} is diminished by τ_{surf}, which has no implemented temperature dependency in this model. This may be the reason for the small difference of the TCs, even at high x, where TC_τ is considerably higher in ESS 1.3 than in REF 1.3. It was shown that the measured TCs correlates with TC_τ. This is not the case for the PERC-model, strengthening the hypothesis that the SRVs are overestimated. However, it seems that this overestimation of the SRVs does not lead to an error in the magnitude of the predicted

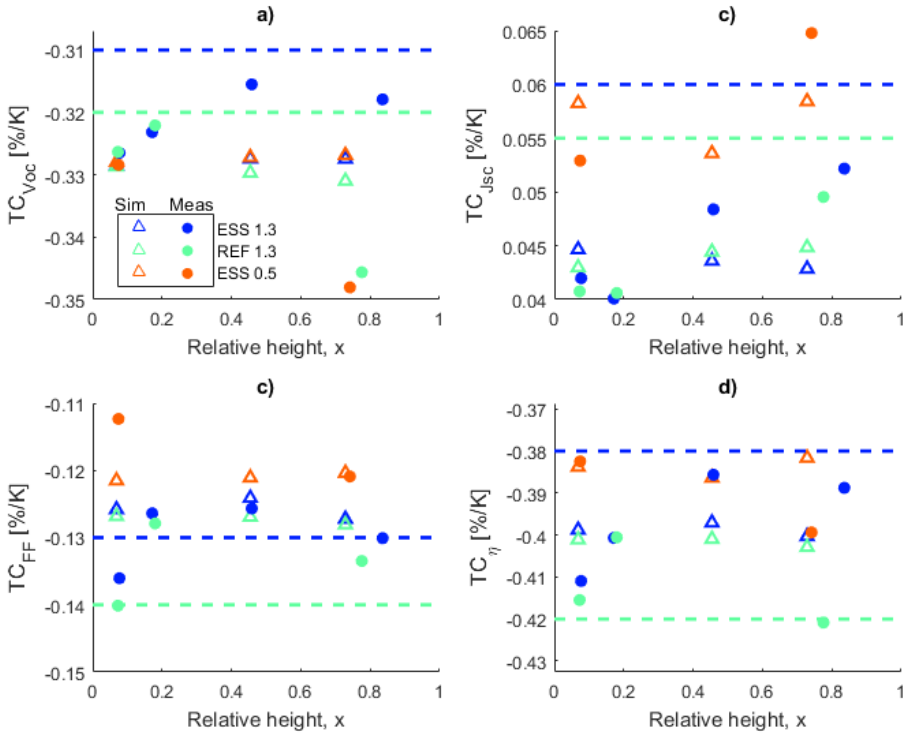

Figure 4.9: TCs of the IV-parameters of the PERC-model (triangles), plotted together with the TCs from the measured PERC cells (circles). The simulations have been run with real lifetimes from the measurements in section 4.1, and real doping levels from Scheil's equation. The dashed lines correspond to the TCs measured by (Berthod et al., 2016), with the same color-coding.

TCs.

The front SRV greatly depends on the doping profile in the emitter, which depends on the background doping levels. As will be seen in section 4.3.4, this results in an increase in $TC_{J_{sc}}$ as p_0 increases, which is probably what causes the high $TC_{J_{sc}}$ in ESS 0.5, both in the model and in the measured cells.

One effect that has to be taken into account is the injection level Δn the cells are operating at (see **Figure 3.6**). According to PC1D, the operating point of the PERC-model is between $\Delta n = 1 \times 10^{13}\,\mathrm{cm}^{-3}$ and $\Delta n = 1 \times 10^{14}\,\mathrm{cm}^{-3}$ at 1 sun. When T increases, the operating point moves to higher Δn. If there is a positive slope in $\tau_{bulk}(\Delta n)$ this results in an increase in τ_{bulk}, even though τ_{bulk} doesn't change with T. However, there is almost no slope between $\Delta n = 1 \times 10^{13}\,\mathrm{cm}^{-3}$ and $\Delta n = 1 \times 10^{14}\,\mathrm{cm}^{-3}$ in the $\tau_{bulk}(\Delta n)$-curves that have been applied in these simulations, so this effect is negligible. It may be considerable for the ideal cell-model, however.

Section Summary. To sum up, the simulation of the PERC-model predicts the efficiency of the cells based on ESS 1.3 to be slightly higher than the efficiency of REF 1.3-cells due to a higher V_{oc}, except at low x. ESS 0.5-cells are predicted to be $\sim 0.5\%_{abs}$ less efficient. This tendency varies little with x. Further, the simulation results aligns well with the measurements at low ingot positions, but the tendencies in the performance as it changes with x is not caught in the model. This is partly ascribed a relative insensitivity to variations in τ_{bulk}, which is ascribed high SRVs, and partly ascribed 2D/3D-effects that are not caught in the model.

The range of values of the TCs predicted by the PERC-model align very well with measured TCs, both the ones presented in section 4.2 and the ones measured by (Berthod et al., 2016). However, also here the tendencies between the different cells as they vary with x are not caught. This is likely due to too high SRVs in the model.

The reason the back SRVs are too high in the PERC-model (if they are too high at all) is that they were used as free parameters to fit the model to the measurements. This is explained in section 3.3. This probably lead to the underestimation of other detrimental effects, and it may be argued that this was not a wise choice. However, in the next section the ideal cell-model will be run, in which the front and back SRVs is set to 0, so that the bulk lifetime is more important. If the tendencies in the IV-parameters and their TCs predicted by that model are similar to those of the measurements, it means the relative variation in IV-parameters between the cells is mainly due to the bulk lifetime, and that the SRVs of the PERC-model are overestimated.

4.3.2 Modeling of Ideal cell, all effects taken into account

IV-parameters. By doing the same simulation as in the last section, only with the ideal cell-model, the effect of changing lifetime stands out much clearer. Since the surface recombination is turned off, it is only the bulk lifetime τ_{bulk} that is decisive for the effective lifetime τ_{eff} of the cells.

And indeed, in **Figure 4.10** it seems that it is τ_{bulk} that has the largest impact on the performance of the cells. This may be stated since the simulation of the ESS 1.3-cells performs better than all other cells, except for the cell at $x = 0.07$, which performs equally well as the REF 1.3-cell at the same position. As can be seen in section 4.1, ESS 1.3 has the highest τ_{bulk} of all the materials, except at $x = 0.07$ where it is almost equal to REF 1.3. Also, ESS 0.5, which has the lowest lifetimes, consequently has the lowest performance. Thus the correlation between η and τ_{bulk} is high in the ideal cell-model. This is as expected.

Further, the biggest difference between ESS 1.3 and REF 1.3 is found in FF and V_{oc}. The difference increases with x, and it increases more in FF than in V_{oc}. Since the difference in τ_{bulk} also increases with x, this indicates that FF, apart from being directly dependent on V_{oc}, also is independently correlated with τ_{bulk}. However, FF of REF 1.3 decreases with x from low to middle ingot positions, but τ_{bulk} increases with x. This must be ascribed the other mechanisms coming into play in FF, like the effect of ρ and the ideality factor. The advantage for ESS 1.3 in V_{oc} and J_{sc} increases with x, in correlation with τ_{bulk}. This is as expected, given what was discussed in section 2.7.

The two main tendencies of the measurements that was not emulated by the simulation of the PERC-model was the increasing difference in η between ESS 1.3 and REF 1.3, and

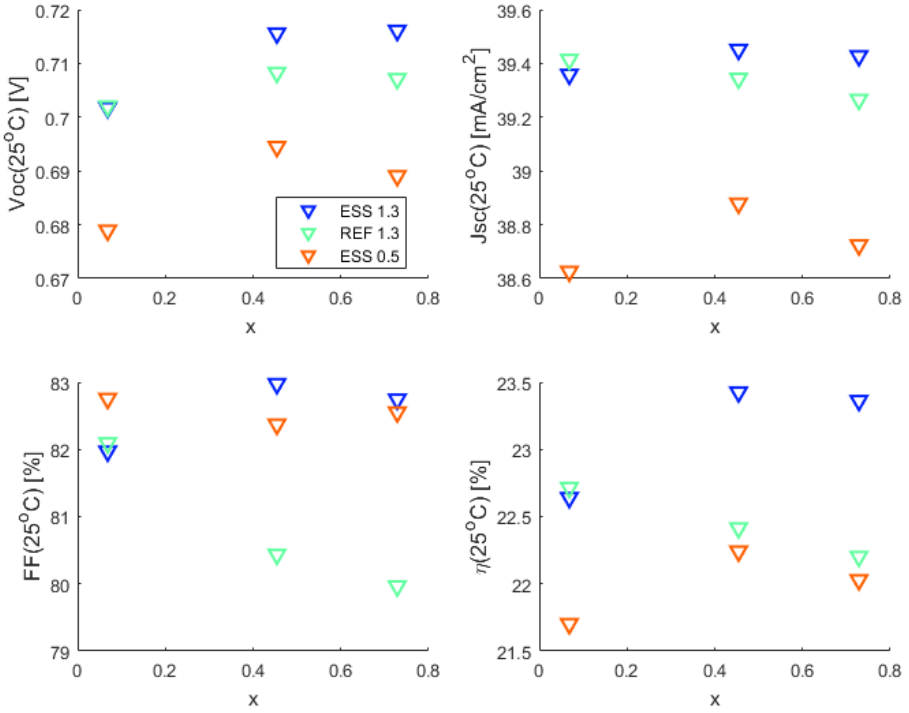

Figure 4.10: IV-parameters of the ideal cell-model, simulated with real lifetimes from the measurements in section 4.1 and real compensation and doping levels from Scheil's equation.

the decrease in η of all cells at high x. The first tendency is emulated by the ideal model, but the latter is not. Since the ideal model is more sensitive to changes in bulk lifetime, this indicates that the spread is due to bulk lifetime. Further, the decrease in η with x of the measurements may still be ascribed the lifetime, since the bulk lifetimes that have been used in the ideal model are overestimated as compared to the average over the wafers at these positions.

Temperature Coefficients. As is seen in **Figure 4.11**, the ideal model predicts all the TCs of the ESS 1.3-cells to be the smallest in magnitude, and the TCs of the ESS 0.5-cells to be the largest. REF 1.3 is somewhere in between, except at low x.

Since the ideal model is not inhibited by high SRVs, it is expected that the TCs will be less negative than in the PERC-model. This is the case, meaning surface recombination indeed does inhibit the temperature dependency of the effective lifetime in the PERC-model. However, the tendencies in the TCs of the ideal model are not very similar to the measured TCs. Except for $TC_{V_{oc}}$ of ESS 1.3 and REF 1.3, the tendencies in the TCs of the ideal model seems rather arbitrary, compared to the measured TCs. These seems

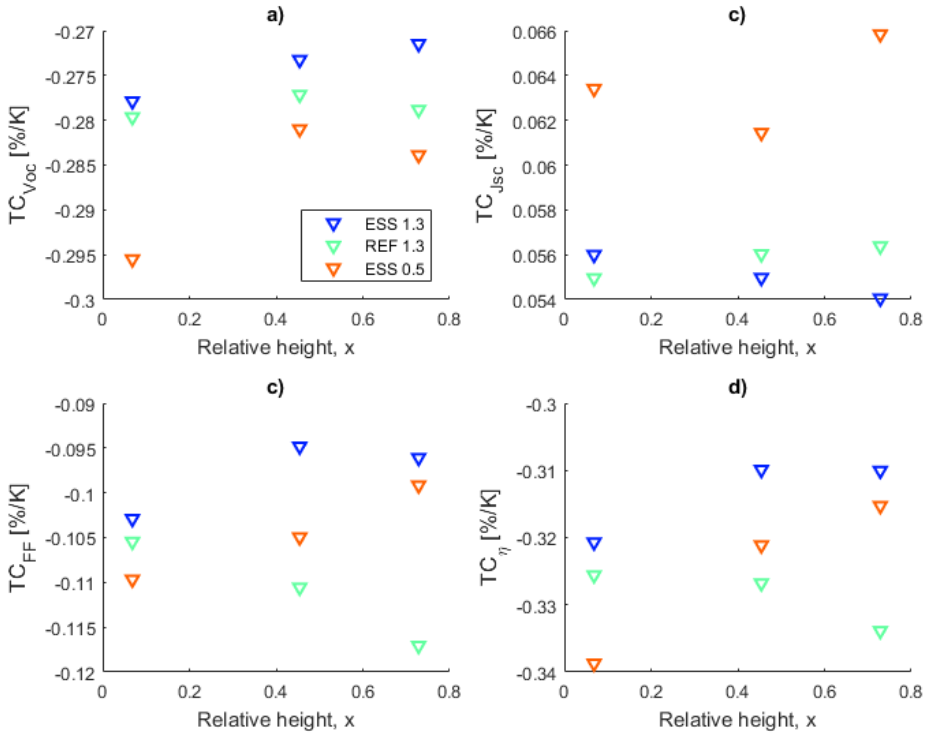

Figure 4.11: TCs of the IV-parameters of the ideal cell-model.

to indicate that τ_{bulk} is not the most important determinant of the TCs of the measured PERC-cells.

The fact that the simulated TC_η of ESS 1.3 is less negative than the other materials cannot be explained by the difference in TC_τ, since TC_τ is higher in ESS 0.5 than in ESS 1.3 at low and middle ingot positions. The benefit in the TCs of all the IV-parameters except J_{sc} of ESS 1.3 compared to REF 1.3 increases with x. This too cannot be explained by TC_τ, since ESS 1.3 has no advantage in TC_τ at the low and middle ingot positions. Thus no considerable correlation between TC_τ and TC_η is seen in the ideal model, and there must be something else in the ideal model that is decisive to the TCs of the cells.

Considering the tendencies of ESS 1.3 and REF 1.3 in **Figure 4.11**, one candidate for this is τ_{bulk} itself. Since ESS 1.3 has the highest τ_{bulk} at all ingot positions, and since the benefit relative to REF 1.3 increases with x, there seems to be a strong correlation between τ_{bulk} and TC_η here. The problem with this explanation is that ESS 0.5 does not follow this tendency: Its τ_{bulk} decreases from middle to high ingot positions, and is the lowest of all the materials at all x. However, ESS 0.5 has a high TC_τ at all ingot positions, and the combination of τ_{bulk} and TC_τ may explain its TC_η.

The impact of τ_{bulk} and TC_τ on the TCs will be investigated further in section 4.3.5.

It is worth to note that the biggest difference between ESS 1.3 and REF 1.3 is seen in TC_{FF}, which, according to this simulation, increases with x in ESS 1.3, but decreases in REF 1.3. In both the measurements and in the simulations with the PERC-model, no such tendency is seen. This might seem to be due to the normalization by FF in the calculation of TC_{FF}, because of the bigger absolute values of FF in ESS 1.3. However, by looking at the un-normalized TCs (**Figure 6.6** in the Appendix), it is seen that this is not the case. Thus there must be another physical phenomenon behind this behavior. The nature of this phenomenon is unknown at the moment.

Also worth noting is the fact that ESS 0.5 has by far the highest $TC_{J_{sc}}$. this is not directly due to the normalization by J_{sc}. Even though J_{sc} is low in ESS 0.5, this benefit is also seen in the un-normalized $TC_{J_{sc}}$ (**Figure 6.6** in the Appendix). This means that there is a physical cause of the benefit in $TC_{J_{sc}}$. In section 4.3.4, it will be argued that this is caused by the effect of a high p_0 on the front SRV.

Section Summary. As was expected, the correlation between performance and lifetime is very high for the ideal cell-model. It seems that both the spread in η of the ESS 1.3- and REF 1.3-cells, and the decrease in η in all the cells at high x, may be explained by the bulk lifetime. This indicates that τ_{bulk} is more determining for the performance of the PERC-cells presented in section 4.2 than what was predicted by the PERC-model. Also, a possible independent correlation between τ_{bulk} and FF is found.

Further, the TCs predicted by this model also correlate with the bulk lifetimes, and does not follow the same tendencies as the measured TCs, which correlate with TC_τ. This correlation with τ_{bulk}, however, does not explain all the tendencies in the TCs, suggesting that other material parameters may also come into play. Thus we remain with a question as to how, and how much, C_l and p_0 actually impact the performance and TCs of the ideal cell, independently of TC_τ. An investigation is called for.

4.3.3 The Effect of Compensation Level

By holding the effective doping level $p_0 = N_A - N_D$ and the bulk lifetime fixed (the lifetime of ESS 1.3 at $x = 0.45$ has been used), and letting C_l vary between 1 and 13, the effect of C_l is investigated. The reason C_l is increased all the way up to 13, and not further, is that the model did not handle higher compensation levels than this; the simulations failed to converge. When the lifetime is fixed, TC_τ is also held constant. In this case the ideal cell-model has been applied, so as to magnify the effect of changing C_l. The physical mechanisms that are dependent on C_l are band gap size E_g, mobility μ and incomplete ionization $i.i.$ The size of the band gap is implemented through the band gap narrowing (BGN) model of (Schenk, 1998), μ through the model of (Schindler et al., 2014) and $i.i$ through the model of (Altermatt et al., 2006). To assess the relative impact of each mechanism, the simulation was run four times with different physical models activated each time. The first round, none of the compensation-dependent mechanisms were activated, essentially making the simulation run with the models implemented in PC1D 5 (Clugston and Basore, 1997). For each subsequent simulation one of the models was activated, until in the end all three mechanisms were active.

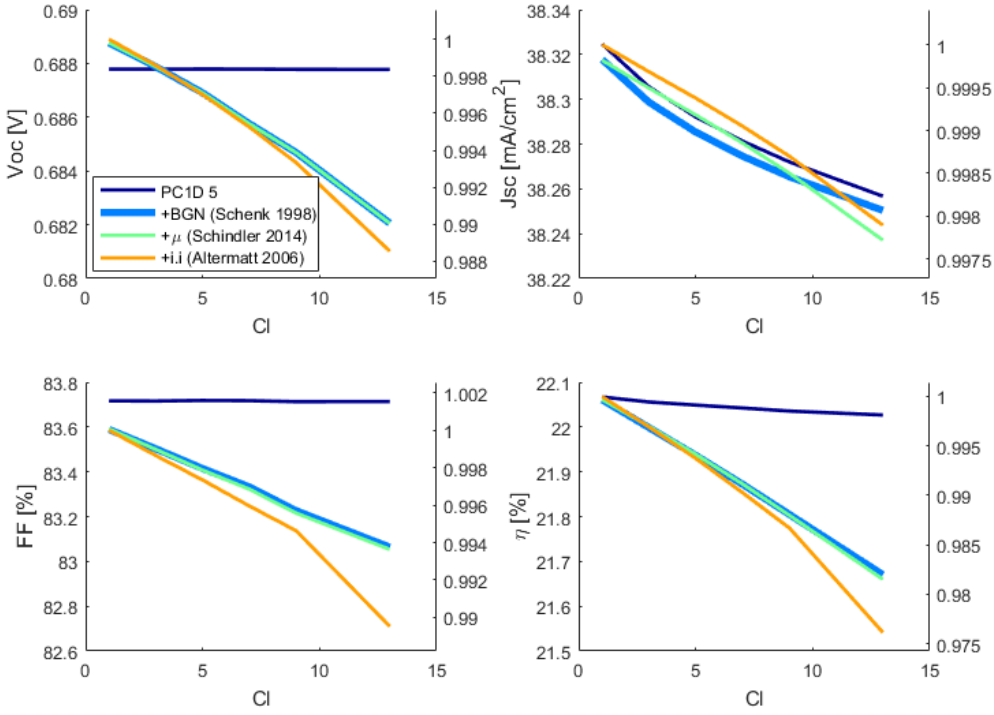

Figure 4.12: IV-parameters as they change with compensation level C_l at 25 °C. The effective doping level is set to $p_0 = 1 \times 10^{16}\,\mathrm{cm}^{-3}$ and the lifetime is that of ESS 1.3 at $x = 0.45$. Four simulations have been run with different mechanisms activated. The first simulation is simply run with the models implemented in PC1D 5. For each subsequent simulation the models mentioned in the legend are activated. The right side y-axes show the IV-parameters normalized to the maximum value of the simulation with all models activated.

IV-parameters As is seen in **Figure 4.12**, increasing C_l is negatively correlated with all IV-parameters. The big difference in the C_l-dependence happens when the BGN-model is activated. There is only a minor difference when the μ-model is turned on, and a slightly bigger difference when $i.i$ is activated. Thus we may conclude that what makes the biggest impact on the C_l-dependency is BGN, according to this model. The small dependency on μ is due to the fact that that the diffusion length L is larger than the cell with W, so that most of the carriers are collected. A small change in μ does not affect this.

The reason there is little change in J_{sc} is that there are two models for BGN in the model: One for the electrical band gap, and one for the optical band gap. The size of J_{sc} depends on the optical band gap, and a dependency of the optical band gap on C_l has not been implemented. However, no known relationship between J_{sc} and C_l exists, as far as the literature study of this thesis goes, so this probably does not affect the accuracy of the models.

Looking at the simulation with all the models implemented (the yellow curve), the sensitivity of the performance to change in C_l stems from V_{oc} and FF, which are both reduced by $\sim 1\%_{rel}$ when C_l goes from 1 to 13. J_{sc} is reduced by $\sim 0.02\%_{rel}$. These are small changes, but they all add up to reducing η by $\sim 2.5\%_{rel}$ ($\sim 0.5\%_{abs}$). Of course, $C_l = 1$ corresponds to a non-compensated material, like in REF 1.3. As is seen in **Table 3.1**, ESS 1.3 and ESS 0.5 have a C_l of around 2.0-4.8 and 1.3-1.9 respectively, increasing with ingot position x. Looking at **Figure 4.12 d)**, η varies by less than $\sim 0.5\%_{rel}$ ($\sim 0.15\%_{abs}$) within these compensation levels in the ideal model. Thus we may conclude that the independent effect of C_l on the performance of the cells is negligible, according to the ideal cell-model.

The variance with C_l is slightly larger in the PERC-model. However, the tendencies are virtually identical, and therefore these results were left out of the thesis.

The way incomplete ionization affects the performance of the cell is that when the doping levels are increased, the incomplete ionization ratio will also increase, causing the hole density at equilibrium $p_{0,i.i} = N_A^- - N_D^+$ to decrease slightly, even though $p_0 = N_A - N_D$ is held constant. This has a detrimental effect on the performance in the range of p_0 used here. The effect of changing p_0 (and therefore changing $p_{0,i.i}$) will be investigated in the next section.

Of course there may be effects of C_l that exist in reality that have not been implemented in PC1D. Examples of such effects may be a dependency of the density of dislocations and grain boundaries on C_l. This would affect the lifetime as well as the lateral carrier logistics in the cell. As was discussed in section 4.2, a 2D model is required to implement this.

Temperature Coefficients The TCs vary even less with C_l than the IV-parameters. **Figure 6.7** (in the Appendix) effectively shows that the impact of C_l and the different models is visible only in the third significant digit of η, and is thus negligible. This is according to the ideal model, but the same is seen in the PERC-model.

There is a slight positive correlation between $TC_{J_{sc}}$ and C_l, which may be ascribed the change in J_{sc}: Since $TC_{J_{sc}}$ is normalized by J_{sc}, a smaller J_{sc} gives a bigger $TC_{J_{sc}}$. Also, it seems like Schenk's mobility model moves $TC_{J_{sc}}$ down by $0.001\%/\mathrm{K}$.

As for the other TCs, there are some tendencies that are not proportional to the IV-parameters, especially in TC_{FF}. However, these tendencies are minimal in magnitude and will not be dwelt upon any further.

Section Summary. The independent effect of increased compensation level is to slightly reduce all IV-parameters, according to the model applied here. This comes down to the dependency of BGN on C_l. However, the magnitude of this effect is negligible within the compensation levels of the measured cells in this thesis. The change in the TCs with C_l is also negligible.

The effect of changing C_l in the model mostly stems from how the band gap scales with C_l. $i.i$ also comes into play, since it causes the hole density at equilibrium $p_{0,i.i} = N_A^- - N_D^+$ to decrease with C_l. The effect of p_0 on the performance will be investigated further in the following section.

4.3.4 The Effect of Effective Doping Level

By holding the bulk lifetime constant (the lifetime of ESS 1.3 at $x = 0.45$ has been used again), and varying p_0 between $1.3 \times 10^{15}\,\mathrm{cm}^{-3}$ and $1.3 \times 10^{17}\,\mathrm{cm}^{-3}$, the independent effect of p_0 on the performance of the models could be investigated. This was done with both models, and with two different compensation levels; $C_l = 1$ (non-compensated) and $C_l = 2.45$ (compensated), the latter being the compensation level of ESS 1.3 at $x = 0.45$.

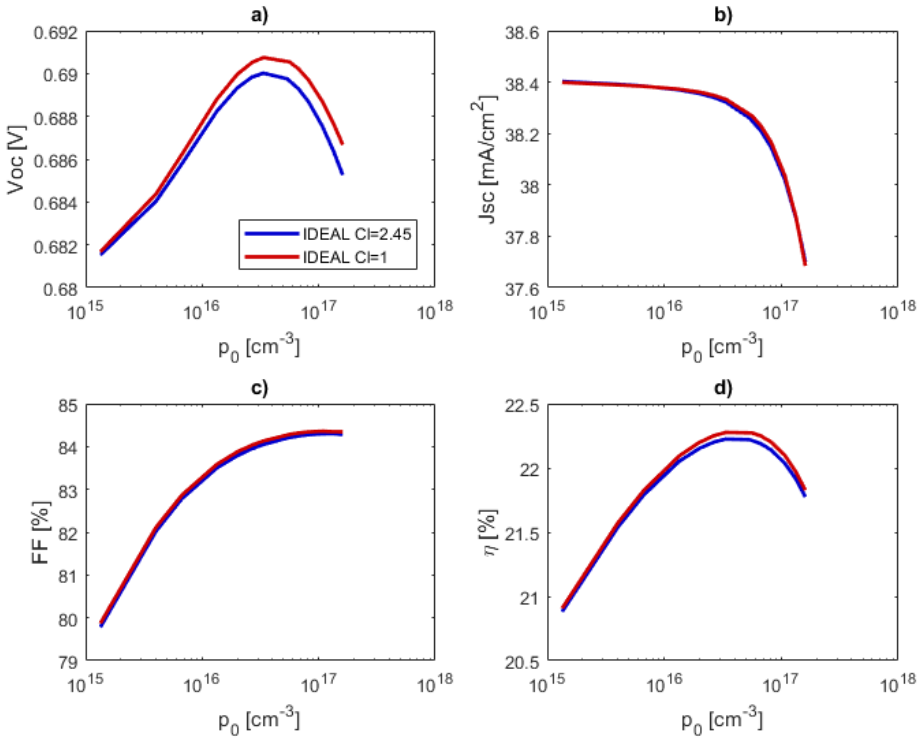

Figure 4.13: IV-parameters as they change with effective doping level p_0 in the ideal cell-model. The simulation was run with compensation level set to $C_l = 2.45$ (compensated) and $C_l = 1$ (non-compensated), and the lifetime is that of ESS 1.3 at $x = 0.45$.

IV-parameters of ideal cell-model. As is seen in **Figure 4.13**, p_0 has a much larger impact on the IV-parameters than C_l. According to this simulation, which has been run with the ideal cell-model, V_{oc} and FF increases, and J_{sc} decreases slightly, with p_0, as long as $p_0 < 3 \times 10^{16}\,\mathrm{cm}^{-3}$. This goes for both $C_l = 1$ and $C_l = 2.45$. FF flattens out as p_0 increases, V_{oc} turns and starts declining, and J_{sc} starts declining at a larger rate. This results in η behaving in much the same way as V_{oc}: it increases with p_0 up to a certain point, then starts decreasing. The maximum in $\eta(p_0)$ is at $p_0 \sim 4 \times 10^{16}\,\mathrm{cm}^{-3}$ for both compensation levels. This corresponds to $\rho \sim 0.43\,\Omega\mathrm{cm}$.

The reason for the benefit of increasing p_0 up to $3 \times 10^{16}\,\mathrm{cm}^{-3}$ on the performance of the ideal cell-model is mainly due to FF. There is a gain of $5\%_{rel}$ in FF in this region, and only a gain of $\sim 1.2\%_{rel}$ in V_{oc}. This may seem surprising, given the similar shapes of $\eta(p_0)$ and $V_{oc}(p_0)$, as well as the knowledge that V_{oc} and η are often closely connected. However, this is not so surprising when considering the physical connection between FF and the bulk resistivity p_0. Since FF decreases with increased internal resistance, and ρ decreases with p_0, it is expected that FF increases with p_0. In the ideal cell-model at $p_0 < 4 \times 10^{16}\,\mathrm{cm}^{-3}$, this benefit overshadows the other mechanisms, causing p_0 to correlate positively with η.

The reason for the increase in V_{oc} with p_0 below $p_0 \sim 3 \times 10^{16}\,\mathrm{cm}^{-3}$ is due to the higher junction potential due to the increased doping level (Xiao et al., 2014). However, there is a decrease in both V_{oc} and J_{sc} at $p_0 \sim 5 \times 10^{16}\,\mathrm{cm}^{-3}$, causing a decrease in η when p_0 rises above this point. This decrease is caused by the increased Auger recombination. As is stated in section 2.4.1, Auger recombination lifetime is inversely proportional to p_0. At a certain point, the Auger recombination lifetime becomes so low, decreasing the effective lifetime so much, that this overshadows the benefit in a higher junction potential and lower internal resistance. This means that, according to the ideal cell-model, the advantage of increasing p_0 is lost at $p_0 \sim 4 \times 10^{16}\,\mathrm{cm}^{-3}$ due to Auger recombination. This causes a sharp decrease in both V_{oc} and J_{sc} above this doping level.

The V_{oc} is slightly higher for the non-compensated cell, according to this model. This effect increases with p_0. This cannot be due to increased incomplete ionization, since $i.i$ would give a lowering of the hole density $p_{0,i.i}$, effectively moving the compensated V_{oc}-curve to higher p_0 relative to the non-compensated one, and not decreasing the magnitude of V_{oc}. However, the largest effect of changing C_l was shown in the previous section to be the band gap size. This is not only connected to C_l, but to N_A and N_D in general. Thus this simulation indicates that increasing p_0 has a negative effect on the band gap size, as expected.

IV-parameters of PERC-model. When it comes to the PERC-model, the tendencies are the same as in the ideal model, as is seen in **Figure 4.14**. The biggest difference is that there is no peak in V_{oc} within the doping levels assessed here. Remember that the largest difference between the ideal model and the PERC-model is that the SRVs are non-zero in the latter, and that the back SRV scale linearly with p_0.

For the same reason as in the ideal model, there is a big change in FF with p_0; it increases with $\sim 5.2\%_{rel}$ over the range of simulated p_0s. However, in this model the biggest change happens in J_{sc}, which goes down by $\sim 7.3\%_{rel}$. This was ascribed Auger recombination in the ideal model. In the PERC-model, however, the decrease in J_{sc} is much larger, and starts at a smaller p_0. Thus it cannot be explained by Auger recombination alone. However, in the ideal model there is no surface recombination. Thus, this can be ascribed the SRVS, or more specifically: the scaling of the back SRV with p_0, which is described in section 3.3. It seems then that it is mainly J_{sc} that is affected by the increase in SRVs.

The behavior of V_{oc} with p_0 is less intuitive. Although there is a general positive correlation between V_{oc} and p_0, the small dip in V_{oc} at low p_0 has unknown causes. Also, the decrease at high p_0 that was observed in the simulations with the ideal model is not

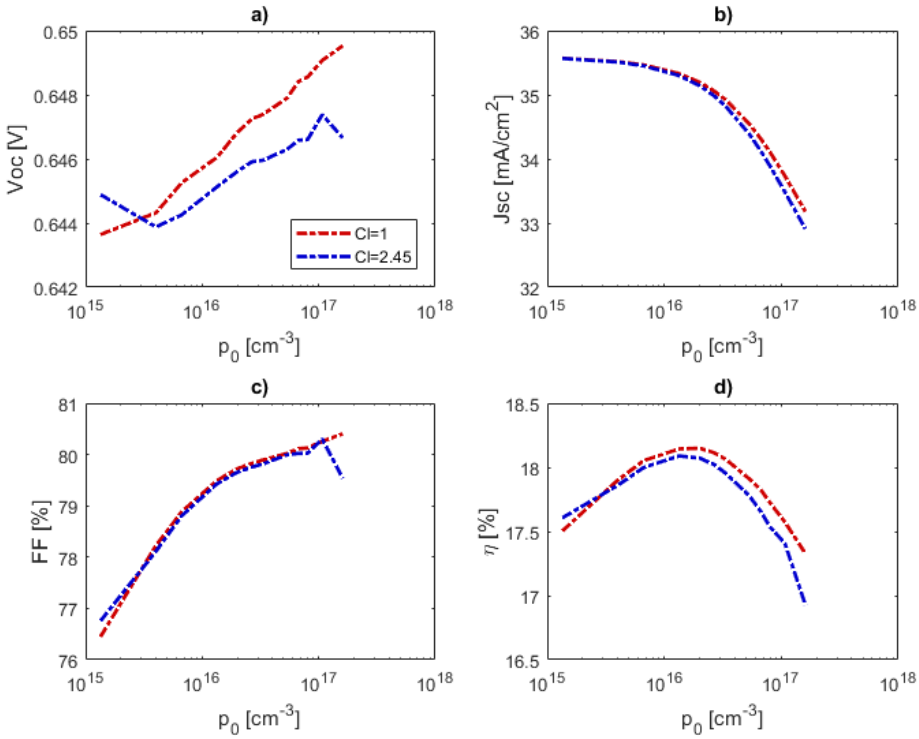

Figure 4.14: IV-parameters as they change with effective doping level p_0 in the PERC-model. The simulation was run with compensation level set to $C_l = 2.45$ (compensated) and $C_l = 1$ (non-compensated), and the lifetime is that of ESS 1.3 at $x = 0.45$.

present in the PERC-model. In the ideal-cell model, this was ascribed the lowering of the Auger lifetime τ_{Aug} with p_0. However, τ_{Aug} is strongly dependent on injection level Δn. As can be seen in **Figure 3.6**, the PERC-model operates at a lower Δn than the ideal model, where τ_{Aug} is considerably higher. This means the PERC-cell is not inhibited by Auger recombination within the doping levels applied here.

Further, the high SRVs are limiting τ_{eff} in this model. τ_{surf} also decreases with p_0, but not as fast as τ_{Aug}. The result is that the intrinsic advantage of increasing p_0 on V_{oc} defeats the disadvantage of increasing SRVs, and V_{oc} increases with p_0 in these doping levels.

Note also the difference in V_{oc} between compensated and non-compensated material. This difference gives a $\sim 0.1\%_{rel}$ advantage to the non-compensated cell in η at high p_0. This difference was ascribed the dependency of the band gap on C_l in the ideal model. This probably serves to explain some of the difference here too. However, according to section 4.3.3. C_l is expected to affect FF too. But there is virtually no difference in FF between the two. The cause of this is unknown.

At any rate, the result is a $\eta(p_0)$-curve that has a maximum at around $p_0 \sim 1.5 \times 10^{16}\,\mathrm{cm}^{-3}$

for both non-compensated and compensated Silicon. This corresponds to a resistivity of about $1.16\,\Omega\mathrm{cm}$.

At this point it is important to mention the coupling between p_0 and τ_{bulk}: as was discussed in section 4.1, an increase in p_0 leads to a decrease in τ_{bulk}. If this had been implemented in the model, it would have resulted in a negative effect of increasing p_0 in all the parameters. In specific, it means that the turning point in $\eta(p_0)$ in reality will happen at an earlier point, and that η will have a lower maximum at a lower p_0.

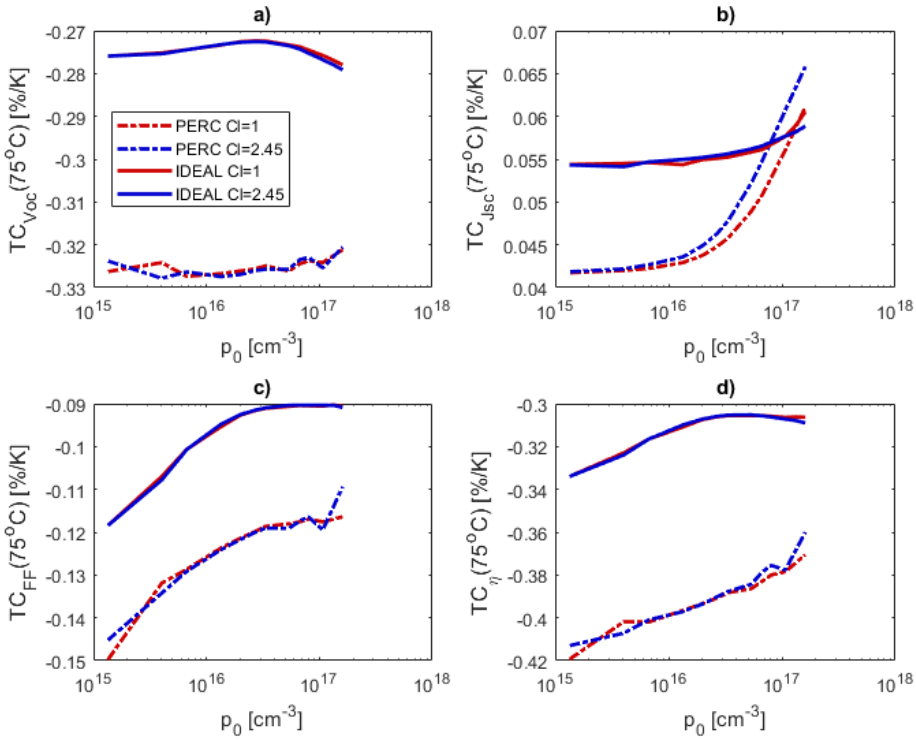

Figure 4.15: TCs of the IV-parameters as they change with effective doping level p_0 in the the ideal cell-model (solid lines) and the PERC-model (dashed lines). The simulation was run with compensation level set to $C_l = 2.45$ and $C_l = 1$, and the lifetime is that of ESS 1.3 at $x = 0.45$.

Temperature Coefficients. Considering the TCs in **Figure 4.15** it seems that p_0 correlates positively to TC_{FF} and $TC_{J_{sc}}$ for all p_0s and both models. $TC_{V_{oc}}$ varies little with p_0 in both models. In sum this results in TC_η increasing monotonously in the PERC-model, and increasing with p_0 until $p_0 \sim 5 \times 10^{16}\,\mathrm{cm}^{-3}$, where it decreases slightly, in the ideal model. The decrease after $p_0 \sim 5 \times 10^{16}\,\mathrm{cm}^{-3}$ is due to $TC_{V_{oc}}$, which increases slightly with p_0 until $p_0 \sim 4 \times 10^{16}\,\mathrm{cm}^{-3}$, where it starts decreasing.

At this point it is worth remembering the definition of the TCs. When looking at the

shape of the TC-curves of the ideal model, they seem to resemble the curves of the IV-parameters to a large degree. This is because of the normalization of the TCs. Even if there is no change in the slope of the IV-parameters as functions of T when p_0 is varied, the TCs may still change because there is a change in the IV-parameters themselves. In order to assess whether this is the whole reason for the variability of the TCs, we can plot the un-normalized values of the TCs, defined as $\Delta X/\Delta T = \frac{X(T)-X(25^\circ\mathrm{C})}{T-25^\circ\mathrm{C}}$ for each IV-parameter X. This was done (the plot is found in **Figure 6.8** in the Appendix), and it is clear that the change in the un-normalized TCs with p_0 is vanishingly small.

In the PERC-model, however, the change is small only in $\Delta V_{oc}/\Delta T$, but not in $\Delta FF/\Delta T$, and even less in $\Delta J_{sc}/\Delta T$. So there is a physical effect of changing p_0 on $TC_{J_{sc}}$ and TC_{FF} that needs to be explained. Remember, the biggest difference between the ideal model and the PERC-model is the SRVs and their dependency on p_0. The detrimental effect of p_0 on the back SRV is seen in J_{sc}. This does not directly affect $TC_{J_{sc}}$. However, from this it can be argued that when the SRVs are big enough, the detrimental effect on J_{sc} of increasing T is diminished. This happens because, as the back SRV increases, τ_{surf} decreases, and it becomes more and more determining for the effective lifetime. No explicit dependency in the SRVs on T has been implemented in the model. However, the front SRV depends on the doping profile in the emitter, which depends on the carrier densities, which again depends on both p_0 and temperature. This results in the effective lifetime not being as negatively influenced by increasing p_0 and T in the PERC-model as in the ideal model. This seems like the most likely candidate for the benefit of increased p_0 on $TC_{J_{sc}}$. This also explains the lack of a fall in $TC_{V_{oc}}$ with p_0, as well as the relatively steady increase in TC_{FF}.

At any rate, the independent effect of increasing p_0 is positive for TC_η of both models, if only up to $p_0 \sim 5 \times 10^{16}\,\mathrm{cm}^{-3}$ in the ideal model.

Section Summary. p_0 comes into play in several different mechanisms in a cell, and the net result is a hill-shaped $\eta(p_0)$-curve. Given constant lifetimes, there is a maximum in η at $p_0 \sim 4 \times 10^{16}\,\mathrm{cm}^{-3}$ in the ideal cell-model, corresponding to $\rho \sim 0.43\,\Omega\mathrm{cm}$. This is a result of the trade-off between an increase in FF due to reduced ρ, and a decrease in V_{oc} and J_{sc} due to increased Auger recombination. In the PERC-model the maximum is at $p_0 \sim 1.5 \times 10^{16}\,\mathrm{cm}^{-3}$, corresponding to $\rho \sim 1.16\,\Omega\mathrm{cm}$. The reason the maximum is at lower p_0 in the PERC-model is the detrimental effect of p_0 on surface recombination.

When it comes to the TCs, it turns out p_0 generally correlates positively with the TCs. However, the TCs of the ideal cell-model are largely ruled by the magnitude of the IV-parameters. It turns out increasing p_0 is beneficial to TCs of the PERC-model, resulting in a TC_η that rises steadily within the doping levels used here.

4.3.5 The Effect of Bulk Lifetime

By running the simulation of the ideal cell-model with different lifetime input, the impact of varying the SRH lifetime τ_{SRH} by 4 orders of magnitude could be investigated. The τ_{bulk}-curves of ESS 1.3 at $x = 0.45$, subtracted by the intrinsic recombination, multiplied by a given factor (τ-multiplier), were used in each simulation run. This way the magnitude of the lifetime is changed, but TC_τ is held constant. If not otherwise stated, the simulations

were run with $C_l = 2.45$ and $p_0 = 1.34 \cdot 10^{16}\mathrm{cm}^{-3}$. The IV-parameters are presented in **Figure 4.16**. In order to assess the relative importance of τ_{SRH} and TC_τ on the TCs of the IV-parameters, the simulation was run with TC_τ equal to 0, 0.5 and 1, and $p_0/10^{16}\,\mathrm{cm}^{-3}$ equal to 0.8, 1.34 and 4.0.

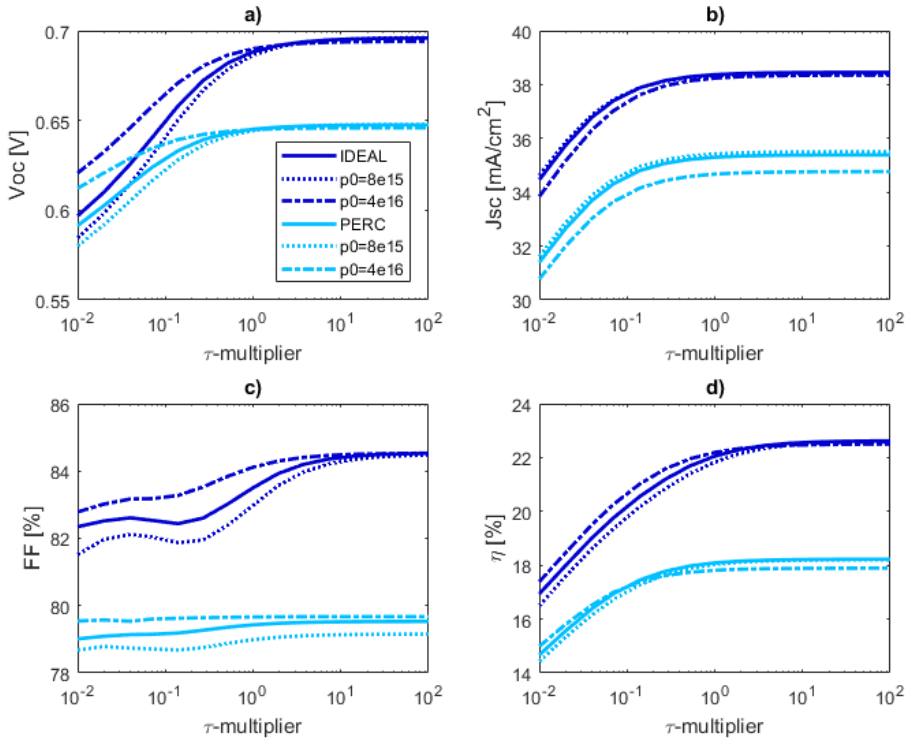

Figure 4.16: IV-parameters as they change with SRH lifetime τ_{SRH} and p_0 in the ideal cell- and PERC-model. If not otherwise stated, the simulations were run with $C_l = 2.45$ and $p_0 = 1.34 \cdot 10^{16}\mathrm{cm}^{-3}$, and the lifetime is that of ESS 1.3 at $x = 0.45$ multiplied by τ-multiplier, which goes between 0.01 and 100.

IV-parameters. The first thing to notice in **Figure 4.16** is that the IV-parameters increase with τ-multiplier until τ-multiplier reaches a certain τ_{crit}, before they saturate (we will come back to the feature in FF at τ-multiplier between 0.01 and 0.1 later). This means the cell reaches a limit, beyond which the effect of increasing the lifetime is negligible. This limit depends on the cell architecture and its parameters, something which has been studied extensively before (Steinkemper et al., 2016). As can be seen, the PERC-model saturates at a lower τ_{crit} than the ideal model, meaning the point in having a high quality feedstock is lost if the cell is not designed for high performance. It is worth to note, though, that even in the ideal cell-model, the gain of increasing the bulk lifetime above that

of ESS 1.3 (τ-multiplier$= 1$) is limited.

Surface recombination is not a limiting factor in the ideal cell-model, since the SRVs have been set to 0 there. This means that it must be intrinsic recombination that limits τ_{eff} at τ-multiplier > 1. Richters model for intrinsic recombination (Richter et al., 2012), which has been used in this case, predicts an intrinsic recombination lifetime between $7\,\mathrm{ms}$ and $9\,\mathrm{ms}$ in the relevant injection levels. This roughly corresponds to lifetimes around 15 times higher than the lifetime of ESS 1.3 at $x = 0.45$. This means that at τ-multiplier$= 10$, the gain of increasing τ_{bulk} is very limited. As is seen, this is the case, meaning intrinsic recombination is ultimately the reason for the saturation of the performance.

J_{sc} saturates at a lower τ_{bulk}. This means there must be another mechanism limiting J_{sc} than intrinsic recombination. The magnitude of J_{sc} cannot be larger than the ideal current $J_{Lg} = qG$. If all carriers are collected, $J_{sc} = J_{Lg}$. Thus when $L \gg W$, where $L \propto \sqrt{\tau\mu}$ is the diffusion length and W is the thickness of the cell, all the carriers are collected, and the gain in increasing τ is lost. Since μ is equal in the ideal and the PERC-model, τ_{crit} of J_{sc} is expected to be equal in the two models. As can be seen, this is the case, supporting the notion that $L \gg W$.

V_{oc}, on the other hand, is determined by the splitting of the quasi-Fermi levels, which depends on the carrier densities in the base and the emitter. Thus V_{oc} is not only determined by L, but also by the recombination rate itself, and increases as long as τ_{eff} increases. τ_{eff} is limited by the SRVs in the PERC-model, and by Auger recombination in the ideal model. This is the reason V_{oc} saturates at higher τ than J_{sc}, and at higher τ in the ideal model than in the PERC-model. As can be seen, at low τ, V_{oc} of the ideal and the PERC-model is almost equal. This is because the SRVs do not limit the performance of the PERC-model when τ_{bulk} is that low.

The behavior of the FF of the ideal model is less intuitive. First of all it seems to saturate at a higher τ than V_{oc}. It is well known that FF depends on V_{oc} (see equation (2.45)). However, the behavior of FF at low and medium bulk lifetimes seems to point to another limiting mechanism which depends on τ_{bulk}. The nature of this mechanism is unknown.

The FF of the PERC-model is virtually independent of τ, especially when p_0 is high. Further, the variation due to p_0 is much larger than the variation due to τ. This relatively small dependency of FF on τ may be caused by the low lifetime in the emitter. The lifetime in the emitter is independent of the bulk lifetime, but dependent on p_0, causing a small dependency of FF on τ, and a larger dependency on p_0.

As is seen, the effect of p_0 depends on the bulk lifetime. In the ideal model, when p_0 goes from $8 \times 10^{15}\,\mathrm{cm}^{-3}$ to $4 \times 10^{16}\,\mathrm{cm}^{-3}$, the performance increases by $\sim 1\%_{abs}$, as long as τ-multiplier is below 0.5. Interestingly, the simulation run with an increased p_0 saturates at a lower η, and at an earlier τ_{crit}. The simulation run with a lower p_0 also saturates at a lower η, but at a later τ_{crit}. Also, while p_0 is beneficial in FF and V_{oc}, it is detrimental in J_{sc}. None of this is surprising, considering the result of section 4.3.4. It was argued there that Auger recombination increases with p_0. This means that the higher the p_0, the lower the τ_{Aug}. A lower τ_{Aug} means a lower J_{sc} and a lower τ_{crit}. However, p_0 is beneficial for V_{oc}, and the net result on the performance of the cell depends on the bulk lifetime of the cell.

The same tendencies are seen in the PERC-model: p_0 is positively correlated with the

performance at low τ, and negatively correlated with p_0 at high τ. However, the results are slightly different in J_{sc} due to the dependency of the back SRVs on p_0. The simulation with the highest p_0 saturates at a considerably lower J_{sc}, and thus a lower η, than the others. This is exactly what was seen in section 4.3.4.

The calculation of the TCs of the ideal cell- and the PERC-model are presented in **Figure 4.17** and **4.18** respectively.

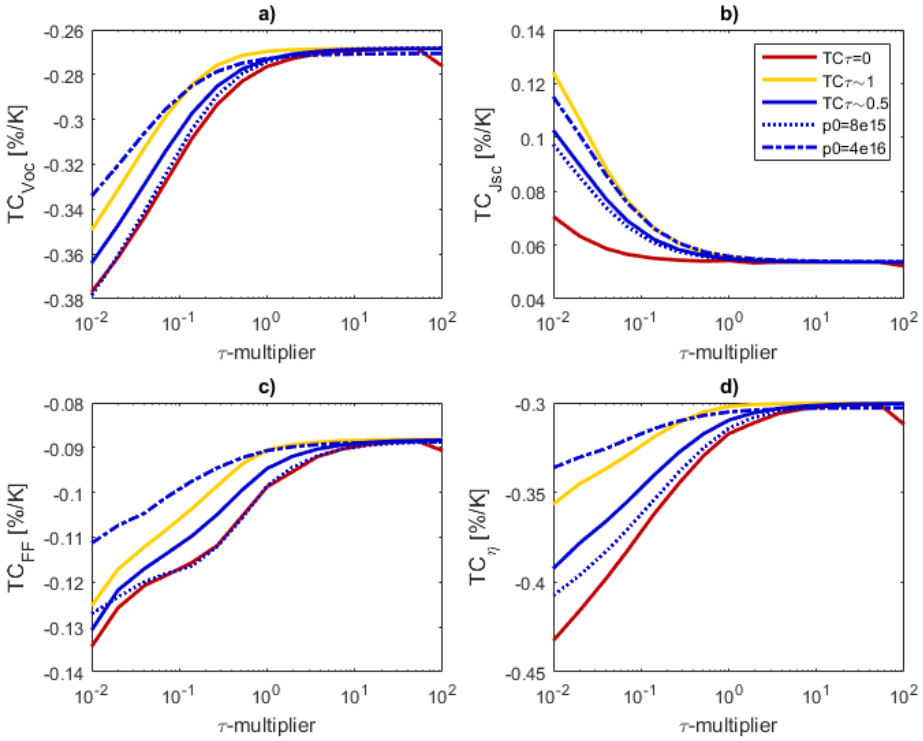

Figure 4.17: TCs of the ideal cell-model as they change with bulk lifetime τ_{bulk} and TC_τ. Five simulations were run, one with $TC_\tau = 0$, one with $TC_\tau = 1$, and three with the TC_τ of ESS 1.3 (~ 0.5) where p_0 was changed, as indicated in the legend. In all runs, $Cl = 2.45$.

Temperature Coefficients of Ideal Model. As was mentioned in the introduction to this section, the TCs have been calculated with varying TC_τ: Five simulations were run, with varying TC_τ and p_0. If not otherwise stated, the simulation is run with $TC_\tau \sim 0.5$ and $1.34 \times 10^{16}\,\mathrm{cm}^{-3}$. This way it is possible the quantify the relative impact of TC_τ and p_0.

Looking at **Figure 4.17**, two observations may be made:

(a) The magnitude of the TCs decreases with τ_{bulk},

(b) the TCs saturates at a certain level, and

(c) the maximum magnitudes of the TCs are not dependent on TC_τ, but they vary slightly with p_0;

(a) This may actually seem counter-intuitive. The lower τ_{bulk} is, the more τ_{bulk} decides the magnitude of τ_{eff}. Since there is a positive temperature dependency in τ_{bulk}, this effect alone should result in a less negative impact of increasing T when τ_{bulk} is low. However, the opposite trend is seen in TC_{FF} and $TC_{V_{oc}}$. An explanation might be that the TCs are mostly decided by the normalization of the TCs. By looking at the un-normalized TCs in **Figure 6.9** in the Appendix, though, it can be seen that this is not the case; the un-normalized TCs also have the same dependency on τ. The most likely explanation, then, is the dependency of TC_{FF} and $TC_{V_{oc}}$ on V_{oc}. Since V_{oc} increases with τ, and $\frac{dFF}{dT}$ and $\frac{dV_{oc}}{dT}$ increase with V_{oc}, TC_{FF} and $TC_{V_{oc}}$ follow the same trends as V_{oc}. When it comes to $TC_{J_{sc}}$, however, this follows the trend that seems intuitive; that the lowering of τ_{bulk} leads to a benefit due to a positive TC_τ. This is confirmed by the simulation with $TC_\tau = 0$ being almost independent of τ.

(b) The fact that the TCs saturate at a certain level of τ_{bulk} means they are limited by something other than τ_{bulk}. The reason TC_{FF} and $TC_{V_{oc}}$ saturate is the same reason the IV-parameters saturate, namely Auger recombination. The temperature dependence of Auger recombination is very slight, leading to a quenching of the positive effect on the TCs of increasing T when τ_{bulk} is high. Further, the saturation of $TC_{J_{sc}}$ is due to $L \gg W$. The saturation magnitude, $TC_{J_{sc}} = 0.054$, corresponds to the optical effect of BGN, which is constant with T in this model.

(c) The reason the magnitudes of the TCs at high τ_{bulk} do not vary with TC_τ follows from the previous discussion: since the saturation magnitude of the TCs is limited by Auger recombination here, increasing TC_τ does not help when τ_{bulk} is large. As can be seen, TC_η may reach $-0.3\%/\mathrm{K}$ even when $TC_\tau = 0$. However, the saturation happens at higher τ_{bulk} if $TC_\tau = 0$ than if $TC_\tau \sim 1$. Also, at low τ_{bulk}, the benefit of increasing TC_τ from 0 to 1 is large. The dependency of the TCs on p_0 is extensively discussed in section 4.3.4.

Now, to assess the relative impact of τ_{bulk} and TC_τ on the TCs, lets look at the variation of τ_{bulk} and TC_τ in the measurements in section 4.1. There, the maximum bulk lifetime varies by a factor of 8 between the different wafers, but the temperature coefficient of the lifetime only varies between $0.3 < TC_\tau < 0.75$. Looking at the area around τ-multiplier$= 1$, varying τ_{bulk} by a factor of 8 leads to a change in TC_η of $\sim 0.03\,\%/\mathrm{K}$, while changing TC_τ from 0 to 1 only changes TC_η by $\sim 0.02\,\%/\mathrm{K}$. This means that changing τ_{bulk} has a slightly larger impact on TC_η within the lifetime values measured in this thesis, according to the ideal model.

If we instead look at the area around τ-multiplier$= 0.1$, changing τ_{bulk} a factor of 10 and changing TC_τ from 0 to 1 both changes TC_η by $\sim 0.045\,\%/\mathrm{K}$. This means that if τ_{bulk} is lower, the effect of TC_τ is bigger.

Another thing that is clear when looking at **Figure 4.17** is that the size of p_0 plays a relatively large role in deciding the TCs. The three values of p_0 that have been chosen in the simulations correspond to: the actual effective doping level of ESS 1.3 at $x = 0.45$ ($1.34 \times 10^{16}\,\mathrm{cm}^{-3}$), the optimal doping level, according to section 4.3.4 ($4 \times 10^{16}\,\mathrm{cm}^{-3}$), and an arbitrary low doping level ($0.8 \times 10^{16}\,\mathrm{cm}^{-3}$). As can be seen, it is $TC_{V_{oc}}$ and TC_{FF} that are most affected by p_0.

Further, increasing p_0 is beneficial to all the TCs, in the range of p_0s applied here. This is exactly what to expect, given the results in section 4.3.4. The important exception to this is seen at high τ, where the simulation with the highest p_0 has a lower TC_η. This stems from the dependency of Auger recombination on p_0, which has been extensively discussed already. It is expected that the negative impact of p_0 at high lifetimes will be more pronounced in the PERC-model.

Of course, the coupling between p_0 and τ_{bulk}, which is not included in the model, would come into play in reality. Since an increase in p_0 leads to a decrease in τ_{bulk}, the benefit of increasing p_0 is not as large in reality as it seems here.

Curiously, $TC_{V_{oc}}$ and TC_{FF} of the simulation with $0.8 \times 10^{16}\,\mathrm{cm}^{-3}$ and the one with $TC_\tau = 0$ almost overlap, and even follow the exact same trend in TC_{FF}. This may be a coincidence, or it may indicate that the same physical phenomenon kicks in in these two simulations.

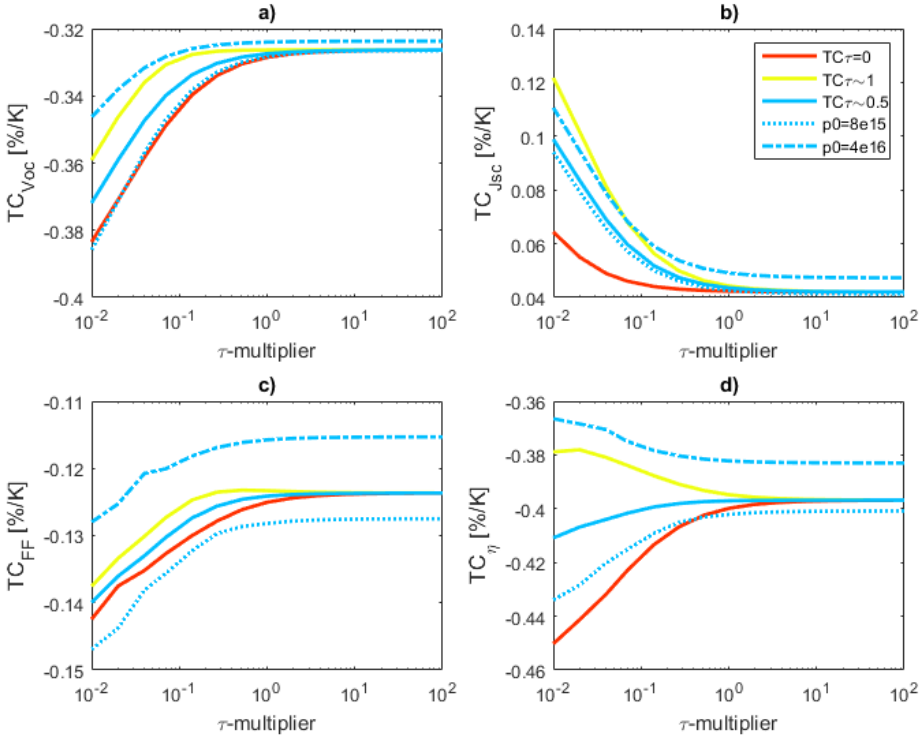

Figure 4.18: TCs of the PERC-model as they change with bulk lifetime τ_{bulk} and TC_τ. Three simulations were run, one with $TC_\tau = 0$, one with $TC_\tau = 1$, and three with the TC_τ of ESS 1.3 (~ 0.5) where p_0 was changed, as indicated in the legend. In all runs, $Cl = 2.45$.

Temperature Coefficients of PERC-Model. Looking at **Figure 4.18**, three immediate observations may be made:

(a) the magnitude of TC_η does not scale monotonously with τ_{bulk},

(b) TC_η varies more with TC_τ than with τ_{bulk}

(c) a high p_0 is beneficial to all TCs, and

(d) as in the ideal model, the simulations with equal p_0 saturate at the same level.

(a) Although the magnitude of both TC_{FF}, $TC_{V_{oc}}$ and $TC_{J_{sc}}$ decrease monotonously with τ_{bulk}, the result is that the magnitude of TC_η increases with τ_{bulk} when p_0 is high and $TC_\tau = 1$. Otherwise it decreases. This stems from the relative size of $TC_{J_{sc}}$, wich changes more with τ than TC_{FF} and $TC_{V_{oc}}$.

(b) The fact that TC_η varies more with TC_τ than with τ_{bulk} stems from the counterbalancing effects of TC_{FF}, $TC_{V_{oc}}$ and $TC_{J_{sc}}$ when it comes to variation with τ_{bulk}, and the mutually strengthening effects when it comes to variation with TC_τ. Although the variation of TC_η with τ_{bulk} is probably underestimated relative to reality here (since the SRVs are too high), the notion that TC_τ is more decisive for the TCs of a cell with bad surface passivation is probably true. This is confirmed by the TCs of the measured cells in section 4.2.2 which correlate well with TC_τ, at least qualitatively.

(c) The fact that increasing p_0 is not surprising, given the results in section 4.3.4. However, here it is shown that this holds for all bulk lifetimes.

(d) This was argued to be due to Auger recombination in the ideal model. In the PERC-model it is due to the onset of surface recombination, which depends on p_0, and not on TC_τ.

Section Summary. The maximum cell efficiency ($\eta \sim 22.6\%$) of the ideal cell-model is reached when τ_{SRH} is ten times that of ESS 1.3 at $x = 0.45$. Above this point the effective lifetime is limited by intrinsic recombination. However, the gain in increasing τ_{SRH} of ESS 1.3 tenfold is only $0.5\%_{abs}$.

The efficiency of the PERC-model, on the other hand, saturates at a lower τ_{SRH}, because it is limited by surface recombination, and the gain in increasing τ_{SRH} in this model is negligible. The fact that the two models are limited by intrinsic and surface recombination causes the optimal effective doping level to depend on bulk lifetime.

When it comes to temperature sensitivity, it turns out the magnitude of the lifetime is more decisive for the TCs than TC_τ in the ideal model. In the PERC-model, however, it is TC_τ that is decisive. Further, p_0 seems to be unequivocally positive to the TCs of the PERC-model.

To conclude, this implies that the most decisive factors of the TCs of solar cells are τ_{bulk}, TC_τ and p_0. The relative importance of these parameters, however, depends on the cell. If the SRVs are high, both p_0 and TC_τ are important. If the SRVs are low, the magnitude of τ_{bulk} is most important.

4.4 General Discussion

A lot has been said now about the correlation between p_0, C_l, τ_{bulk} and TC_τ, and the IV-parameters and their TCs. In this final section, an attempt at knitting together all the previous partial conclusions will be made, thus reaching a comprehensive understanding of the effect and relative significance of the different parameters. Specifically, the degree to which the simulation results are applicable to real life needs to be assessed, and the resulting conclusions need to be drawn.

We will start this discussion by pointing out the big takeaway of this thesis: that everything goes back to the lifetime.

What is meant by this is that the most important parameter, the one most strongly determining the performance of a solar cell at all temperatures, is τ_{bulk}. The reason this can be stated is most strongly seen in section 4.3.5. Although it seems, when looking at plot d) in **Figure 4.16**, that within the doping levels and lifetimes measured in the samples of this thesis, increasing p_0 may be more decisive than increasing τ_{bulk}, this conclusion is wrong. There is a coupling between p_0 and τ_{bulk} that has not been included in the model: raising p_0 may lead to a lowering of τ_{bulk}. This is seen in section 4.1 by the fact that ESS 0.5, the most heavily doped material, has a lifetime up to 8 times lower than ESS 1.3. Further, this is the reason the ESS 1.3-cells perform better than the ESS 0.5-cells, which is seen in **Figure 4.5**. In section 4.3.4 it is shown that varying p_0 affects the performance of a cell. However, judging from the measurements, the indirect effect p_0 has on the performance of a cell through its effect on τ_{bulk} is bigger than the direct effect it has on the performance. This means that it is first of all τ_{bulk} we need to look at when it comes to the performance of a cell.

Further, from plot d) in **Figure 4.17**, it can be seen that, when the SRVs are low, the magnitude of the lifetime is more determining for TC_η than TC_τ is, within the doping levels and lifetimes measured in the samples of this thesis. When the SRVs are high, however, TC_τ is more determining for $TC\eta$, as can be seen in **Figure 4.18**. It seems this is the case for the measured PERC-cells too, since a high correlation between TC_τ and TC_η is seen there. For instance, TC_η of the ESS 0.5-cells, which have high TC_τ, are among the least negative. However, due to the low bulk lifetimes in these cells, their performance at 25 °C is worse than the other cells, and the good TCs do not make up for this, as is seen in **Figure 4.5**. This goes to emphasize the point that, even though you want as small TC_η as possible, you don't want this if it decreases the performance of the cell.

However, there is no one-to-one relationship between TC_τ and τ_{bulk}. Comparing the measured TCs of the cells made of ESS 1.3 and REF 1.3 in **Figure 4.2.2**, the cells that perform equally well also end up with almost identical TCs. The pair of cells from the ingot position where ESS 1.3 exhibits less negative TCs is the only pair that has different $\eta(25°\mathrm{C})$, and the $\eta(25°\mathrm{C})$ of ESS is higher. It was argued that the small TC_η can not be explained by the normalization by η, but that it is due to a higher TC_τ, as well as a higher V_{oc}, leading to a less negative $TC_{V_{oc}}$. The higher V_{oc} is explained by the higher bulk lifetime. This leads to a cell with both a higher $\eta(25°\mathrm{C})$ and a less negative TC_η.

The modeling of the PERC cells indicate that the SRVs of the measured cells are not as high as in the PERC-model. Also, the tendencies in the measured IV-parameters as they vary with material and ingot position correlate well with τ_{bulk}, which is emulated by the ideal model. This indicates that the ideal model is more similar to the measured

PERC-cells than initially assumed. Thus, τ_{bulk} is more decisive for the IV-parameters of the measured PERC-cells than the PERC-model shows. And in the ideal model, i.e. when SRVs are low, τ_{bulk} is also shown to be the most decisive parameter for the TCs. Further, considering the development in the industry when it comes to cell production, surface passivation is only expected to improve. This will lead to tendencies more and more in line with what was concluded about the ideal cell-model.

Thus we see that the bulk lifetime is ultimately more decisive than TC_τ when it comes to the performance of a cell at all (relevant) temperatures. This means that the notion that it all goes back to the lifetime is warranted. Although the degree to which τ_{bulk} determines the TCs depends on the material as well as the cell architecture, it is τ_{bulk} that in the end is most decisive for the performance..

This leads to the conclusion that the previously measured benefit in the TCs of ESS-cells relative to equally rated polysilicon reference cells (Berthod, 2016; Berthod et al., 2016) can be traced back to higher lifetimes. Further, a hypothesis may be proposed. First, note that if two cells of different bulk material are to be compared in terms of their TCs, they need to perform similarly at $25\,^{\circ}\mathrm{C}$. The hypothesis is that *if an ESS-cell performing equally well to a polysilicon cell has a less negative TC_η, it is due to a higher bulk lifetime*. This high bulk lifetime will result in a higher TC_τ, a higher V_{oc}, leading to a less negative $TC_{V_{oc}}$, and a less negative TC_η. According to (Berthod, 2016; Berthod et al., 2016), a statistical significant amount of ESS-cells with comparable η to polysilicon-cells exhibit a less negative TC_η. These cells in average have higher V_{oc}s, indicating higher lifetimes. However, the lifetime is not measured in these experiments, and the connection is not made.

The reason why ESS-cells need to have higher lifetimes to perform equally well as polysilicon-cells will not be attempted justified here. However, the notion that ESS generally has higher lifetimes than the polysilicon reference used here is confirmed by the lifetime measurements presented in section 4.1. This may be due to a different content of impurities.

The above hypothesis is strengthened by the IV-measurements of the cells from high x presented in section 4.2. At low x, the cells that perform equally well also have almost equal lifetimes and equal TCs. However, the reference material was designed to have resistivity $\rho \sim 1.3$. Scheil's equation shows that it probably has a lower p_0, and thus a higher ρ, than ESS 1.3 at low ingot positions (see **Figure 3.1**). This may be the reason why the lifetime of REF 1.3 and ESS 1.3 is equally large at low x. At any rate, this means that the cells of comparable η have different p_0, and according to the modeling results, p_0 has an important part to play. Thus these cells are not directly comparable.

Of course, it is important to note that if the above stated hypothesis is true; that any benefit in the TCs of ESS-cells relative to similarly rated polysilicon-cells stems from a higher bulk lifetime, this still means that these ESS-cells will perform better than the reference cells in high temperatures. This should be reflected in the pricing of the corresponding PV-modules. This is not to say that ESS necessarily always has higher bulk lifetimes than polysilicon. As was mentioned in section 3.1, the polysilicon reference used in this thesis has a certain blend-in ratio of Silicon produced in a fluidized bed reactor, and is therefore not the purest Silicon you can acquire. However, both ESS and the reference are cheap alternatives to EG-Silicon, and comparing them is warranted.

This means that, in the end, the way to improve the temperature sensitivity of a solar cell is to improve the performance of the cell. Thus, what is most important for the material producer, regardless of what temperature the cells will operate in, is to maximize the performance. To a certain extent, this means maximizing the bulk lifetime. For the material producer, this is done by minimizing the impurity contents, and optimizing the doping levels. However, the exact value of an optimal p_0 will not be the p_0 yielding the highest bulk lifetime. Since there are other effects of increasing p_0, like a benefit in V_{oc}, the optimal p_0 is slightly higher than this.

One benefit of doing compensation engineering is that one can get a more even resistivity profile in the ingot. This means that it is possible to find the optimal p_0 given the material quality, and make sure this doping level is reached for an increased fraction of the wafers cut from the ingot.

Chapter 5

Conclusion

The motivation of writing this thesis was to reach an increased understanding of the temperature sensitivity of solar cells in general, and cells made of Elkem Solar Silicon®(ESS) in specific. This has been achieved, and the conclusions reached are summed up here.

To split it up, we go back to the goals set in the Introduction, which were:

1. to measure the minority carrier lifetime in wafers made of ESS and polysilicon,
2. to measure the IV-parameters and the temperature coefficients (TCs) of cells made of ESS and polysilicon,
3. to assess the impact of lifetime and doping levels on the IV-parameters and their TCs of solar cells made from ESS and polysilicon, and
4. ultimately to explain the reason for the previously measured advantages in the TCs of ESS-cells.

1.) This was done, as seen in section 4.1, and the measurements showed that the ESS-wafers with $\rho \sim 1.3$ (ESS 1.3) had higher lifetimes than the polysilicon reference (REF 1.3), except at low ingot positions x. ESS 1.3 showed to have a higher temperature coefficient of the lifetime TC_τ at high x. The measurements also showed that the low resistivity ρ (high p_0) ESS-wafers had significantly lower bulk lifetimes than the other cells, but it had the highest TC_τ. The variation in the lifetime within the ESS-wafers corresponds well with the expected correlation between bulk lifetime and p_0.

2.) The IV-parameters and the TCs were measured, as seen in section 4.2, and the IV-parameters showed to have a strong correlation to the bulk lifetimes τ_{bulk}. The TCs showed to correlate with TC_τ as well as V_{oc}.

3.) In section 4.3, through the modeling of the measured PERC-cells, as well as the sensitivity analysis done on the different material parameters, it was shown that it is mostly the bulk lifetime, p_0 and TC_τ that determines the performance and temperature sensitivity. More specifically, the relative impact of the different parameters depends on the quality of the surface passivation: If the surface recombination velocities (SRVs) are high, τ_{bulk}

decides the performance, and p_0 and TC_τ decides the TCs. If the SRVs are low, τ_{bulk} is decisive for both. Further, there is an optimal p_0 for all cells. Assuming no coupling between p_0 and τ_{bulk}, the optimal level is $\sim 1.5 \times 10^{16}\,\mathrm{cm}^{-3}$ according to the PERC-model, and $\sim 4 \times 10^{16}\,\mathrm{cm}^{-3}$ according to the ideal model. However, in reality there is a negative correlation between p_0 and τ_{bulk}, so that the beneficial impact of increased p_0 is reduced.

4.) In the General Discussion (section 4.4) a hypothesis is made, stating that *if an ESS-cell performing equally well to a polysilicon cell has a less negative TC_η, it is due to a higher bulk lifetime*. In other words, an ESS-cell will often need higher lifetimes to perform as well as a cell made of the polysilicon reference material, which will lead to a higher TC_τ as well as a higher V_{oc}, giving it a less negative TC_η. This might explain why ESS-based PV modules in average show higher performance ratios than modules based on the reference material.

Chapter 6

Further Work

There are several ways to reach a more thorough understanding of the topic of this thesis, as well as either strengthening or falsifying the statements made. Some of these involve acquiring a bigger, more robust data set, and some of them involve improving the modeling part.

Starting with the acquisition of data, the most helpful initiative would be to get a more robust set of lifetime measurements. This would constitute a solid foundation for making statements about the lifetime of ESS compared to other materials as it varies with doping levels, as well as making it possible to identify the impurity content through TIDLS. By using temperature dependent PL-imaging, lifetime maps of the wafers can be acquired, so that this can be done on each position of the wafers. Further, if this is done on wafers from the same positions in the ingots as previously measured cells, this gives a more robust foundation for linking lifetime to cell performance as it varies with temperature. IV-measurements have already been performed on a large amount of cells by Berthod et al, and wafers from the same ingots as these cells are good candidates for these lifetime measurements. Specifically, this would make it possible to falsify the hypothesis that the benefit in the TCs of ESS-cells comes from higher lifetimes.

The modeling is most obviously improved by going over to a 2D or 3D modeling software like Silvaco or Quokka. Then it is possible to emulate the lateral carrier logistics, which arguably is important in cell architectures like PERC. Further, the effect of grain boundaries and defects in the bulk, in other words non-homogeneous lifetimes in the wafer, is possible to account for by using analytical circuit-models like Griddler. The model can be further improved by fitting more of the cell parameters to the measured cells, as well as implementing a temperature dependence in the surface recombination rates, and a more realistic dependency of τ_{bulk} on p_0. Even if a more accurate model is not developed, the scope of the simulations can be increased, possibly making a many-dimensional map of the IV parameters as they change with T, τ, the SRVs, p_0 and TC_τ.

Bibliography

Aberle, A. G., 1999. Crystalline silicon solar cells : advanced surface passivation and analysis. Centre for Photovoltaic Engineering, University of New South Wales Sydney.

Altermatt, P. P., Schenk, A., Heiser, G., 2006. A simulation model for the density of states and for incomplete ionization in crystalline silicon. I. Establishing the model in Si:P. Journal of Applied Physics.

Antonio Luque, S. H., 2011. Handbook of Photovoltaic Science and Engineering, 2nd Edition. Wiley.

B M Girisch, R., P. Mertens, R., F. De Keersmaecker, R., 03 1988. Determination of si-sio2 interface recombination parameters using a gate-controlled point-junction diode under illumination 35, 203 – 222.

Berthod, C., 2016. Temperature coefficients of silicon solar cells.

Berthod, C., Strandberg, R., Odden, J. O., 2015. Temperature Coefficients of Compensated Silicon Solar Cells - Influence of Ingot Position and Blend-in-ratio. In: Energy Procedia.

Berthod, C., Strandberg, R., Odden, J. O., Saetre, T. O., 2016. Reduced Temperature Sensitivity of Multicrystalline Silicon Solar Cells with Low Ingot Resistivity (4898), 1–5.

Brody, J., Rohatgi, A., 2001. Analytical approximation of effective surface recombination velocity of dielectric-passivated p-type silicon. Solid-State Electronics 45 (9), 1549–1557.

Clugston, D., Basore, P., 1997. PC1D version 5: 32-bit solar cell modeling on personal computers. Conference Record of the Twenty Sixth IEEE Photovoltaic Specialists Conference - 1997, 207–210.
URL http://ieeexplore.ieee.org/document/654065/

Cuevas, A., Forster, M., Rougieux, F., Macdonald, D., 2012. Compensation engineering for silicon solar cells. Energy Procedia 15 (2011), 67–77.
URL http://dx.doi.org/10.1016/j.egypro.2012.02.008

Dubois, S., Enjalbert, N., Garandet, J. P., 2008. Effects of the compensation level on the carrier lifetime of crystalline silicon. Applied Physics Letters 93 (3).

Dupré, O., Vaillon, R., Green, M. A., 2015. Physics of the temperature coefficients of solar cells. Solar Energy Materials and Solar Cells 140, 92–100.

F. Tanay, S. Dubois, N. E., Veirman, J., 2011. Low temperature-coefficient for solar cells processed from solar-grade silicon purified by metallurgical route. PROGRESS IN PHOTOVOLTAICS: RESEARCH AND APPLICATIONS 19, 966–972.
URL http://dx.doi.org/10.1002/pip.1104

Forster, M., Cuevas, A., Fourmond, E., Rougieux, F. E., Lemiti, M., 2013a. Impact of incomplete ionization of dopants on the electrical properties of compensated p-type silicon. IEEE Journal of Photovoltaics.

Forster, M., Rougieux, F. E., Cuevas, A., Dehestru, B., Thomas, A., Fourmond, E., Lemiti, M., 2013b. Incomplete ionization and carrier mobility in compensated p-type and n-type silicon. IEEE Journal of Photovoltaics.

Green, M. A., 2003. General temperature dependence of solar cell performance and implications for device modelling. Progress in Photovoltaics: Research and Applications 11 (5), 333–340.

Green, M. A., 2008. Self-consistent optical parameters of intrinsic silicon at 300 K including temperature coefficients. Solar Energy Materials and Solar Cells 92 (11), 1305–1310.

Haug, H., 2014. New Methods for Investigation of Surface Passivation Layers for Crystalline Silicon Solar Cells, 169.

Haug, H., Greulich, J., 2016. PC1Dmod 6.2 - Improved Simulation of c-Si Devices with Updates on Device Physics and User Interface. In: Energy Procedia.

Haug, H., Greulich, J., Kimmerle, A., Marstein, E. S., 2015. PC1Dmod 6.1 state-of-the-art models in a well-known interface for improved simulation of Si solar cells. Solar Energy Materials and Solar Cells 142 (August), 1–7.
URL http://www.sciencedirect.com/science/article/pii/S0927024815002640

Haug, H., Wiig, M. S., S??nden??, R., Wong, J., 2016. Simulating the Effect of Lifetime Non-uniformity on Solar Cell Performance Using cmd-PC1D 6 and Griddler 2. In: Energy Procedia.

ISE, 2017. Photovoltaics Report (July).
URL https://www.ise.fraunhofer.de/content/dam/ise/de/documents/publications/studies/Photovoltaics-Report.pdf

Klaassen, D. B. M., 1992a. A unified mobility model for device simulation-II. Temperature dependence of carrier mobility and lifetime. Solid State Electronics 35 (7), 961–967.

Klaassen, D. B. M., 1992b. Simulation–I . Model Equations and Concentration Dependence. Solid-State Electronics 35 (7).

MacDonald, D., Cuevas, A., 2011. Recombination in compensated crystalline silicon for solar cells. Journal of Applied Physics 109 (4).

Min, B., Muller, M., Wagner, H., Fischer, G., Brendel, R., Altermatt, P. P., Neuhaus, H., 2017. A Roadmap Toward 24% Efficient PERC Solar Cells in Industrial Mass Production. IEEE Journal of Photovoltaics (September), 1–10.
URL http://ieeexplore.ieee.org/document/8048349/

Modanese, C., Acciarri, M., Binetti, S., Søiland, A.-K., Di Sabatino, M., Arnberg, L., 2012. Temperature-dependent Hall-effect measurements of p-type multicrystalline compensated solar grade silicon. Prog. Photovolt: Res. Appl.
URL http://dx.doi.org/10.1002/pip.1160

Murphy, J. D., Bothe, K., Krain, R., Voronkov, V. V., Falster, R. J., 2012. Parameterisation of injection-dependent lifetime measurements in semiconductors in terms of Shockley-Read-Hall statistics: An application to oxide precipitates in silicon. Journal of Applied Physics 111 (11).

Neamen, D., 1997. Semiconductor Physics And Devices, 2nd Edition. McGraw-Hill, Inc., New York, NY, USA.

Nelson, J., 2003. The physics of solar cells.

Nguyen, H. T., Rougieux, F. E., Mitchell, B., Macdonald, D., 2014. Temperature dependence of the band-band absorption coefficient in crystalline silicon from photoluminescence. Journal of Applied Physics 115 (4).

Pizzini, S., 2012. Advanced Silicon Materials for Photovoltaic Applications. John Wiley & Sons, Ltd.
URL http://dx.doi.org/10.1002/9781118312193

Ponce-Alcántara, S., Connolly, J. P., Sánchez, G., Míguez, J. M., Hoffmann, V., Ordás, R., 2014. A Statistical Analysis of the Temperature Coefficients of Industrial Silicon Solar Cells. Energy Procedia 55 (March), 578–588.
URL http://linkinghub.elsevier.com/retrieve/pii/S1876610214012533

Rand, B. P., Genoe, J., Heremans, P., Poortmans, J., 2007. Solar Cells Utilizing Small Molecular Weight Organic Semiconductors. Prog. Photovolt: Res. Appl. 15 (February 2013), 659–676.
URL http://dx.doi.org/10.1002/pip.1160

REC, 2016. Rec achieves milestone efficiency for multicrystalline solar cells.
URL http://www.recgroup.com/en/rec-achieves-milestone-efficiency-multi

Rein, S., 2005. Lifetime Spectroscopy - A method of Defect Characterization in Silicon for Photovoltaic Applications. Springer.

Reinders, A., Verlinden, P., Sark, M., Freundlichvan, A., 2017. Photovoltaic solar energy. Wiley.

Richter, A., Werner, F., Cuevas, A., Schmidt, J., Glunz, S. W., 2012. Improved parameterization of Auger recombination in silicon. Energy Procedia 27, 88–94.
URL http://dx.doi.org/10.1016/j.egypro.2012.07.034

Rougieux, F. E., MacDonald, D., Cuevas, A., Ruffell, S., Schmidt, J., Lim, B., Knights, A. P., 2010. Electron and hole mobility reduction and Hall factor in phosphorus-compensated p -type silicon. Journal of Applied Physics 108 (1).

Schenk, A., 1998. Finite-temperature full random-phase approximation model of band gap narrowing for silicon device simulation. Journal of Applied Physics 84 (7), 3684–3695.
URL http://aip.scitation.org/doi/10.1063/1.368545

Schindler, F., Forster, M., Broisch, J., Schön, J., Giesecke, J., Rein, S., Warta, W., Schubert, M. C., 2014. Towards a unified low-field model for carrier mobilities in crystalline silicon. Solar Energy Materials and Solar Cells.

Sio, H. C., Phang, S. P., Zheng, P., Wang, Q., Chen, W., Jin, H., Macdonald, D., 2017. Recombination sources in p-type high performance multicrystalline silicon. Japanese Journal of Applied Physics 56 (8S2), 08MB16.
URL http://stacks.iop.org/1347-4065/56/i=8S2/a=08MB16?key=crossref.5b1400443404e224805e52c92d664503

Solar Power Europe, 2016. Global Market Outlook For Solar Power / 2016-2020.

Søndenå, R., Berthod, C., Odden, J. O., Søiland, A.-K., Wiig, M. S., Stensrud Marstein, E., 2015. Temperature dependent quantum efficiencies in multicrystalline silicon solar cells. Energy Procedia 77 (77), 639–645.
URL www.sciencedirect.com

Sproul, A. B., 1994. Dimensionless solution of the equation describing the effect of surface recombination on carrier decay in semiconductors. Journal of Applied Physics 76 (5), 2851–2854.

Steinkemper, H., Hermle, M., Glunz, S. W., 2016. Comprehensive simulation study of industrially relevant silicon solar cell architectures for an optimal material parameter choice. Prog. Photovolt: Res. Appl. 24 (April 2016).
URL http://dx.doi.org/10.1002/pip.1160

Tayyib, M., Odden, J. O., Ramchander, N., Prakash, M. B., Surendra, T. S., Muneeshwar, R., Sarma, A. V., Ramanjaneyulu, M., Saetre, T. O., 2013. Performance assessment of a grid-connected mc-Si PV system made up of silicon material from different manufacturing routes. In: Conference Record of the IEEE Photovoltaic Specialists Conference.

Tayyib, M., Odden, J. O., Ramchander, N., Prakash, M. B., Surendra, T. S., Muneeshwar, R., Sarma, A. V., Ramanjaneyulu, M., Saetre, T. O., 2014a. Two years performance comparison of Elkem Solar multicrystalline silicon with polysilicon in a PV grid-connected system. In: 2014 IEEE 40th Photovoltaic Specialist Conference, PVSC 2014.

Tayyib, M., Odden, J. O., Saetre, T. O., 2014b. Influence of spectral composition on the temperature coefficients of solar cells from Elkem Solar. In: 2014 IEEE 40th Photovoltaic Specialist Conference, PVSC 2014.

Tayyib, M., Odden, J. O., Saetre, T. O., 2014c. Irradiance dependent temperature coefficients for MC solar cells from Elkem solar grade silicon in comparison with reference polysilicon. In: Energy Procedia.

Wasmer, S., Greulich, J., Hoffler, H., Wohrle, N., Demant, M., Fertig, F., Rein, S., 2017. Impact of material and process variations on the distribution of multicrystalline silicon perc cell efficiencies. IEEE Journal of Photovoltaics 7 (1), 118–128.

Xiao, C., Yang, D., Yu, X., Gu, X., Que, D., 2012a. Influence of the compensation level on the performance of p-type crystalline silicon solar cells: Theoretical calculations and experimental study. Solar Energy Materials and Solar Cells 107, 263–271.
URL http://dx.doi.org/10.1016/j.solmat.2012.06.046

Xiao, C., Yang, D., Yu, X., Wang, P., Chen, P., Que, D., 2012b. Effect of dopant compensation on the performance of Czochralski silicon solar cells. Solar Energy Materials and Solar Cells 101, 102–106.
URL http://dx.doi.org/10.1016/j.solmat.2012.02.023

Xiao, C., Yu, X., Yang, D., Que, D., 2014. Impact of solar irradiance intensity and temperature on the performance of compensated crystalline silicon solar cells. Solar Energy Materials and Solar Cells 128, 427–434.
URL http://dx.doi.org/10.1016/j.solmat.2014.06.018

Zhao, J., Wang, A., Robinson, S. J., Green, M. A., 1994. Reduced temperature coefficients for recent highperformance silicon solar cells. Progress in Photovoltaics: Research and Applications 2 (3), 221–225.

Appendix

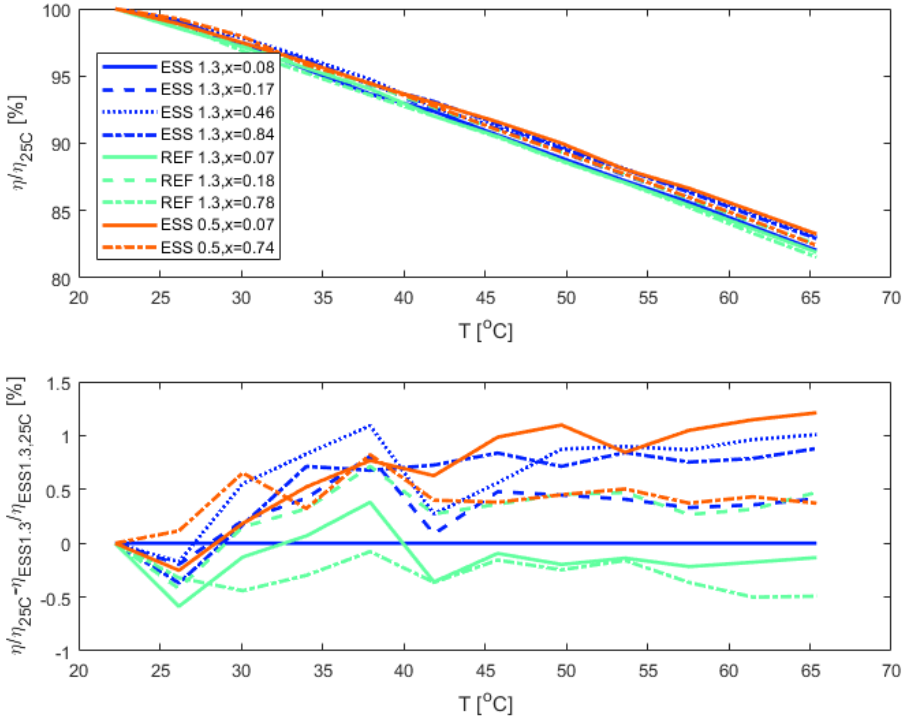

Figure 6.1: First: Temperature dependent efficiency of measured cells, normalized by efficiency at 25°C. Second: Difference between the normalized efficiencies.

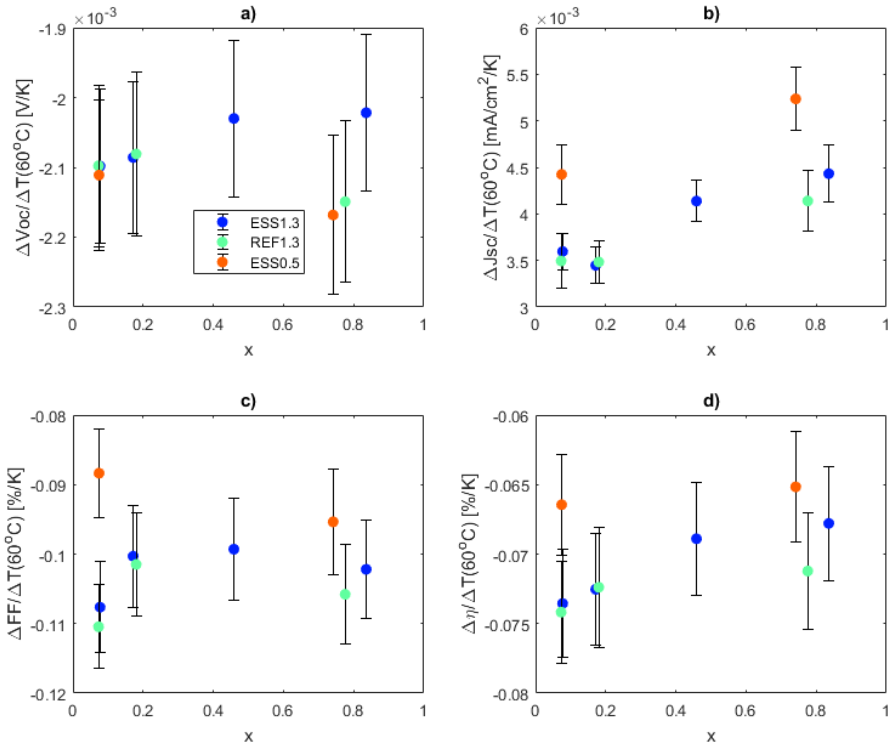

Figure 6.2: Un-normalized TCs, defined as $\Delta X/\Delta T = \frac{X(T)-X(25^{\circ}C)}{T-25^{\circ}C}$, of the IV-parameters of the measured cells presented in **Figure 4.5**.

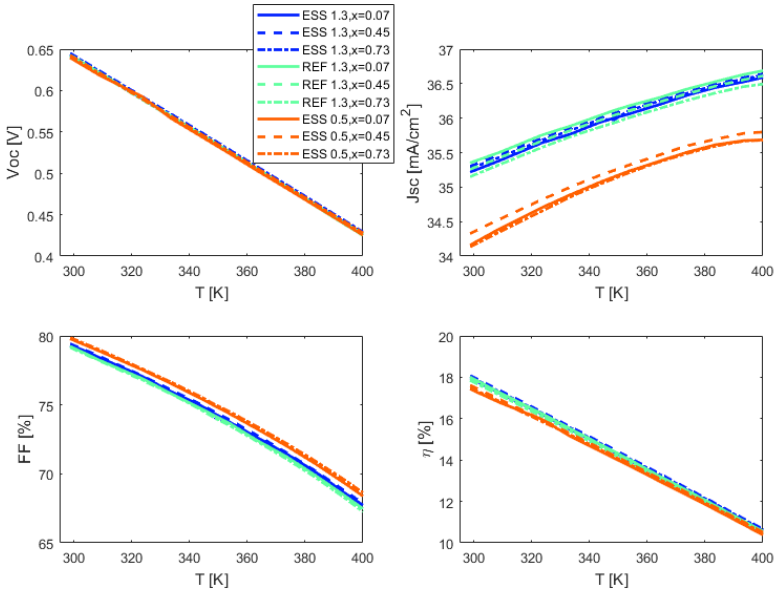

Figure 6.3: IV-parameters of the PERC-model as they vary with T, simulated with real lifetimes from the measurements in section 4.1 and real compensation and doping levels from Scheil's equation.

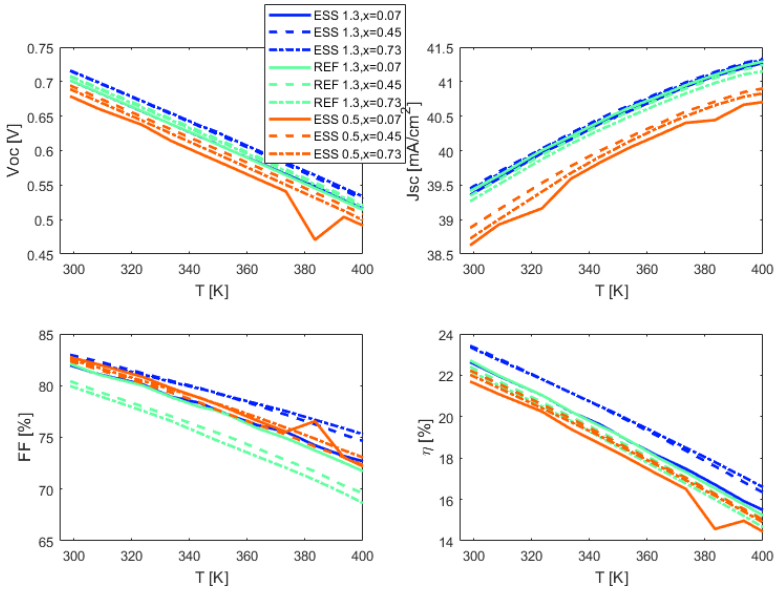

Figure 6.4: IV-parameters of the ideal cell-model as they vary with T, simulated with real lifetimes from the measurements in section 4.1 and real compensation and doping levels from Scheil's equation.

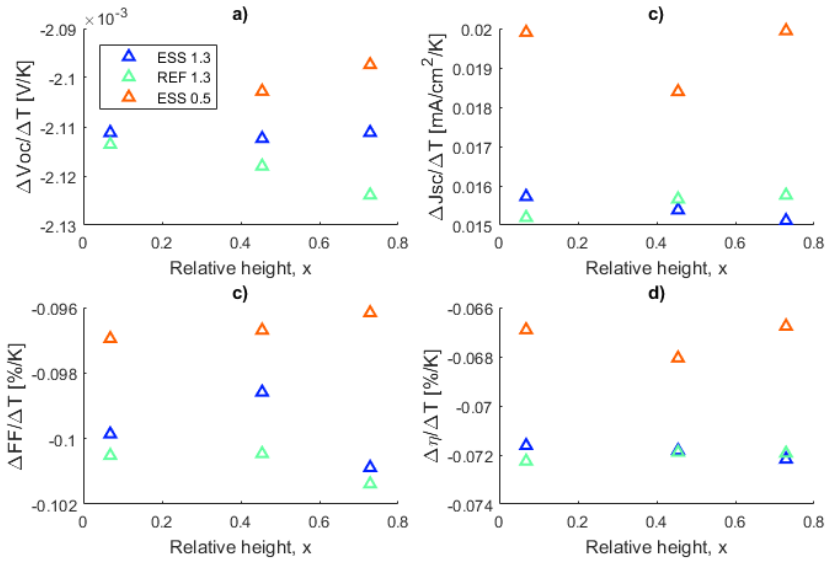

Figure 6.5: Un-normalized TCs, defined as $\Delta X/\Delta T = \frac{X(T)-X(25^{\circ}\mathrm{C})}{T-25^{\circ}\mathrm{C}}$, of the PERC-model (triangles) and measurements (circles).

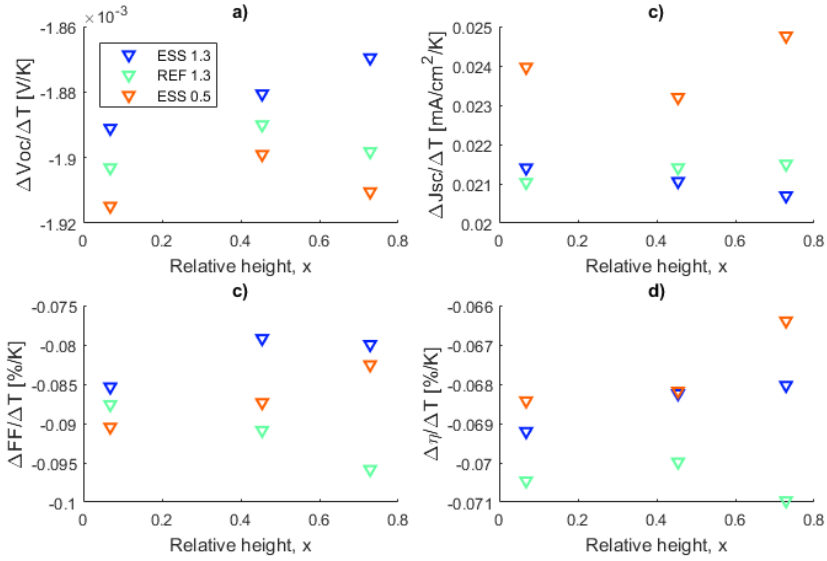

Figure 6.6: Un-normalized TCs, defined as $\Delta X/\Delta T = \frac{X(T)-X(25^{\circ}\mathrm{C})}{T-25^{\circ}\mathrm{C}}$, of the ideal cell-model, derived from the data presented in **Figure 6.4**.

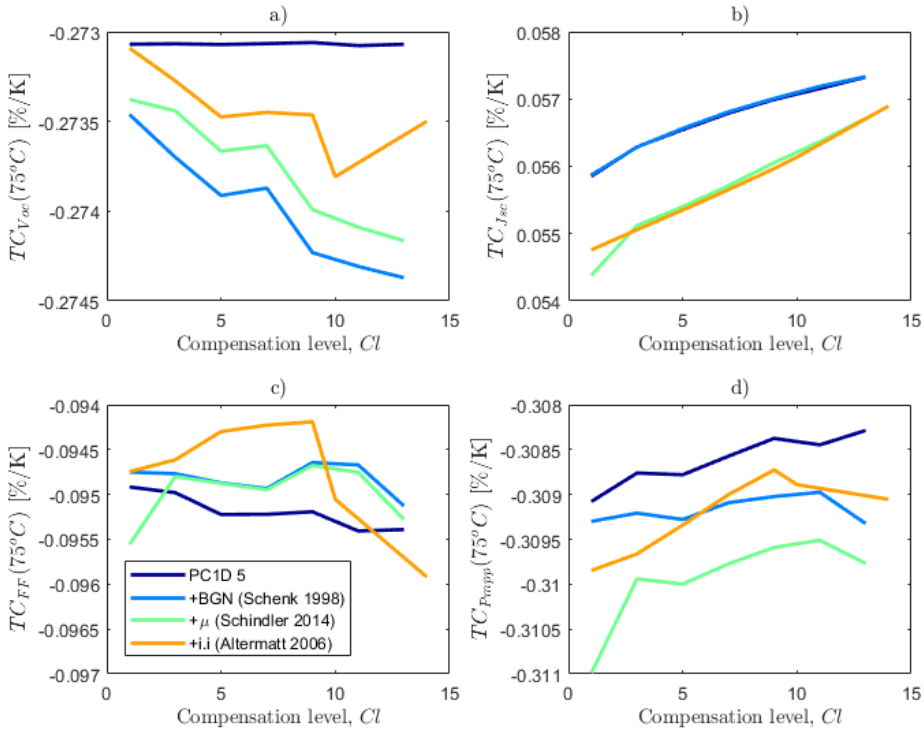

Figure 6.7: TCs of the IV-parameters as they change with compensation level C_l. The effective doping level is constant; $p_0 = 1 \times 10^{16}$ cm^{-3}, and the lifetime is that of ESS 1.3 at $x = 0.45$.

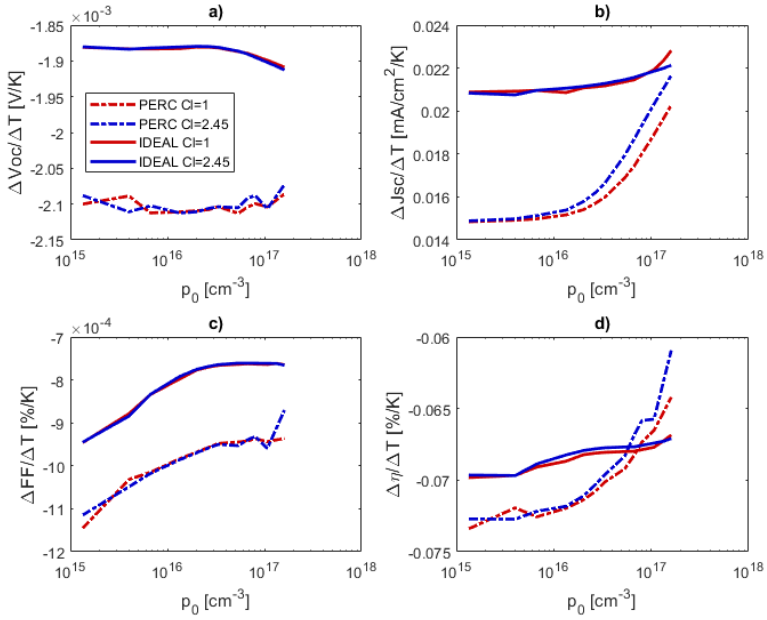

Figure 6.8: Un-normalized TCs, defined as $\Delta X/\Delta T = \frac{X(T)-X(25°C)}{T-25°C}$, of the IV-parameters as they change with effective doping level p_0.

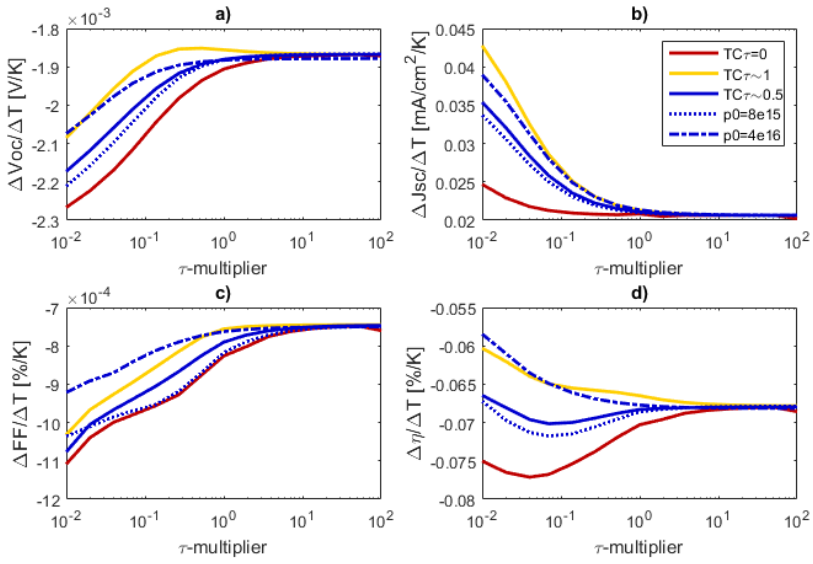

Figure 6.9: Un-normalized TCs, $\Delta X/\Delta T$, of the ideal cell-model as they change with bulk lifetime τ_{bulk}, TC_τ and p_0.

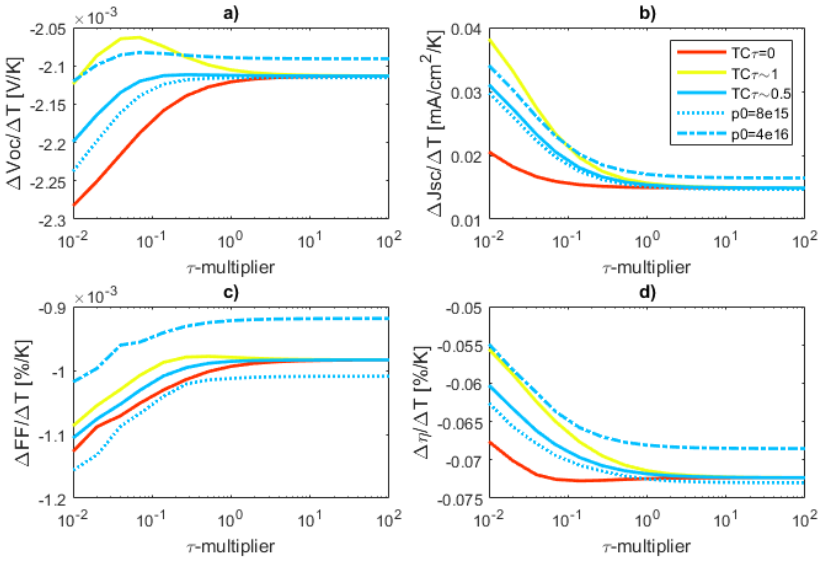

Figure 6.10: Un-normalized TCs, $\Delta X/\Delta T$, of the PERC-model as they change with bulk lifetime τ_{bulk}, TC_τ and p_0.